D2.4

Portability of failure mode detection/prognosis orientations

Grant agreement nº 745625

ROMEO

Deliverable No.	D2.4	Work Package No.	WP2	Task/s No.	Task 2.3 Task 2.4
Work Package Title		WP2 Wind Turbine diagnosis/prognosis solution for a New Design. Physical.			
Linked Task/s Title		Tasks T2.3, T2.4 and T2.5			
Status		Final	(Draft/Draft Final/Final)		
Dissemination level		PU-Public	(PU-Public, PP, RE-Restricted, CO-Confidential) (https://www.iprhelpdesk.eu/kb/522-which-are-different-levels-confidentiality)		
Due date deliverable		2021-08-31	Submission date		2021-08-27
Deliverable version		Portability of failure mode detection/prognosis orientations 1.3			

Document Contributors

Deliverable responsible		SGRE DE	
Contributors	Organization	Reviewers	Organization
Daniel Kjeldsmark Andreasen	Siemens Gamesa	Javier de la Peña	Zabala
Cristian Rodenas-Soler	SGRE DE	Leonardo Casado	Zabala
Ulrich Oertel	Bachmann	Athanasios Kolios	Strathclyde
Kilian Krügel	Bachmann		
Igor Reinares	Laulagun		
Ioseba Sanz Mendia	Siemens Gamesa		
Jesper Hjortshøj Nielsen	Siemens Gamesa		
Anders Olsen	Siemens Gamesa		
Amadou Tinni	EDF R&D		
Darius Vizireanu	EDF R&D		
Jalal Cheaytani	EDF R&D		
Pierre Bousseau	EDF R&D		

Document History

Version	Date	Comment
0.1	2021-06-25	Initial Version
0.2	2021-06-28	Initial Comments from SGRE.
0.3	2021-06-29	Improvements from SGRE
0.4	2021-06-30	Graphs and Definitions added
0.5	2021-07-01	Inclusion and refining of Blade Bearing and Electrical contents.
1.0	2021-08-06	Completing all technical contents and final candidate for the release.
1.1	2021-08-19	Inclusion of comments and general introduction and closure.
1.2	2021-08-26	Inclusion of Zabala suggestions and Laulagun suggestions.
1.3	2021-08-27	General cosmetic modifications, scientific language and orto.

Table of contents

List of figures

List of tables

List of abbreviations

Table 1. List of abbreviations.

Abbreviation	Description
AD5	Adwen 5MW Wind Turbine
CMS	Condition Monitoring System
DD	Siemens Gamesa Direct Drive
LCOE	Levelized Cost of Energy
ROMEO	Reliable OM decision tools
SCADA	Supervisory Control and Data Acquisition
SWP	Siemens Wind Power
TCM	TCM® for Turbine Condition Monitoring (see Definitions)
WP	Work Package
WTG	Wind Turbine Generator

List of definitions

Table 2. List of definitions.

Definition	Description
Data	Individual facts, figures, signals, measurements
Diagnosis	Diagnosis is a subfield of control engineering which concerns itself with monitoring a system, identifying when a fault has occurred,

Definition	Description
	and pinpointing the type of fault, the failure mode detected and its location.
CMSSTD	Bachmann' condition monitoring Data processing software.
DPS	Bachmann's Data Processing Server.
Failure Cause	The physical or chemical processes, design defects, quality defects, part misapplication or other processes which are the basic reason for failure, or which can initiate the physical process by which deterioration proceeds to failure.
Failure Mode	The way in which a failure is observed, describes the way the failure occurs, and its impact on equipment operation
Information	Organized, structured, categorized, useful or condensed Data.
Knowledge	Concept of idea, notion, learning, synthetisation, discussed or consensus results of an Information and Data acquisition process.
Month	Month of the Project ROMEO, starting from June 2017 (M1)
Portability	Capability of a technology development to be deployed in different technological platforms. Cross-platform.
PT100	Platinum resistance thermometer. It is a common type of temperature sensor.
Siemens Gamesa / SGRE DE	Siemens Gamesa and/or SGRE DE are subsidiaries of the Siemens Gamesa group of companies. Every time Siemens Gamesa is referred in this document, the collaborative work of the different companies of the Siemens Gamesa group that participate in ROMEO is assumed to be included within this reference.
Technology Development	A Technology Development is a technical innovation representing progressive or radical advances in the engineering field. Technology Developments are usually developed by the Research, Development and Innovation departments from engineering companies to gain a competitive advantage for the exploitation of their products.
TCM	The TCM®, is a commercial product from Gram & Juhl. It is a condition monitoring system that measures vibration.
U	Voltage
WebLog Expert®	Bachmann's condition monitoring diagnosis software.
Windbox	Windbox is a Test Bench for blade bearings and pitch components that ROMEO project used as an enabler to connect for the first time the Laulagun CMS and to acquire Data regarding a degrading test on Blade Bearings. The test ran in WP2 Tasks 2.4.1 and 2.4.2.
'x'	Non defined value

Definition	Description
μ-bridge	Bachmann's stress wave sensor for low speed condition monitoring applications.
Ω-Guard	Bachmann's modular condition monitoring hardware system

D2.4 - Portability of failure mode
detection/prognosis orientations
CO-Confidential

1. Executive Summary

This document covers part of the work conducted within ROMEO WP2 coordinated by Siemens Gamesa, more particularly the deliverable D2.4, entitled "Portability of failure mode detection/prognosis orientations". The main objective of WP2 is to develop diagnosis and prognosis solutions for new designs and arrangements. This is aligned with the general scope of ROMEO of anticipating failures in order to reduce O&M costs.

This report describes the different approaches that have been checked regarding newest and diverse offshore wind turbines, covering Drive Train, Electrical Drive Train and Blade Bearing systems.

Within WP2, the initial development of diagnosis and prognosis techniques, was validated in test bench, intended to mimic real failure development and symptoms.

The final stage of this work package has been to port applicable algorithms or appropriate methods directly in order to make them work on offshore wind turbines.

Some other interactions with the rest of the project are summarised in Figure 1 and Table 3.
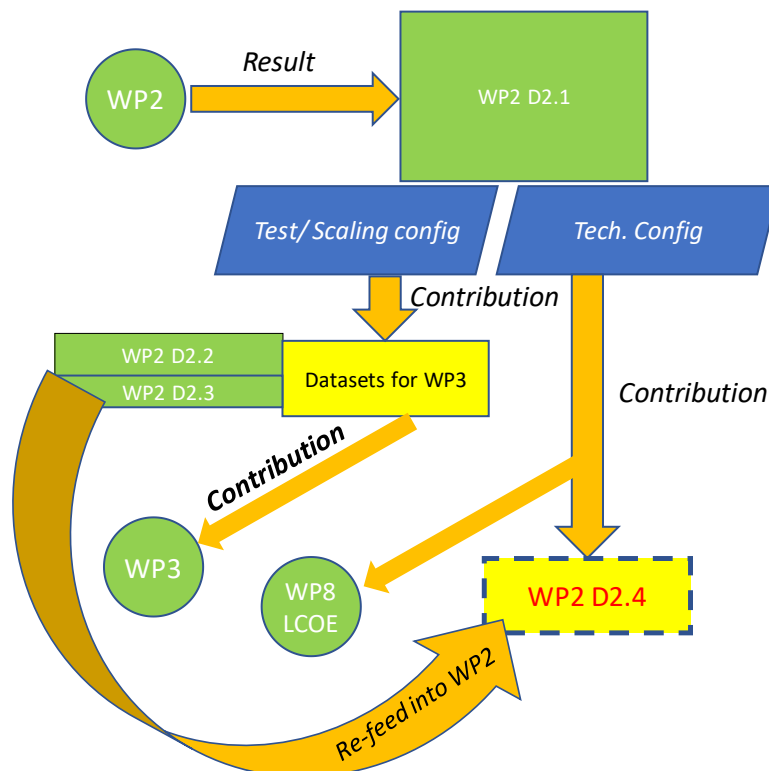
Figure 1. Map of interactions, inputs, outputs to other work packages and deliverables.

D2.4 - Portability of failure mode
detection/prognosis orientations
CO-Confidential

Table 3. Summary of interactions of Deliverable 2.4 with other work packages and deliverables.

Type of interaction	Target	Summary of the interaction
Input	Tech configuration from D2.1 WP2	Input from the Technical Developments as they were subject of technological development.
Output	WP8	Results that are candidate to improve LCOE.
Output	WP9	Exploitable product / Intellectual Property.

The present document, D2.4, as well as D2.1, shall represent, Methods, also described as "diagnosis methods for new design".

This deliverable will be submitted again in February 2022 in order to include the portability considerations applicable to electrical machines and progressive generation of short circuit algorithms.

2. Introduction

This document shall serve as a collection of methods developed during WP2, that have been studied in detail as candidates to be ported to other systems.

The objective of this deliverable is to provide a memorandum on the status of the investigation of each method and suggest improvement or new developments.

WP2 targets three main assemblies, namely the mechanical drive train, the blade bearing and the electrical drive train. One by one, the state of the art of each one of them will be reviewed regarding portability.

2.1. Mechanical Drive Train CMS State-of-the-Art (ROMEO Task 2.3 related)

During the execution of WP2 it was identified that only classical approaches of vibration analysis were used in industrial systems. This gap was identified in order to provide further use of the CMS putting into value some of the detailed data recovered from offshore field, as well as the usage of test bench facilities.

Regarding [D2.1, the different technologies were presented, with a level of detail that covered implementation of each of the algorithms.

This document presents the state of the art of the industrialized versions of the algorithms regarding a final subset of wind turbines from diverse platforms where the analysis has been refined and the techniques have been subsequently ported. Therefore, Section 3.1 gives a better view of what the industry can achieve with the use of a proven example.

2.2. Blade Bearing CMS State-of-the-Art (ROMEO Task 2.4 related)

During the execution of WP2 it was identified that this technology concept was not available by the industry. In order to advance in this gap, an effort was made within Task 2.4 in order to build solutions that can be industrialized in form of a CMS, and at the same time, the algorithms can be used in offshore applications for future wind turbines.

The result is a reviewed knowledge base of methods for detecting blade bearing shown in Section 3.2.

2.3. Electrical Drive Train techniques State-of-the-Art (ROMEO Task 2.5 related)

The most challenging part regarding technology developments on the diagnosis and prognosis field was the electrical drive train. By one side, electrical machines are not easily accessible to sensorics and tests, and by the other side converter failures show signs of degradation with less anticipation.

Knowing of the basis of the updated technologies could be studied within ROMEO, the approach was taken directly by building a small laboratory and taking full scale candidate examples when applicable, in order have better data and focused experiments on the different specific failure modes.

The result is a reviewed knowledge base of methods for detecting electrical drive train is shown in Section 3.3.

As stated in the executive summary, this deliverable will be submitted again in February 2022 in order to include the portability considerations applicable to electrical machines and progressive generation of short circuit algorithms.

3. Failure mode methods ported during ROMEO

3.1. Drive Train

3.1.1. Unbalance algorithm

3.1.1.1. Description

Undetected loads resulting from unbalance can drastically affect the component lifetime of the drive train, support structure and tower. The previous ROMEO deliverable 2.1 presents Bachmann's online blade unbalance calculator enabling operators assessing the rotor balance grade remotely. The algorithm has been successfully translated into a commercial product and is now part of Bachmann's CMS product portfolio.

This section presents the advances made from prototype testing to commercialisation. It summarises necessary hardware, input as well as output of the diagnostic module. Finally, the algorithm was ported to one of ROMEO's pilot farms where it has shown successful performance.

3.1.1.2. Inputs

The blade unbalance calculator is a plugin to Bachmann's condition monitoring software CMSSTD. It computes both mass and aerodynamic unbalance as well as the associated phase angle. The module's input comprises

- 2D acceleration signals measured in fore-aft and side-side direction
- Rotor speed
- Rotor angle (optional: for phase angle measurements)
- Finite element tower model

Note that many wind turbines are already equipped with a 2D acceleration transducer and rotor speed acquisition is essential and thus part of any CMS installation. That means, that for a high number of turbines the unbalance module is a pure software update of their existing CMS solution.

The unbalance algorithm translates the measured acceleration signal into an unbalance value in the unit kgm. It does this by means of a FE model custom made for the particular tower. The advantage is that values in kgm can be compared with threshold values set by the turbine manufacturer or farm operator. In case a threshold is exceeded, an automatic alarm highlights the abnormal operation of this turbine. An effective way to spot affected turbines is to make a fleet comparison and see which turbines have significantly higher unbalance values then the fleet's average (see Figure 3 for example data of ROMEO's offshore pilot farm).

D2.4 - Portability of failure mode
detection/prognosis orientations
CO-Confidential
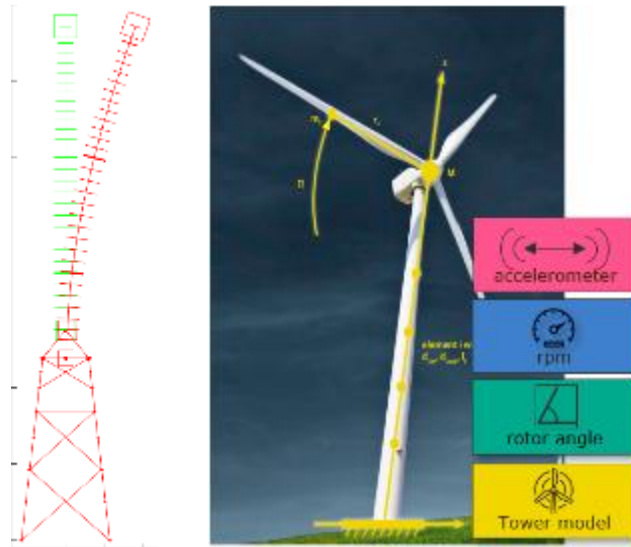
Figure 2: Bachmann's online blade unbalance calculator
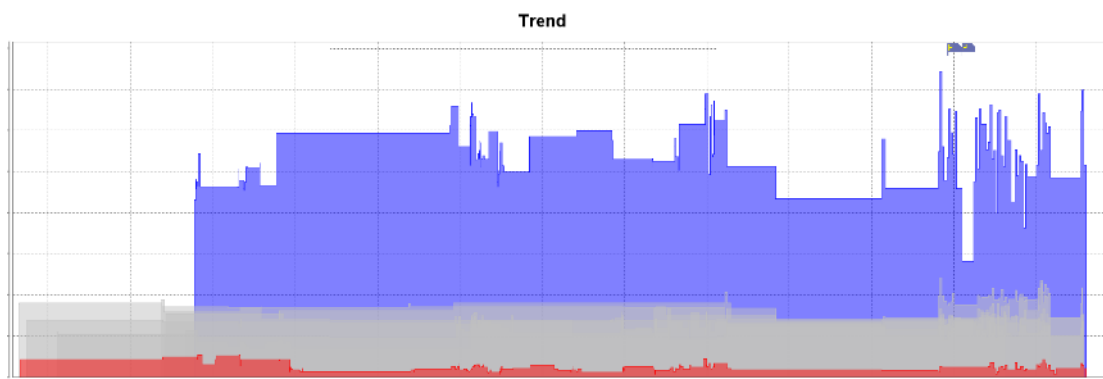
Figure 3: Unbalance fleet comparison showing abnormal unbalance condition of purple turbine

3.1.1.3. Calculations

The calculation procedure of the plugin was presented in deliverable 2.1 This section presents results from one of Bachmann's pilot installations. The data of the onshore turbine showed a high value of mass unbalance of 380 kgm, which is far above the allowable threshold value (see Figure 4). For validation purposes, a partner was sent to measure the unbalance with conventional methods using test-weights. The offline-measured value of 375 kgm confirmed the results of the plugin. Moreover, the phase of 272° matched almost exactly the phase derived with our calculator (see phase histogram in Figure 4).

D2.4 - Portability of failure mode
detection/prognosis orientations
CO-Confidential
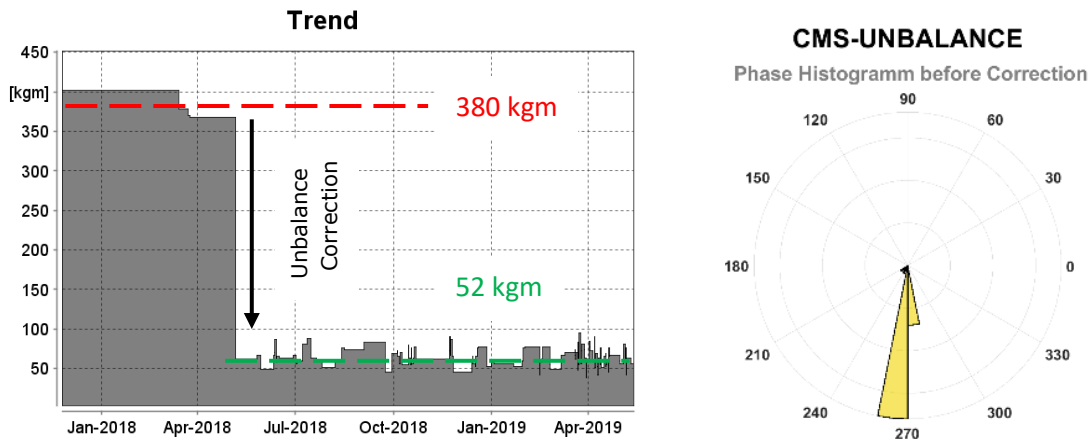
Figure 4: CMS-UNB: Mass unbalance example

3.1.1.4. Portability

The unbalance algorithm developed in WP2 was ported to one of ROMEO's pilot wind farms. In close collaboration, SGRE and Bachmann launched an effort to compare the unbalance status of the operational turbines. Within the project, three abnormal conditions were successfully identified and confirmed by both SGRE and Bachmann. Figure 5 shows an example of an aerodynamic unbalance. It was caused by a faulty blade installation, which could not be registered by the turbine control system. After the CMS detected the high unbalance value, the operator could correct the pitch angle by adding an offset to the control configuration and thus compensating the hardware error.
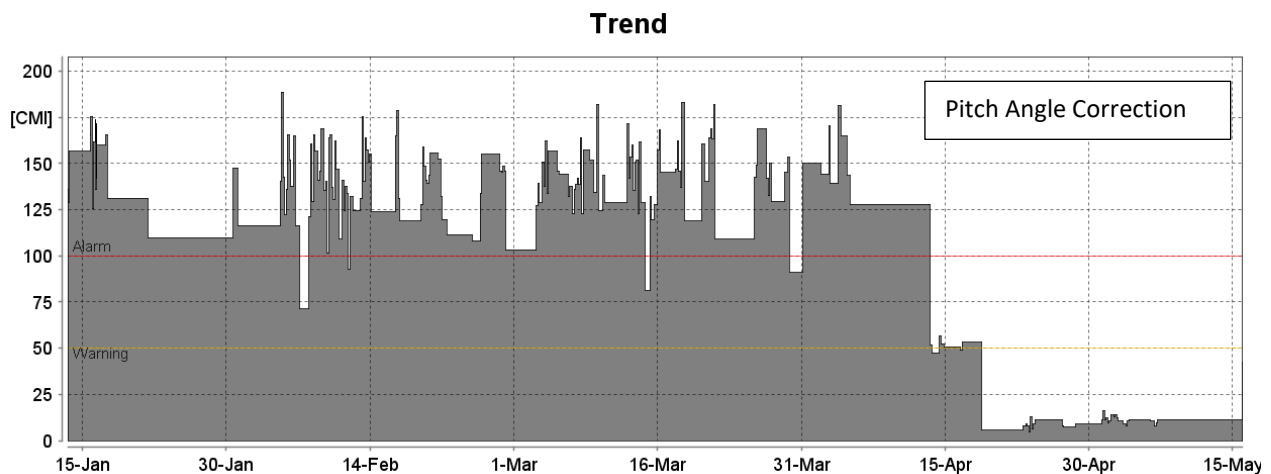
Figure 5: CMS-UNB: Aerodynamic unbalance example from pilot wind farm (CMI – normalised condition monitoring index, 100 equals alarm threshold)

3.1.2. Damage Classification

3.1.2.1. Description

Modern O&M concepts include the use of software platforms, which gather, link and visualise data from various sources. Among others, that comprises metocean data, component availability or current vessel cost. A key role plays condition monitoring data supporting the O&M service to plan and optimise their actions.
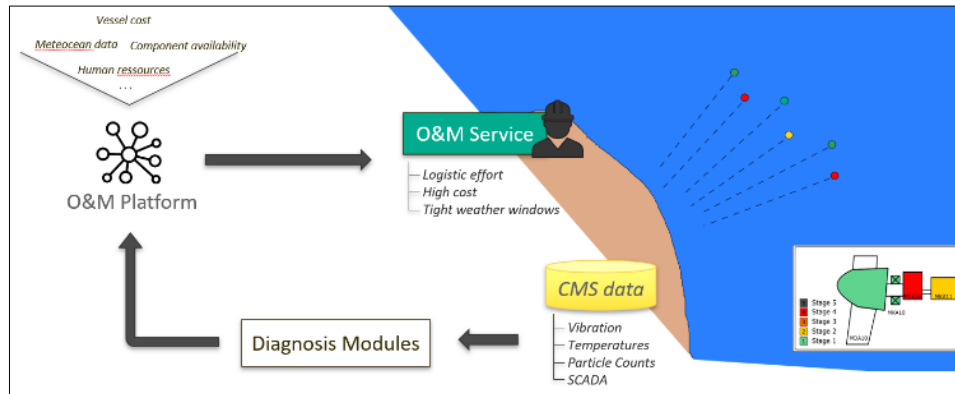
Figure 6 Role of condition monitoring in predictive maintenance concepts

For drive train monitoring, vibration transducers are a cost-effective solution to gain insight in the current condition of components. Time signals are usually acquired in very high resolution, enabling us to detect defects in a sub-component level. E.g. CMS not only allows us to identify a damaged bearing, but also characterise the failure type. That could be the identification of an outer race, inner race, cage or roller defect.

In condition monitoring, vibration data can be complemented with further measurements. Useful information comes from temperatures, particle counts in the oil system and the SCADA system. The total amount of data acquired by a condition monitoring system can be enormous and difficult to interpret. On the other hand, O&M teams require concise status messages on fleet, turbine and component level. This section presents the methodological approach of handling CMS data. It highlights the importance of data reduction and evaluation techniques which are bundled in diagnostic modules.
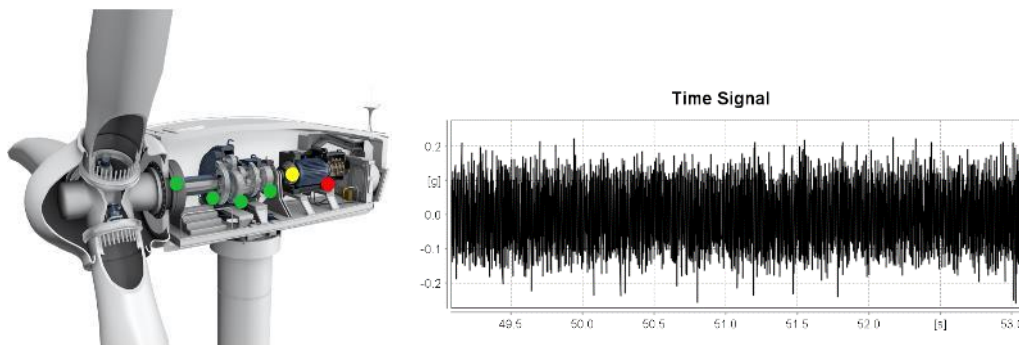
Figure 7 High resolution vibration data for condition monitoring

D2.4 - Portability of failure mode
detection/prognosis orientations
CO-Confidential

3.1.2.2. Identification of fault indicators for damage classification

ROMEO deliverable [D2.1] presented the methodological approach of the failure mode symptom analysis (FMSA). It describes the process of deriving diagnostic indicators based on sensory input. In practice, one failure mode is described by a list of indicators. Using multiple indicators for one failure mode is advantageous, as they provide detailed insights in the component's condition. One indicator may be enough to detect a particular failure. The combination of several enables the severity classification of this failure, though. This section presents how a FMSA is performed for an exemplary bearing component.
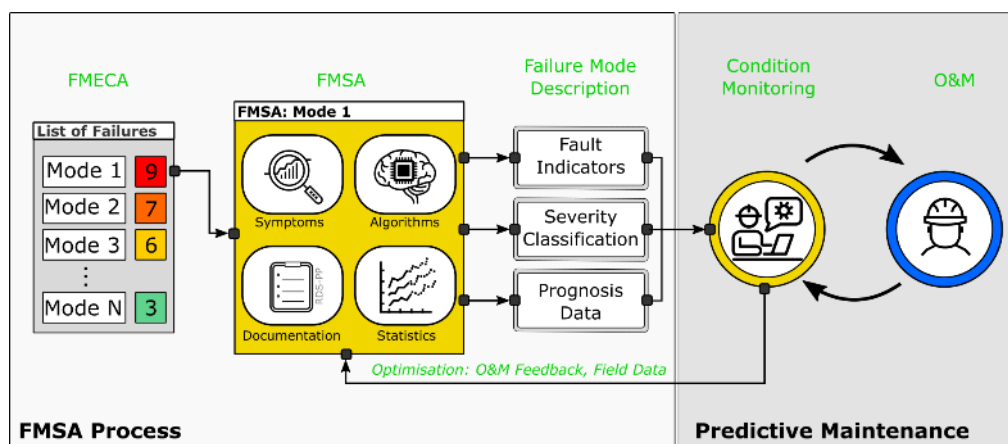
Figure 8: Failure Mode Symptom Analysis (FMSA)

Fault indicators can be derived from various data sources. The main input for condition monitoring comprises data from

- Accelerometers
- Oil particle counters
- SCADA (including temperatures)

- Each condition monitoring task is described by a set of requirements. The aim of the FMSA process is to determine fault indicators which satisfy these requirements. For our exemplary application we state that, the set of indicators shall:
(a) detect raceway damages of a particular bearing type from a very early phase.
(b) yield for a high detection rate.
(c) exclude (minimise) the chance of a false positives.
(d) enable a severity classification.
(e) enable prognostics / point to failure estimation.
(f) work for typical operational states of the turbine.

D2.4 - Portability of failure mode
detection/prognosis orientations
CO-Confidential

- While (a) to (c) are conventional condition monitoring requirements, (d) and (e) introduce novel diagnostic challenges to the FMSA process. Following the VDI 3832 and ISO 10816-21 standards, 5 stages for damage classification are applied. To include the characteristics of the investigated failure mode, we slightly modify the stage descriptions:

stage 1 – as a new undamaged raceway
stage 2 – raceway with sub-surface cracks
stage 3 – raceway with initial surface cracks
stage 4 – intermediate damage / growing phase
stage 5 – very advanced raceway damage, two rollers fall into the damage zone

The computation of fault indicators includes several standard post-processing techniques. For acceleration data, time series, frequency and envelope analysis are standard methods. Their output is used to apply advanced feature selection techniques to diagnose the component's condition. Two exemplary bearing fault indicators are shown in Figure 9. Each point of the scatter plots represents one post-processed time series dataset. The data comes from a real offshore wind turbine with a bearing defect in stage 3. The horizontal and vertical axis represent the rotational speed and value of the damage indicator, respectively. The indicator shown in the left plot seems to be unsuitable for both damage detection and severity classification. For all operational speeds, one cannot identify threshold zones to distinguish between stage 1 (green), stage 2 (yellow) and stage 3 (orange). The right scatter plot shows a more suitable indicator. It clearly separates the three damage stages for all running speeds und thus fulfils requirements (d) and (f). Note that data-based separation of damage stages requires highly experienced and skilled diagnostic staff, which is capable of identifying and classifying signals based on machine dynamics.
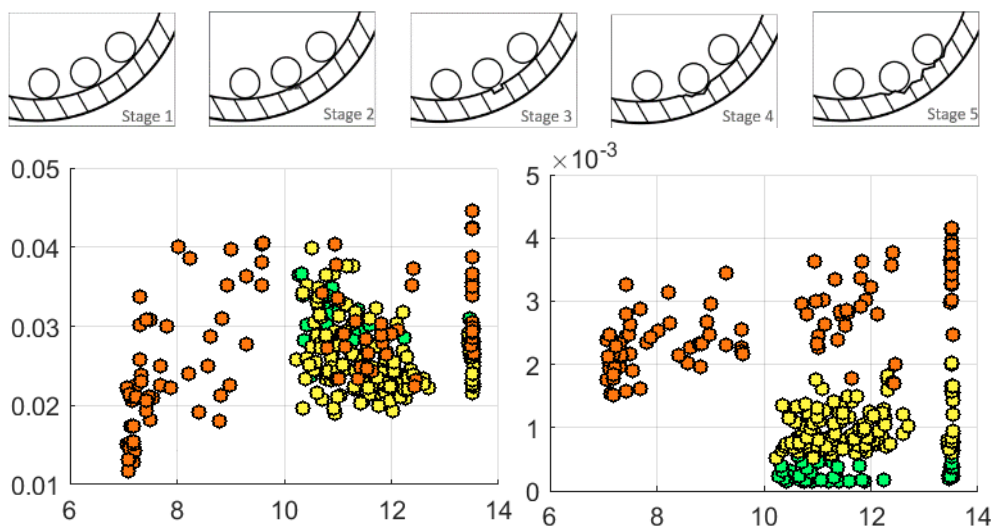
Figure 9: Identification of suitable fault indicators (left: unsuitable indicator, right: suitable indicator, green: damage stage 1, yellow: damage stage 2, orange: damage stage 3).

D2.4 - Portability of failure mode
detection/prognosis orientations
CO-Confidential

Figure 9 demonstrates that individual indicators can be used to distinguish between damage stages. To add robustness, one strategy is to use multiple indicators characterising one damage stage. Moreover, individual characteristics can be used to for monitoring the transition from a particular phase to another. Figure 10 shows two exemplary vibration trends for a bearing condition developing from damage stage 1 to 4. The blue trend is used to detect the transition from stage 1 (undamaged) to stage 2 (sub-surface cracks), indicated by the increase. Several months the trend remains constant. Note that the oil particle count (black dotted line) also remains constant showing that there is not breakout of raceway material. Note also, that the second indicator in purple remains constant, too. It is used to detect the transmission from stage 2 to stage 3 (initial raceway surface damage). Validating the results, its increase correlates with the increase of the particle count trend. After steady increase, both vibration trends stabilise and even decrease slightly indicating stage 4 of the damage classification.

In summary, the FMSA process provides condition monitoring services with a list of failure indicators. They are derived from characteristic damage features and can be logically combined for damage classification and automated diagnosis. The method has been applied on two offshore wind farm turbines of the same type. The selected failure indicators yielded for a detection rate of 100% with zero occurrences of a false positive. After repair and replacement services, the O&M team analysed the condition of every damaged component. The results of this studies were compared with the damage classification based on CMS data. In all cases the CMS estimated the damage class correctly. Moreover, both the O&M and monitoring teams ranked the damage cases according to their severity. As visualised in Figure 11, both rankings have a 100% match.
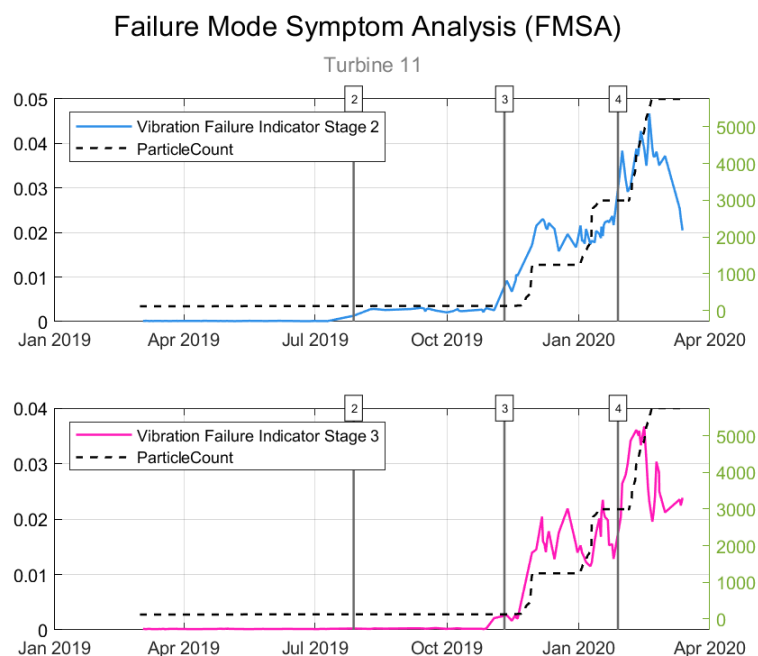
Figure 10: Exemplary failure indicators showing bearing damage stages one to four for one turbine

D2.4 - Portability of failure mode
detection/prognosis orientations
CO-Confidential

Damage Classification
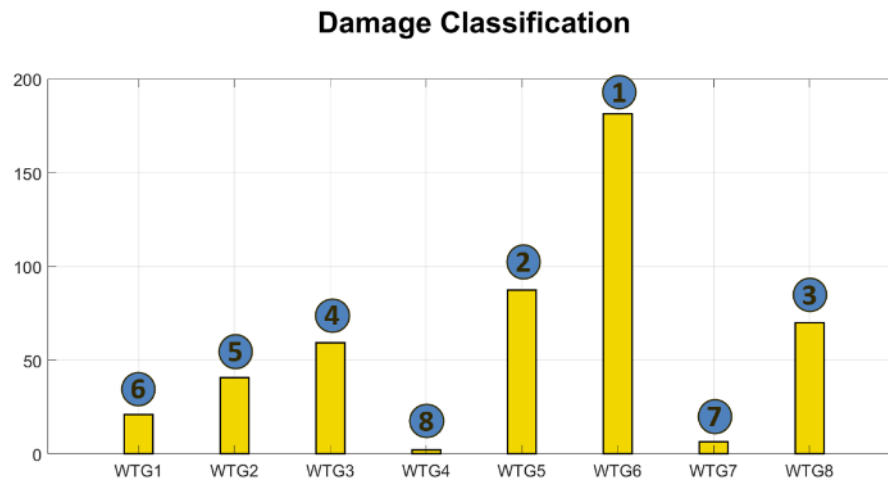
Figure 11: Damage severity classification based on vibration data – comparison of CMS data (yellow bars) and O&M field feedback (blue circles) ranking
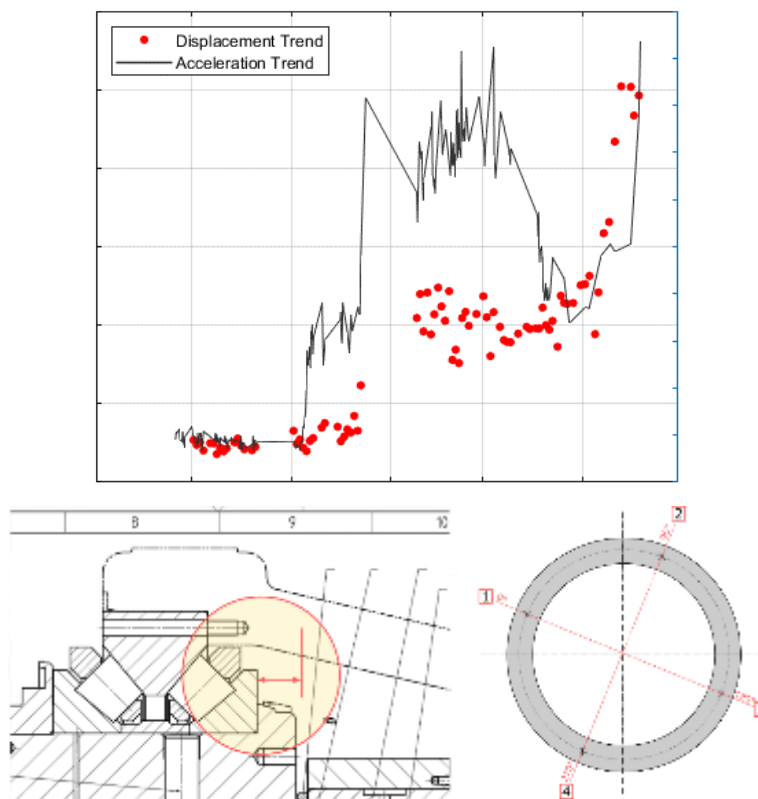
Figure 12 Application of displacement sensors

During the FMSA study the application of new sensors was investigated. For that purpose, several indicators were derived from the displacement sensor installed to measure a bearing's pretension. It could be shown that displacement signals contain information of raceway damages and one can generate well working failure indicators using appropriate post-processing techniques. In comparison to indicators derived from acceleration, they performed surprisingly well (see Figure 12). They are

disadvantageous in very early fault detection but work sufficiently well for the later and more important damage phases.

Despite promising results from the displacement sensor study, the derived failure indicators were not included in the FMSA list for the analysed bearing. The reason is, that the created diagnostic modules were subsequently ported to turbines of one of ROMEO's pilot wind farms. Unfortunately, these turbines do not have displacement sensors installed so further studies on this topic were not feasible.

3.1.2.3. Portability and Prognosis Assessment

3.1.2.3.1. Description

The algorithms and failure indicators presented in section 3.1.2.2 were ported and applied on one of ROMEO's offshore pilots. In this process, the FMSA process and damage classification methods were implemented in Bachmann's condition monitoring architecture WebLog. The main components of this architecture comprise a server for CMS data storage, the *WebLog Portal* accessible for customers via an arbitrary web browser and the *WebLog Expert* client software. The latter features

- CMS configuration
- Data visualisation, diagnosis and prognosis
- Turbine condition history log
- Ticket system for customer communication
- CMS report generator

The implementation of the FMSA allows the user to define failure modes for the individual components of a wind turbine. If required for the project, the mode description can also include damage stages. Next, indicators are configured and assigned to both failure mode and damage stage.

Prognostics features allow statistical evaluation of historical damage cases. From that, P-F intervals and the point to failure are derived, which are valuable measures to plan O&M actions.

3.1.2.3.2. Weblog implementation and results

An exemplary WebLog FMSA implementation is presented in Figure 13. The plot shows vibration indicator 1 presented in section 3.1.2.2. While damage stages are visualised with threshold levels and different background colours, the vertical lines indicate transitions from one stage into the other. For each case, the corresponding timestamps are tracked and stored in a database (see top right window). This way, the system gathers and performs statistical evaluation based on all historical damage cases of a particular failure mode. The prognostic output allows the user make lifetime forecasts for components.

The FMSA is a universal method applicable in monitoring tasks of arbitrary technical systems. In comparison to the preliminary study at two offshore wind locations, the ported diagnosis modules show equal performance on turbines of the selected ROMEO pilot farm. The study yielded a detection rate of 100% with no false positives. The failure indicators for damage classification are robust and give precise information about the current component status of each turbine.

D2.4 - Portability of failure mode
detection/prognosis orientations
CO-Confidential
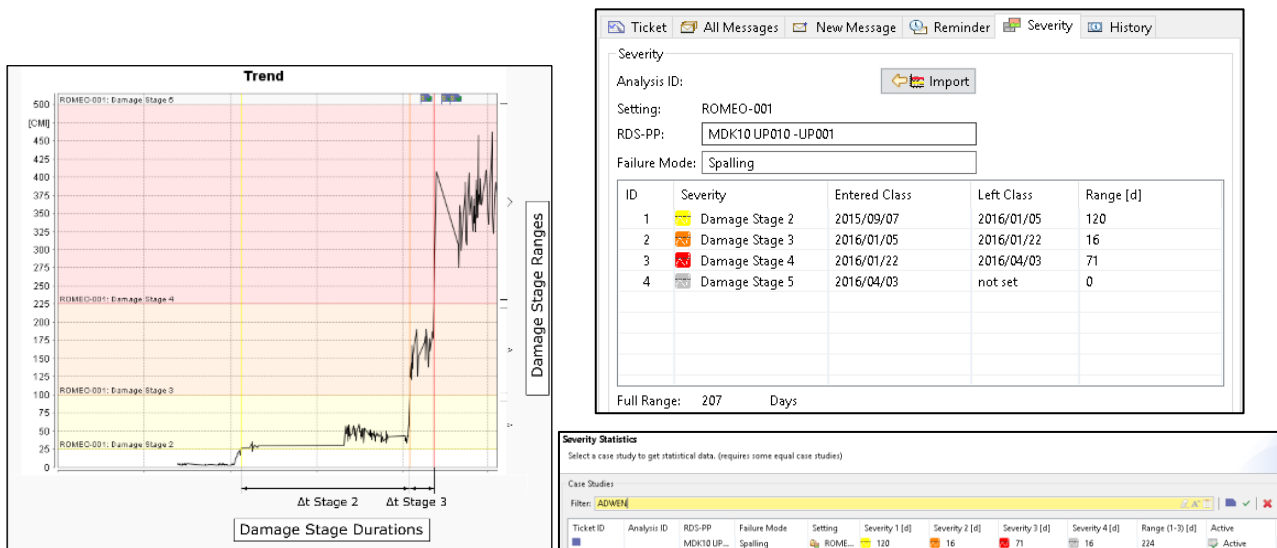
Figure 13 FMSA, damage classification and prognosis assessment in WebLog Expert

3.1.2.3.3. Communication interfaces

Diagnostic results can be communicated to the O&M service through

(a) Diagnostic reports / ticket system
(b) Health-API for direct status transfer to O&M platform

Diagnostic reports are short event descriptions of a particular CMS alarm event. They comprise plots of failure indicators leading to the alarm, detailed charts (e.g. showing spectral analysis), a summarising text describing the component status and recommended O&M actions.

Report based communication between remote monitoring services and O&M service is the conventional and current industry practice. One goal in ROMEO was to facilitate cross-platform communication between the different entities of a predictive maintenance process. Bachmann created the Health-API to transfer output from the diagnosis module to O&M software platforms, a detailed description can be found in Deliverable 3.1. In the project, the RDS-PP functional designation system was used to label farm locations, wind turbines and their components. The use of standardised communication is key and an essential requirement for digitalisation of service tasks.

Figure 14 shows the Health-API in the context of an O&M software platform. The latter gathers information from various sources to plan and optimise their processes. The Health-API provides status

D2.4 - Portability of failure mode
detection/prognosis orientations
CO-Confidential

messages for each turbine and each component, respectively. For components, the status displays the current damage stage.
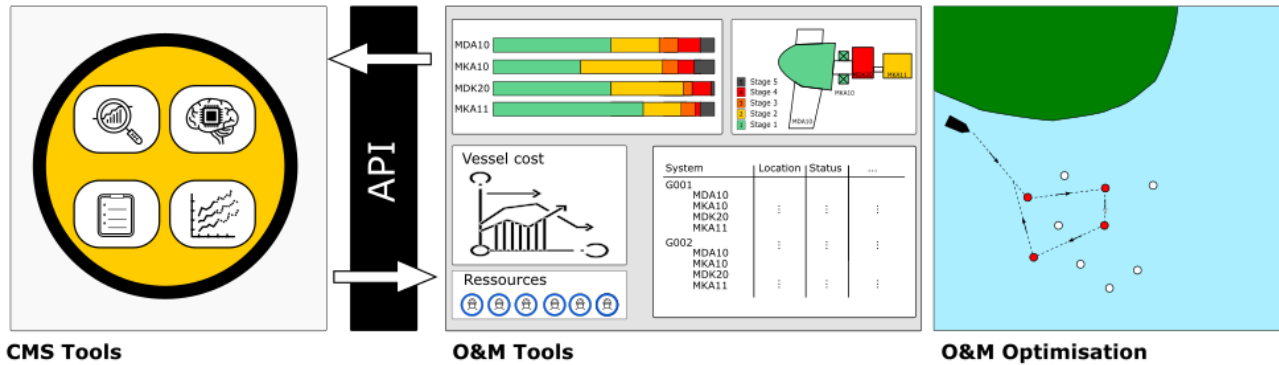
Figure 14 Bachmann's Health API and the role of condition monitoring in O&M optimisation

3.1.3. CMS STD – Continuous Reading - Diagnosis

3.1.3.1. Description of ported algorithm

In order to proof portability of the algorithms generated in task 2.3, Siemens Gamesa (SGRE) and Bachmann launched an effort to test the CMS-STD condition monitoring software at a real scale main bearing the test bench of a direct drive machine, located within the SGRE factories in Brande/Denmark. The focus of the measurement campaign was to evaluate the continuous ISO r.m.s acquisition presented in deliverable 2.1 [D2.1]. Bachmann's other CMS algorithms have been tested on real operating wind farms. The online r.m.s, however, is a hardware calculated value requiring Bachmann's newest AIC214 CMS module, which was released after the project start and is thus not available on one of ROMEO's pilot windfarms.

The main bearing test bench is illustrated in Figure 15. It comprises a foundation and tower adapter, which supports the main frame holding the bearing. To simulate loads, the bearing's outer race is attached to a rotating ballast tube.

The CMSSTD runs on Bachmann's Ω-Guard condition monitoring hardware (Figure 16). Installed at the test bench, it handles signal acquisition, post-processing, and transfer to a WebLog server for data storage.

D2.4 - Portability of failure mode
detection/prognosis orientations
CO-Confidential
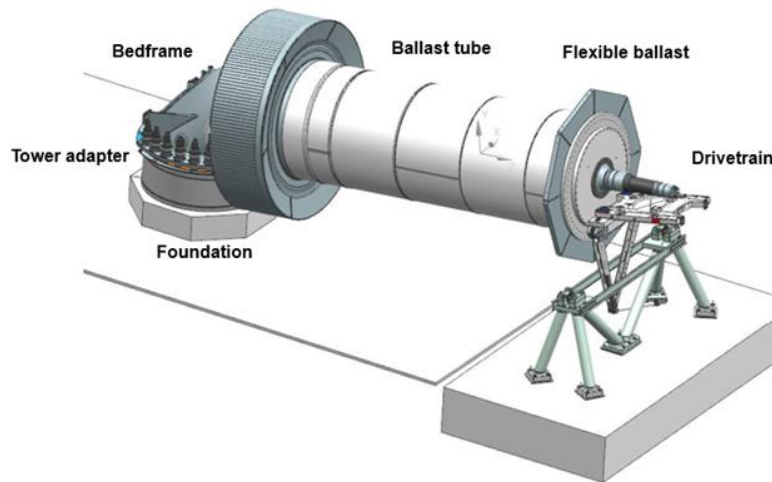
Figure 15: SGRE main bearing test bench

Figure 16 Bachmann's Ω-Guard condition monitoring system

The CMS is configured to detect bearing defects and unwanted operation conditions such as unbalances or misalignments (see Table 4). However, for this task the focus was to evaluate results from continuous r.m.s measurements, which can be used for machine protection. System input, results and evaluation according to the ISO-10816-21 and VDI 3834 are summarised in the subsequent sections.

Table 4: Condition monitoring and machine protection

	Indicator Type	Indicators
Condition Monitoring	Component defect indicators	MB* inner race defect indicators
		MB* outer race defect indicators
		MB* roller defect indicators
	Machine status indicators	Unbalance indicators
		Misalignment indicators
		Rotating looseness indicators
Machine	Machine energy levels	Overall energy levels in various positions

	Indicator Type	Indicators
		Energy levels in various bandwidth according to ISO 10816-21 and VDI 3834

*MB: Main Bearing

3.1.3.2. Inputs

The hardware setup for the main bearing test bench comprises Bachmann modules for data acquisition and post-processing, an LTE router for data transfer to Bachmann's WebLog server. The latter is realised via FTP over the 4g cellular network.

Table 5: SGRE test bench hardware summary - data acquisition

Hardware	Hardware description	Usage
NT255*	Power supply	Power supply for control system
MC210*	Controller	Data Processing
AIC214*	Vibration sensor input module	High speed acquisition, continuous recording, real time r.m.s calculation, RPM measurement
GIO212*	Universal input/output module	Receive 4-20mA current signals from SGRE system. Signals comprise operational test bench parameter.
LTE router	Long-Term Evolution router	Communication for FTP Data transfer over 4g network

*Bachmann Module
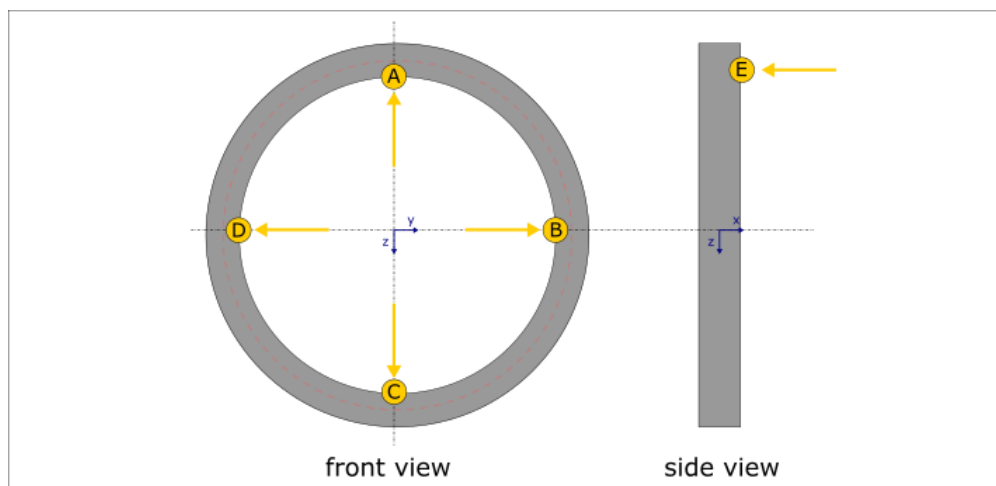
Figure 17: CMSSTD: Main bearing test bench - sensor setup

• The sensor setup is split into two locations. At the test bench load system, two inductive tachometers are installed. Located at the low and high-speed side of the gearbox, this arrangement enables both RPM and phase measurements. Two accelerometers measure vertical and horizontal vibration of the ballast tube bearing on the drive-end side of the test bench. Additionally, 4-20mA current signals were provided by SGRE to include operational parameters in the subsequent Data analysis. The

signals comprise tilt and torque measurements which are recorded synchronously to the vibration measurements.

For the main bearing, a standard setup is applied. It consists of four radial and one axial sensor locations (see Figure 17). Each location is equipped with accelerometers. Location (A) and (D) have additional stress wave sensors, which are advantageous in low speed operation. Furthermore, (A) has redundant accelerometers to compare transducer quality of different types and manufacturers. The Data acquisition configuration parameters are specified according to their application and usage:

•

Table 6 SGRE test bench - data sampling
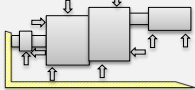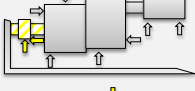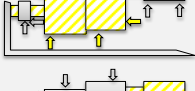
Application	Sample rate [Hz]	Number of samples [-]
Condition Monitoring	6400	1,536,000
Continuous ISO r.m.s	100	60,000
Operational parameter from SGRE	16	3,840

3.1.3.3. RMS operation zones

The VDI 3834-1 and ISO10816-21 standards introduce bandpass filter settings for the individual drive-train components. The filters are defined for both acceleration and velocity, where the latter is derived from the acceleration signal. The r.m.s is a measure for the energy level of these bandwidths. In contrast to diagnostic indicators, it does not provide information of the exact component or failure type. It is used to assess the overall machine vibration level, detect major system faults such as high unbalances, misalignments, or advanced component damages. For each band, the ISO standard and VDI guidelines provide threshold levels, which define operational zones. They range from zone A for a newly commissioned turbine to zone D for a potentially machine damaging operation (see Table 7). Note that these values can be used as a good reference but may need adaptations depending on the actual turbine type.

Table 7: Wind turbine operation zones according to VDI3834-1 and ISO 10816-21 (
Zone A: Newly commissioned turbine, low turbulence operation.
Zone B: long-term operation,

Zone C: investigation recommended,
Zone D: Potentially damaging operation)

3.1.3.4. Calculations

Bachmann's AIC214 condition monitoring module provides hardware filtering and subsequent r.m.s calculation for all ISO r.m.s standard values. The advantage of a hardware calculation is, that it is very fast, separate from other software modules, thus does not affect CPU performance and is providing r.m.s levels continuously 24/7. It allows continuous measurements which are stored in the module's ring buffer for temporary storage. From there, the r.m.s values can be transferred to the turbines SCADA and control system or send to a WebLog condition monitoring server for permanent storage.

Following the standards ISO 10816-21 and VDI 3834-2 for direct-drive machines, three bandpass filters are defined for acceleration and velocity time signals:
Sampling frequencies:

- 0.1 to 10 Hz (acceleration)
- 10 to 2000 Hz (acceleration)
- 10 to 1000Hz (velocity)

To compare r.m.s values calculated in software with those calculated in hardware, these bandwidth settings are also applied for the software post-processing routine. The acquisition and data evaluation period are set to 10 minutes, which enables detailed data comparison with the real time values. For real applications, though, the data logging period for the r.m.s calculation in software is much greater[1]. Contrary, the r.m.s calculated in hardware is a real time measurement, which is meant to be integrated

---

[1] Configurable, typically four trend points per day.

D2.4 - Portability of failure mode
detection/prognosis orientations
CO-Confidential

into the turbine control and/ or SCADA system to guarantee optimal turbine operation and ensure machine protection.

Figure 18 shows data from the SGRE main bearing test bench measurement campaign. The plot compares the software and hardware calculated r.m.s values for a bandpass setting of 0.1 to 10 Hz. The hardware r.m.s shows good compliance. Slight differences are expected due to configuration differences. The software version computes the r.m.s using a ten-minute time signal. The hardware version uses shorter time periods for evaluation. That results in more data points. This refined evaluation allows better detection of single events, such as collisions.
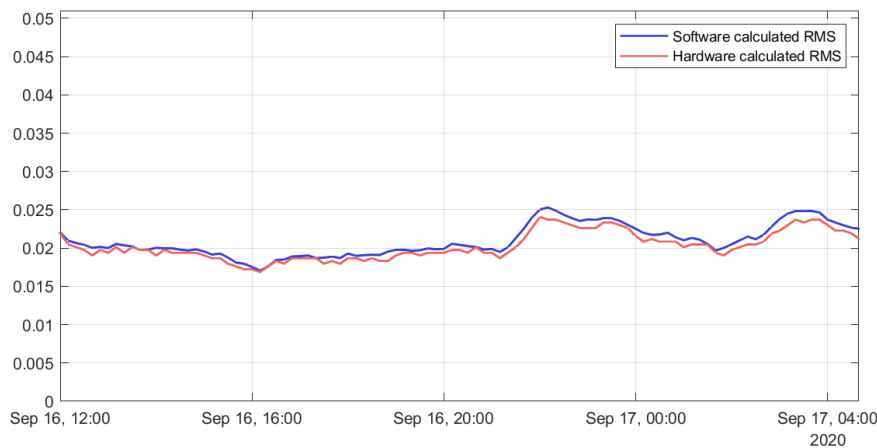
Figure 18 SGRE test bench - comparison of software and hardware calculated r.m.s (0.1-10Hz).

A visualisation from the WebLog Expert client software is presented in Figure 19. Whereas the 10-2000Hz r.m.s is continuously acquired on the CMS, the system is configured to send ten-minute mean values to the server. The r.m.s trend correlates to the operational trends of shaft running speed (blue) and the applied mean torque (yellow).

D2.4 - Portability of failure mode
detection/prognosis orientations
CO-Confidential
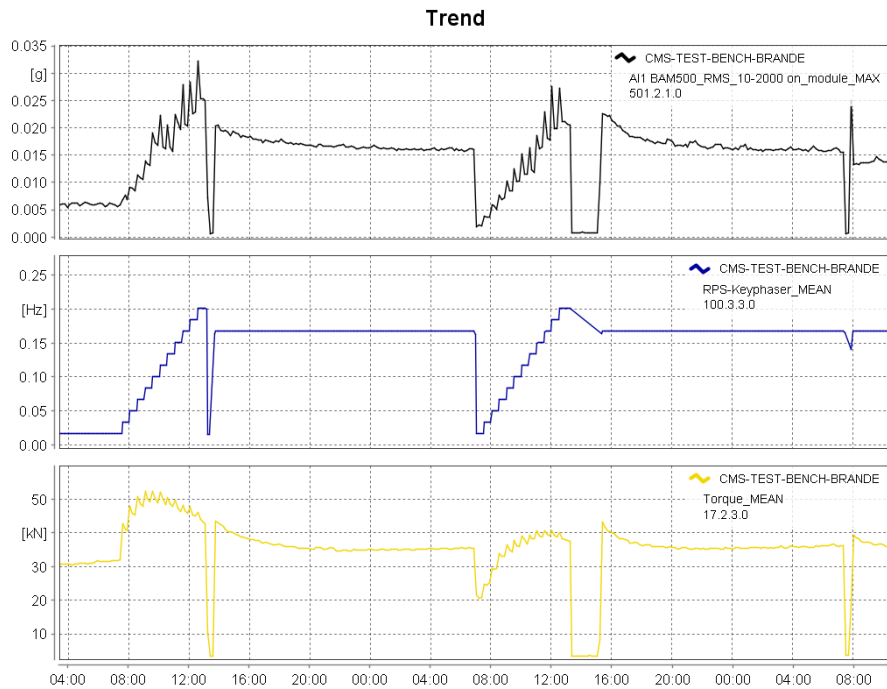
Figure 19: SGRE test-bench - online r.m.s 10-2000Hz (WebLog Expert visualisation)

3.2. Blade Bearing

3.2.1. System Description

3.2.1.1. Summary of the system

The target machine to focus in order to port blade bearing diagnosis algorithm are the Siemens Gamesa Direct Drive turbines. These turbines range from 3MW onshore turbines to the largest and most advanced offshore turbines. They are pitched using a hydraulic pitch system.

The pitching system consist of blade bearing, pistons and accumulators together with a hydraulic pump, which supply the pressure for the accumulators needed for the system to pitch the blades. This is controlled in essence by a feedback loop, where the operating mode and conditions of the turbine sets a pitch reference, which is compared to the actual pitch positions, obtained via the piston extension, and then the discrepancy between reference and position is minimized. An example of a blade bearing together with a hydraulic pitch system is displayed in Figure 20
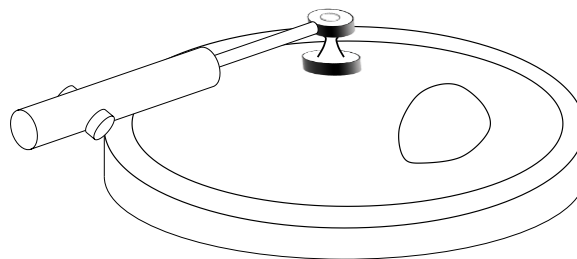
Figure 20: Scheme of a hydraulic pitch system and blade bearing.

3.2.1.2. Instrumentation

There are no sensors installed directly on or next to the blade bearing in the turbines where we aim to port the blade bearing monitoring to. The sensors closest to the blade bearing, which are deemed relevant for blade bearing monitoring are the sensors installed in the hydraulic system used for pitching the blades. Specifically, a linear displacement sensor in the pistons give, for each blade, the extension of the piston; and the relative opening of the proportional valve, controlling the pressure on the working side chamber of each piston, is reported.

In addition to this comes several operational observations like power production, rotational speed, wind speed and direction etc. and several variables indicating the operational mode.

3.2.2. Failure Description

A bearing is a mechanical component and is used in numerous constructions where parts should be able to move/rotate independently of each other. For a blade bearing it is the blade, that should be allowed to rotate independently from the hub. In the SGRE DD-turbine design double row ball bearings are used. They consist of an outer ring attached to the hub and an inner ring attached to the blade. The rings are separated by two raceways filled with balls, that let the inner ring move with minimal friction. Grease is supplied to the raceways as lubrication. To avoid grease leakage from the raceway a seal covers the spacing between the inner and outer ring.
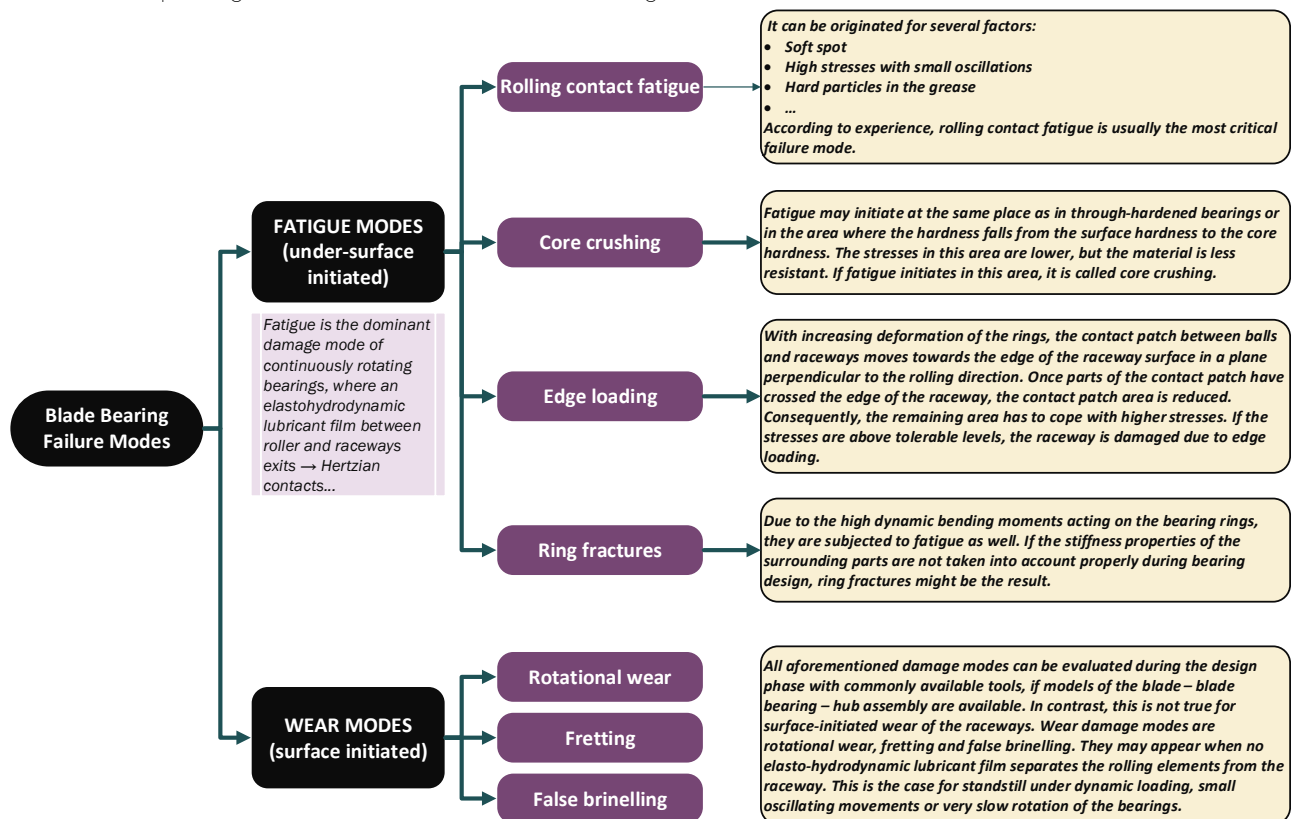
Figure 21: Typical failure modes of blade bearings

To the best of our knowledge, the typical failure modes of rolling bearing, in particular blade bearing, are summarised in Figure 21. In detecting the imminent failure, the focus has been made on the effects of the various failure modes that will potentially prohibit the bearing from functioning. Focus will be on ball spalling and cracks, and raceway spalling. These three failure effects all leave debris in the raceway hindering the balls movements and thus increases the friction in the bearing as the failure mode develops.

Debris is probably the best parameter to understand the health of the raceways of the blade bearings. Unfortunately, there is not a reliable and cost-effective way to monitor the debris in a grease environment due to the high viscosity of it. For example, for oil environments there are many solutions already validated in multiple sectors and many technological suppliers that provide very reliable sensors for this.

For bearings in continuous rotation, e.g. the main bearing in turbines, these failure modes are classically detected and monitored using vibration sensors where spalling/marks/indentation in either ball, the inner, or outer part of the raceway gives rise to distinct failure frequencies, that can be determined using e.g. envelope methods.

The blade bearing moves approximately a quarter of a full rotation, when going from blade feather towards production, and when in normal operation, only a partial amount of that motion is expected. The movement is furthermore slow, all of which make the periodicity that the classical approach builds on disappear.

3.2.3. Portability legacy of previous approaches for blade bearing

3.2.3.1. Portability legacy of rolling contact fatigue damage algorithm

Test bench related systems with algorithms implemented on them are perfectly portable, but they need to be supported and feeded with some specific sub-systems and requirements. In the case of Laulagun´s algorithms and their execution in test benches within the Romeo project, it has been learned that:

- Programming language: Robust and capable software has been used, Matlab 2016. Then, only this version or later version would be valid to update or improve them. An extra option would be to use only executable files from Matlab.
- Operating system: Windows 10 has been operating perfectly. Very reliable system.
- Memory requirements: When the algorithms are run, they start generating measured indicators that need to be treated continuously. Those indicators are being stored in the hard disc of the condition monitoring system, being treated before and avoiding an extra treatment with new data coming from the sensors. So, for this storage a good memory capacity is needed, in order to keep saving all those indicators during the test.
- Mathematical models: The developed algorithms are based in two different sources; signals from the sensors and FEM model of the bearing. So, to run the models, at least two sources need to be covered

and ensure that the system is feeded with a correct and reliable information. Using the methodologies based on simulated modelling of the component will allow the prediction of the expected probability of failure after a certain number of operating hours / cycles for the selected failure mode (Rolling contact fatigue RCF or Ring Structural Fatigue RSF).

- Sensors and Hardware for the acquisition: For rolling contact failure mode, most valid sensors are normally the inductive sensors, especially because of the easy installation and the relationship between the possible clearance generated in the raceway of the bearing and capacity of measuring that with this inductive sensor. Then, related to the hardware, normally digitalized cards are used, capable of acquiring and storing the data coming from the sensors.
- Wiring to avoid electrical noise: It is quite essential to use shielded cables for both, the instrumented signals and power supply cables. If possible, try to separate those cables from others integrated in the test bench or wind turbines that are for other purposes. Doing this properly would allow the system not to get false positives due to the possible electromagnetic noise.

3.2.3.2. Portability legacy of structural damage algorithm

The same portability legacy explained in the previous chapter could also be applied for this algorithm. In fact, both (RCF and SHM) have tested with the same equipment and in the same test bench by Laulagun, so the lessons learned are valid for both.

In this case, the difference is more related to the type of sensors and the protection to be used in this case, that are:

- Type of sensors: Strain gauges with a temperature compensation system. They could be auto-compensated or it could be generated by configuring the Wheatstone bridge of the strain gauge.
- Physical protection: Use the material suggested from the supplier (protective adhesives etc..) and apart from that, cover the gauge with a plastic box that allows the routing of the cables to the external circuit.

D2.4 - Portability of failure mode
detection/prognosis orientations
CO-Confidential

Visual example of a proper installation and wiring

Apart from those minor details, the rest of portability requirements are the same as in the previous point, as it has been stated before.

3.2.4. Common grounds on portability of failure models

The aim in porting blade bearing diagnosis algorithm to the direct drive turbines have been to test, whether the controller data, that can be gather from those turbines, can be exploited for blade bearing diagnostic purposes, when taking a statistical approach to the data. This approach is advantageous to installing new sensors on the turbine, as it adds no additional cost, and allows utilization on existing turbines, assuming the same data is generated.

The statistical approach however is limited by the fact that there is only one case of a turbine having its blade bearing replaced, where controller data have been recovered to a reasonable extent from before and after the replacement. This turbine will be denoted turbine R. In addition, the methods have been tested on two turbines, where a blade bearing have started to degrade. Since the degradation evolves very slowly these bearings could be operated for years before any impact on performance can be seen. These turbines will be denoted DA and DB, respectively. Some methods have also been tested against data from turbines with where all blade bearings are healthy, these will be denoted HA, HB, HC, and so forth.

The number of cases with blade bearing degradation, that any statistical analysis can be based on is very limited. This also greatly affect the possibility to apply various advanced machine learning

D2.4 - Portability of failure mode
detection/prognosis orientations
CO-Confidential

techniques, as the advantageous aspect of these methods often is that they can handle many more variables at one time, than is possible for humans, but having very few cases and introducing many variables makes such methods very prone to overfitting.

3.2.5. Pitch trace smoothness monitoring

3.2.5.1. Description

The idea underlaying monitoring the smoothness of a pitch traces is that when debris from spalling on either raceways or balls is present, it will eventually reduce the free movement of the blade bearing, and we will leave the ideal situation with only rolling friction and introduce both a static and dynamic friction, that will increase with an increasing amount of debris. Following this idea, the hydraulic force will then need to overcome the static friction from standstill situations. This would result in prolonged periods of no movement followed by a sudden movement. Thus, the pitch trace will be less smooth. In Figure 22 the proposed effect is magnified on artificial signals to the extent, where it is visually detectable. The artificial signals represent time traces of a pitch position signal. The signals labelled "bad" experience a jumpier movement, which according to the assumptions would be due to increased friction. To quantify this lack of smoothness the distributions of movements during different lag times (that is the resulting movement during intervals of different duration) is studied.

The general level of friction in a blade bearing is set by the viscosity of the bearing grease, which in its own turn is influenced by the temperature of the grease. This will mask the frictional effect of the spalling debris and will make the friction experienced by the blade bearing dynamically changing depending on the environment temperature introducing potentially daily and seasonal effect, but also largely influenced from the operational mode and its short time history.

It is also noticed that the sealing system could provide a difference on the Friction Torque, but the effect could decrease with wear suffered from the seal itself due to the rotating cycles or pitching of the blade.

D2.4 - Portability of failure mode
detection/prognosis orientations
CO-Confidential
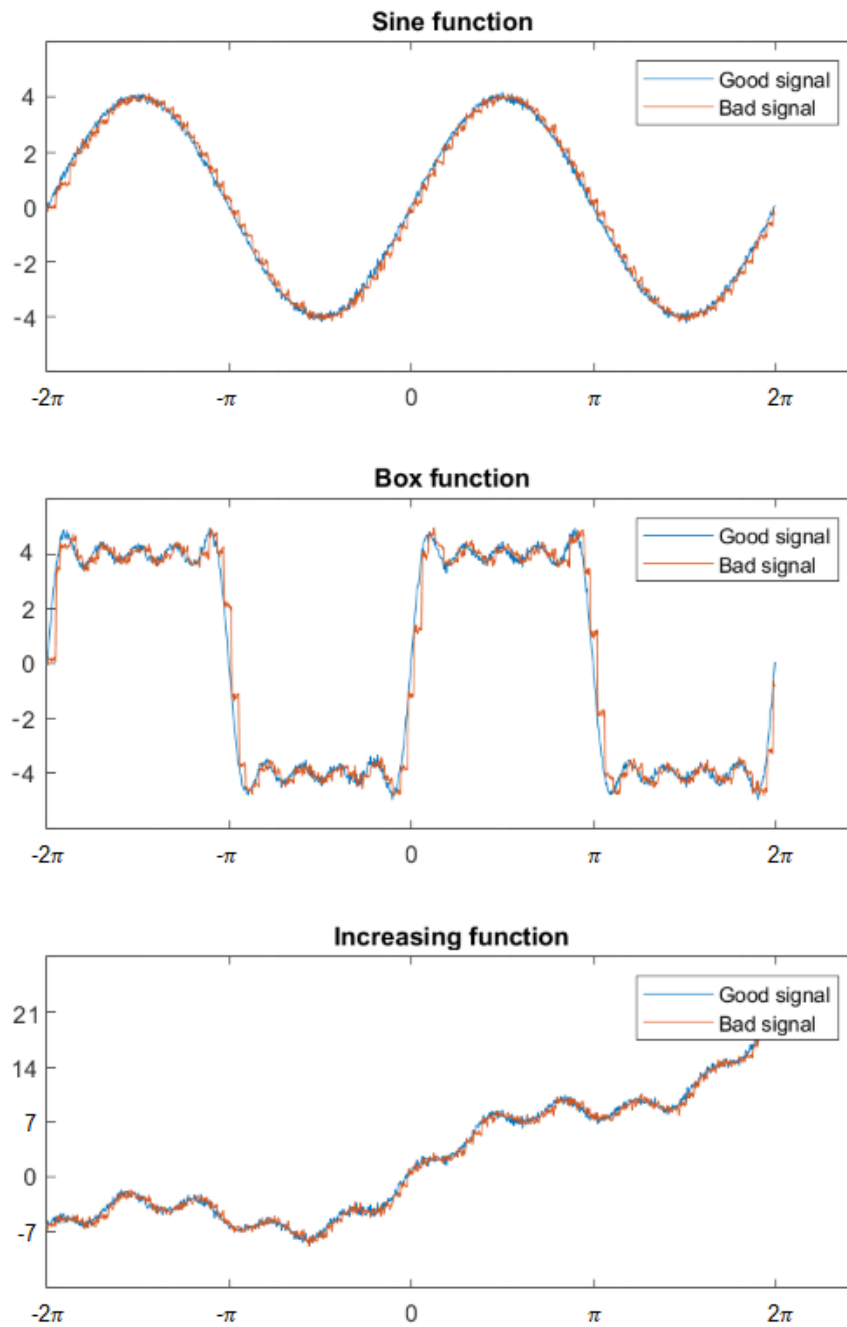
Figure 22: Visual examples of non-smooth signals

3.2.5.2. Inputs

The variables used for this analysis is primarily the piston or pitch position. In addition to this, the hub and environment temperatures together with the power produced and start and stop signals. The data comes from the turbine controller.

D2.4 - Portability of failure mode
detection/prognosis orientations
CO-Confidential

3.2.5.3. Calculations

To assess the effect that can be expected when a blade bearing degrades, we apply the method on turbine R, which had one of its blade bearings replaced due to a broken ball. The broken ball caused metal particles to appear in the grease. The displacements within different time lags are determined by taking the difference of a trace with itself temporally displaced. In **Figure 23** the displacement histograms and their evolution when the time lag is increased are displayed. The top row of plots shows three cases of a pitch to stop, two from before the damaged blade bearing was replaced (subfigure A and B) and one after the replacement (subfigure C). The bottom row similarly shows histograms from three pitch from stop to operation traces. Again, the two first ones from before the damaged blade bearing is replaced (subfigure E and F) and the last from after replacement (subfigure G).
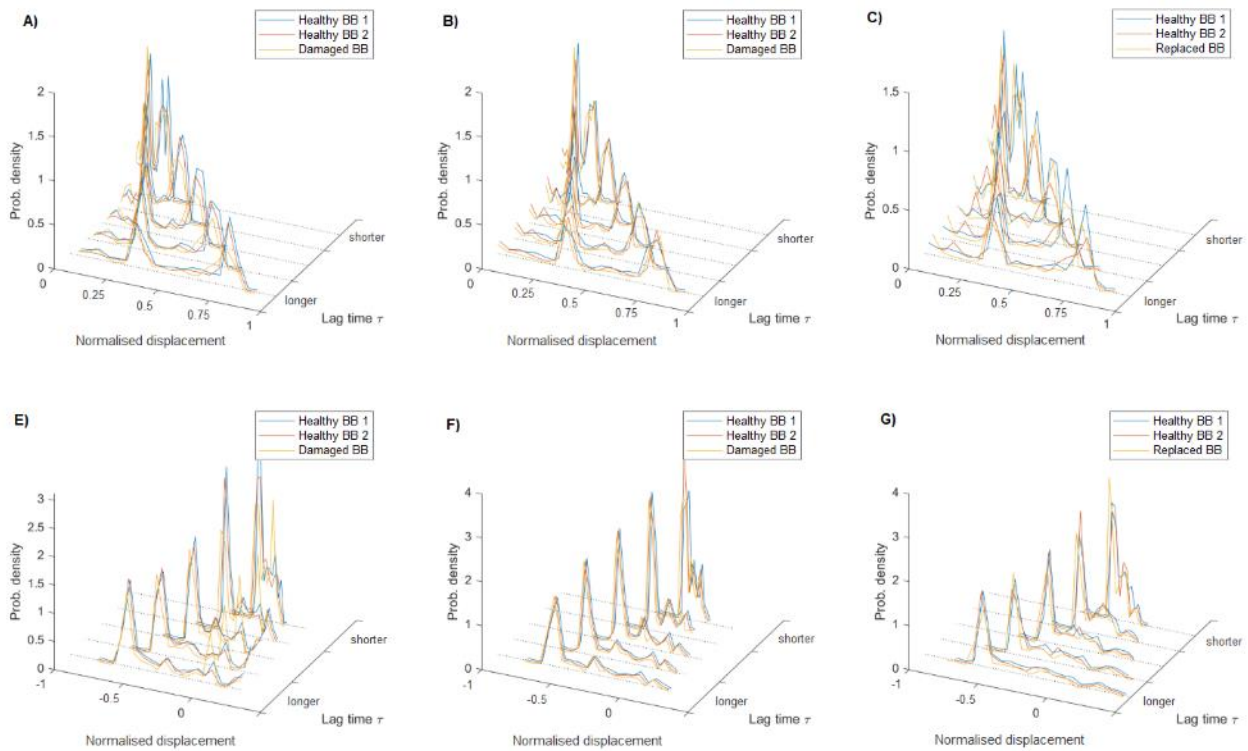
Figure 23: Displacement histograms

3.2.5.4. Parameters

Lag time, the time interval across which the movement is calculated.
Operation mode, determines whether data should be taken from traces, where the blade is being pitched to stop, when the turbine resumes operation (blade is pitched from stop to production) or when the turbine is producing, and active pitching is not needed.

3.2.6. Rate monitoring of minimal changes in blade bearing data

3.2.6.1. Description

As a blade bearing degrades it at some point starts behaving differently form the other two blade bearings installed in the turbine. The idea in the method "Rate monitoring of minimal changes in blade bearing data" is to keep a count on every time a certain variable changes its value by a minimum amount. Then the difference in behaviour of the blade bearings is detected by checking if the count for one blade bearing is repeatedly significantly higher than the count on the other two blade bearings installed on a turbine.
In turbine operation the pitch positions are optimized continuously to maximize AEP and because the blade bearings are moved by individual hydraulic systems, there is a natural variation in the exact movement of the bearing and thus a natural variation in when a variable value changes, which may mask the effect that this method proposes.

3.2.6.2. Inputs

The variables used for this analysis is primarily the piston position.

3.2.6.3. Calculations

A time duration is chosen, and the number of minimal changes recorded per interval is counted for each of the bearings, for each interval the median number of samples are determined and the evolution in the number of samples relative the median is then studied. **Figure 24** and **Figure 25** illustrate the analysis for two cases of blade bearings, that have begun to show signs of degradation, from turbine DA and DB, respectively.

D2.4 - Portability of failure mode
detection/prognosis orientations
CO-Confidential
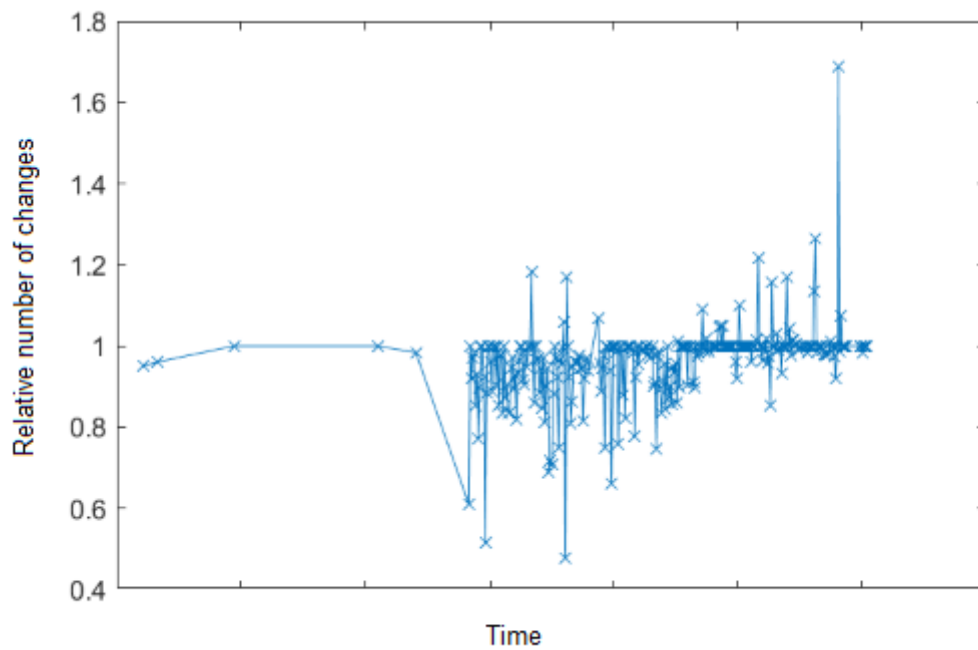
Figure 24: Evolution in number of changes
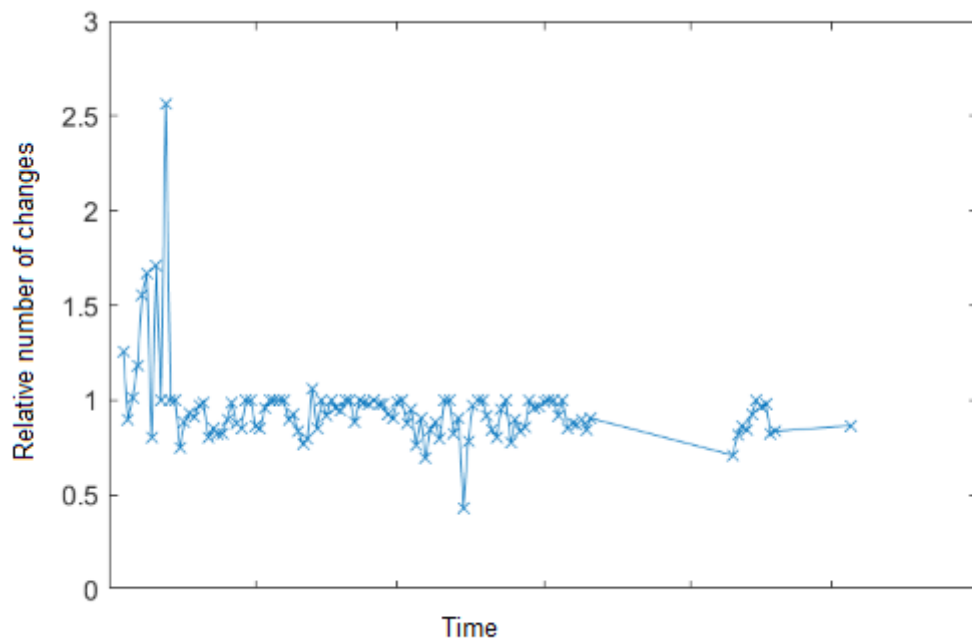
Figure 25: Evolution in number of changes

3.2.6.4. Parameters

Duration for the rate to be estimate across and which pitch system variable to used.

3.2.7. Excess piston extension monitoring

3.2.7.1. Description

The pitch position of each of the three blades of a turbine are moved by each their pistons with the hydraulic forced provided from their accumulators. A pitch reference is continuously updated for the blades and a feedback loop minimizes the difference with the actual pitch position of the blade. During turbine operation the pitch references for all blades sometimes happen to be identical for extended periods. During these periods the individual movement of the blades and the common reference gives a situation where ideally the pitch positions should be identical, but due to differences in the piston-accumulator systems and the loads on the blades and by that also the moments affecting the blade bearings, the pitch positions are in fact not identical. Among the loads are the friction in the blade bearing, and for the method of monitoring the excess piston extension it is assumed, that a damaged blade bearing will experience an excess amount of friction. Other loads will affect all three blades in a random or periodic manner, but with a statistical approach to data, this will just add some variation.

Taking a purely statistical approach to the blade bearing data and studying the correlations among the variables associated to the blade bearing it have been noticed, that the correlations among the piston positions might be different for blade bearing that experience some amount of degradation. Particularly comparing the difference of the piston position for a healthy blade bearing and a blade bearing known to show signs of degradation versus the difference between two healthy blade bearings, the damaged blade bearing can be identified by an offset that grows with the absolute extension of the piston.

3.2.7.2. Inputs

The variables used for this analysis is primarily the piston positions. In addition to this, various variables to filter data. The variable data comes from the turbine controller.

3.2.7.3. Calculations

To get an overview of how the pistons of two blade bearings differ from each other in regard to their extension, we focus first on the turbine R, where a blade bearing has been exchanged due to a damage. We construct the scatter plot of the piston extension difference versus the extension of one of the pistons. **Figure 26** displays data from two different periods before the damaged blade bearing was replaced and **Figure 27** displays data from a period after the blade bearing was replaced. In **Figure 26** the subplots A and B shows data from one period, while C and D shows data from a later period. A and C display the difference between two healthy bearings and B and D shows the difference between one of the healthy bearings and the bearing later to be replaced. In **Figure 27** the situation during a period after the replacement is shown. Here A display the difference between the two remaining (healthy) bearings, while B displays the difference between the new (healthy) bearing and one of the "old" bearings.
From the figures it can be seen, that the piston moving the damaged blade bearing shows a tendency to extend further then the pistons moving the healthy blade bearings. This tendency disappears when the damaged blade bearing is replaced. The tendency is to a very good approximation linear and can thus be characterised by its slope. **Figure 28** shows how the slope of these piston position difference scatters evolved in time from before the damage was detected to after replacement. In the figure a full

line indicates when the blade bearing was replaced, and a stippled line indicates when the damage was first discovered
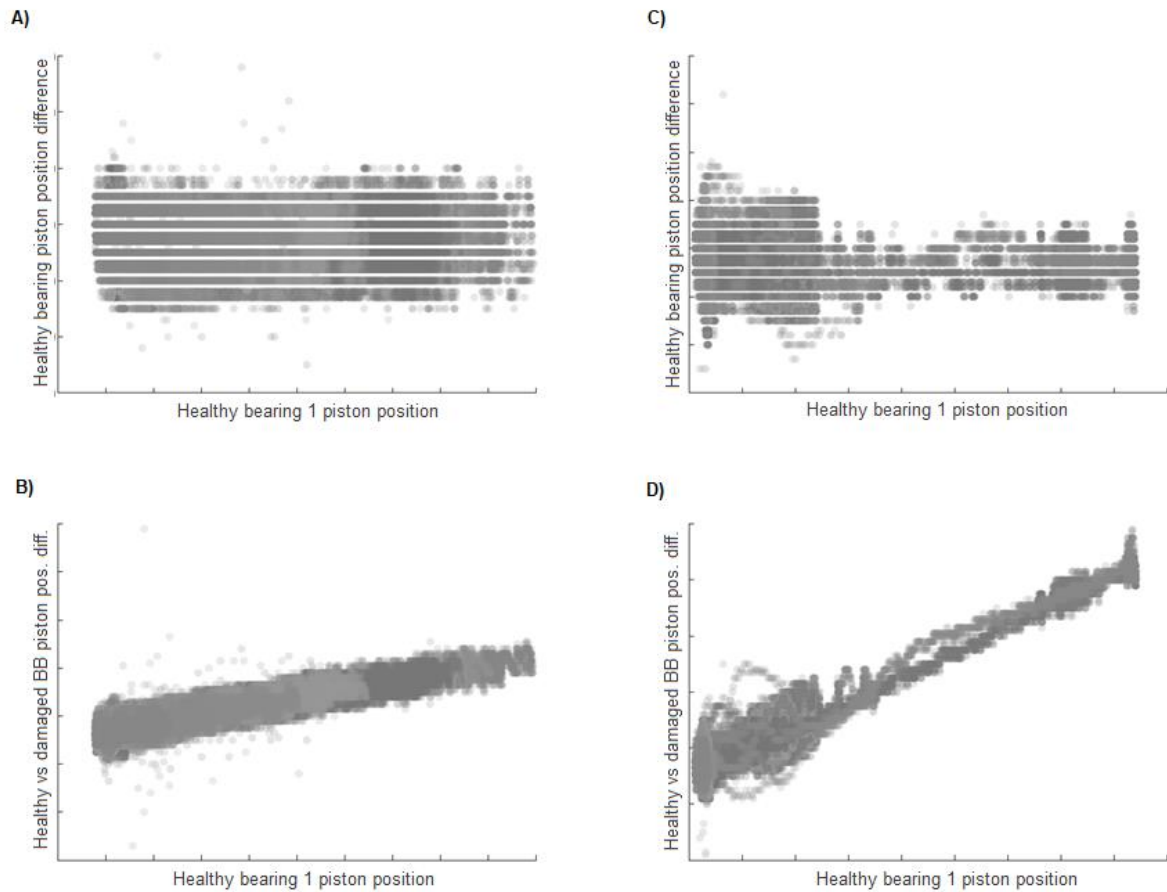
Figure 26: Piston scatters before replacement
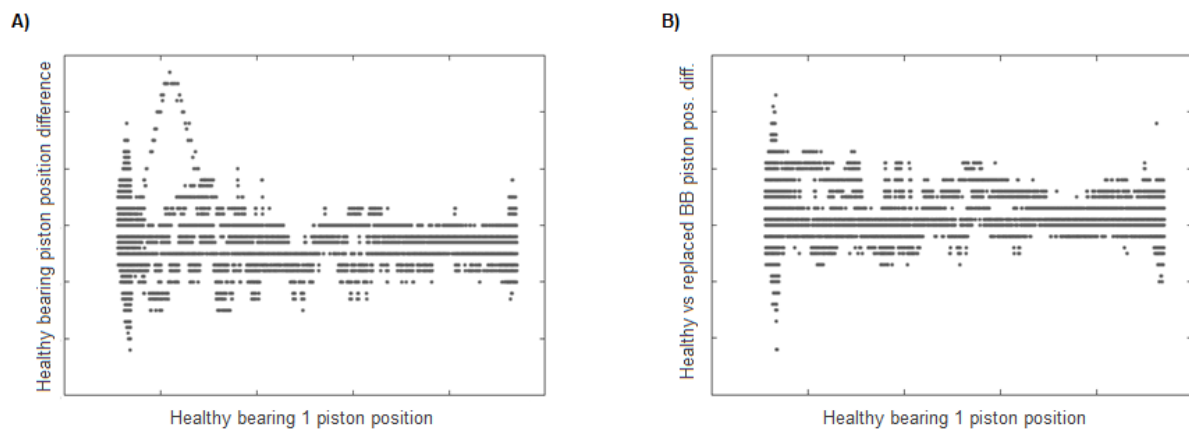
Figure 27: Piston scatters after replacement

D2.4 - Portability of failure mode
detection/prognosis orientations
CO-Confidential
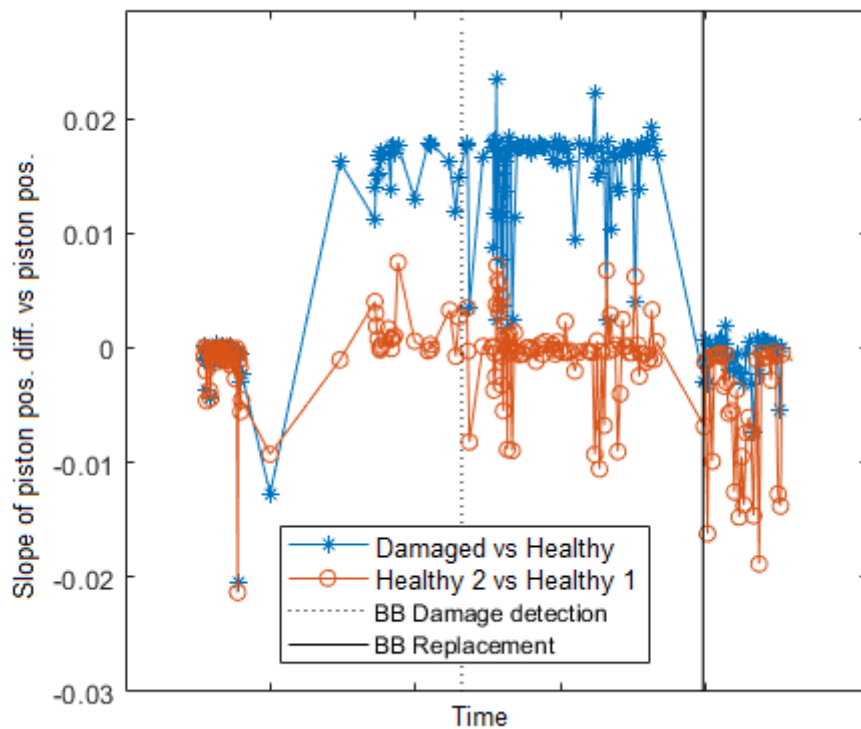
Figure 28: Time evolution of slopes of scatters

The analysis has also been performed on turbine DA and DB, which are both known to operate with a degraded blade bearing and several turbines which have shown no signs of degradation. To get a symmetrical view of the state of the blade bearings they have been compared pairwise, so that each blade is compared to the two others. For each turbine we thus get three-time evolution trends for the slopes. In **Figure 29** the time evolution of the slopes of the piston extension difference vs piston extension is shown for six case turbines, as examples of the analysis. The six cases shown are the turbine DA (in the bottom of the figure) and five of its neighbouring turbines, HA, HB, …, HE above. HA, HB, …, HE are all known to have healthy bearings. Turbine DA shows a tendency for excess piston extension like the one depicted in **Figure 28** for the turbine R, which had a blade bearing replaced, but for the healthy turbines some shows this shows this tendency (e.g. turbine HA and HE), while the others do not or do in a smaller degree. The situation is similar for turbine DB which shows the same tendency for excess piston extension, but to a lesser degree, also less than its two closest neighbour turbines.

D2.4 - Portability of failure mode
detection/prognosis orientations
CO-Confidential
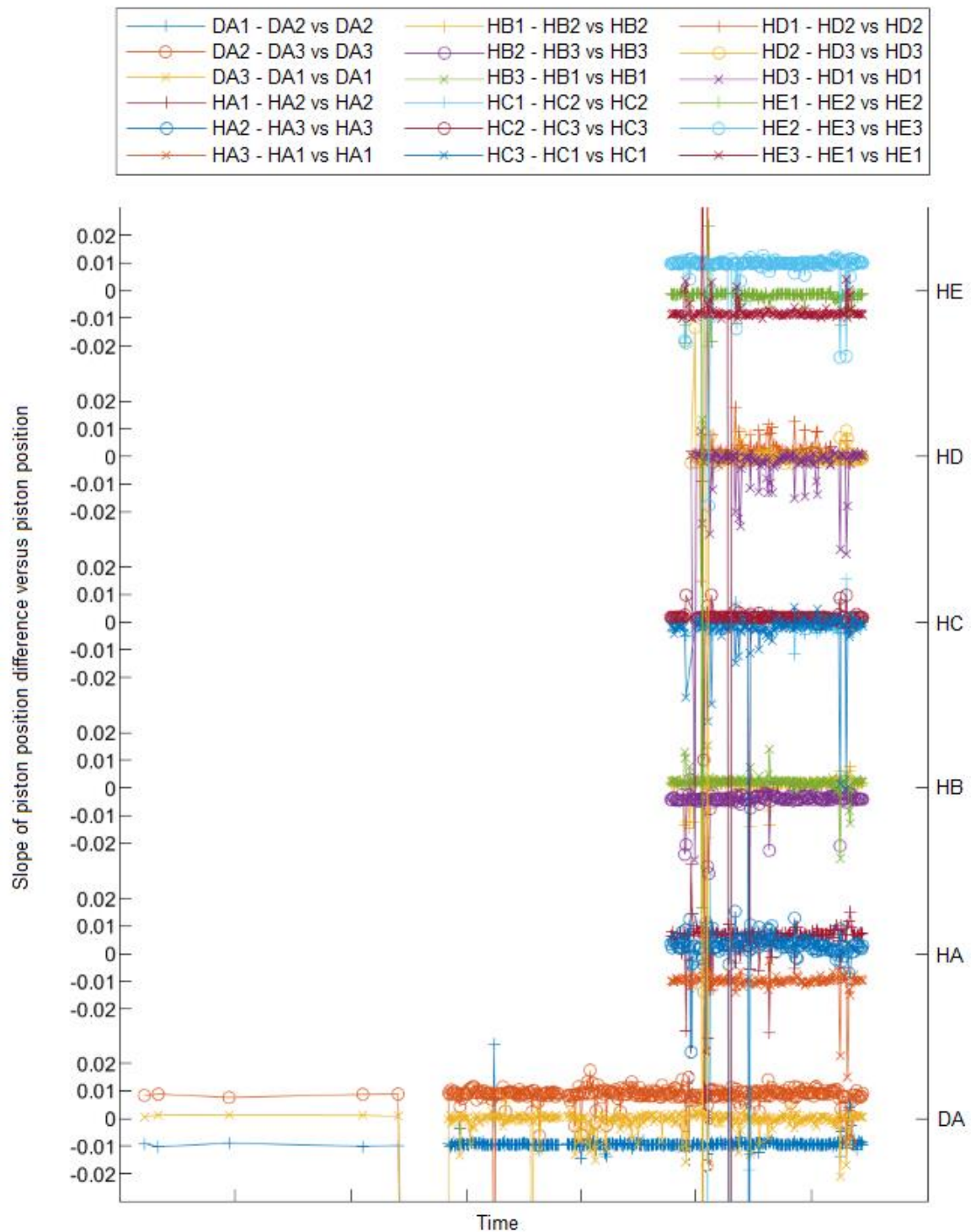
Figure 29: Time evolution of slopes for more turbines

D2.4 - Portability of failure mode
detection/prognosis orientations
CO-Confidential

3.2.8. Delayed and instant tracking error distribution monitoring

3.2.8.1. Description

When a pitch reference is set for a blade, it will naturally take some time before the pitch position reaches this reference. The idea behind this method is again, that as a blade bearing degrades it will react slower due to increased friction, the pitch position will therefore lack further behind the pitch reference compared to a healthy blade bearing. Thus, this method focuses on the difference between the pitch reference and the pitch position. The time/delay from a reference value is set before the pitch position reaches it is dynamically changing depending on operating conditions as well as the condition of the hydraulic system and the blade bearing. It is this delay between a reference is set and it is reached, which is directly interesting to study. Unfortunately, it cannot be determined directly and estimating it introduces other uncertainties. Section 3.2.8.3 will focus on this. Instead this section will focus on a simple and easy to calculate proxy, the tracking error, which is defined as the numerical difference between the reference and the position. Two different kinds of tracking error will be studied, an instant tracking error and a delayed tracking error. The instant tracking error we define as the instantaneous difference between the position and the reference. The instant tracking error can be argued to be unphysical, as the system have had no time to adjust to any new reference. For this reason, a delayed tracking error is also studied, defined as the difference of the pitch position and the reference, that had been set a fixed time offset prior to the position being recorded. As this time offset/delay is fixed, the delayed tracking error is like the instant tracking error in some sense artificial, but both will serve as proxies for the time delay.

To investigate how the state of a degrading blade bearings will manifest itself in the tracking error data a statistical approach is taken, and the distributions of tracking errors are investigated. In doing so the data is filtered after various operating and environmental conditions.

3.2.8.2. Inputs

Pitch position, pitch reference, tracking error and various signals that indicate the operation mode of the turbine together with environmental signals as wind speeds.

3.2.8.3. Calculations

To compare the tracking errors of healthy and damaged blade bearings, histograms of tracking errors are constructed. In order to do this, we first investigate how long time is needed to sample a histogram, such that the histogram is relatively stable. Knowing this period, we first construct histograms for the delayed tracking error for a relative wide range of operating conditions. In **Figure 30** examples are shown for turbine R, which had a damaged blade bearing replaced. The figure shows histograms of delayed tracking error for all three blade bearings from two periods before the damaged bearing was exchange (subfigure A and B) and a period after the bearing was replaced (subfigure C). The histograms are shown both on a linear scale, where the normal events can clearly to distinguished and on a logarithmic scale, where the rare events in the tails of the histograms can be studied. The histograms are shown on linear scale on the subfigures labelled 1 and on logarithmic scale on the subfigures labelled 2. The damage

D2.4 - Portability of failure mode
detection/prognosis orientations
CO-Confidential

bearing clearly distinguish itself for the normal events where it has its main mass shifted compared to the two healthy bearings. After the replacement, though, the new blade bearing does still not behave as the two old ones. This could be interpreted as an indication that this effect stems not from the blade bearing, but from some other artefact in the pitch system. Focusing instead on the tails of the distributions, visible on logarithmic scale, from before replacement (subfigure A2 and B2) one could get the impression, that the damaged blade bearing can be distinguished by having less probability mass in the left tail. This is counter intuitive, since this means the pitch position of a damaged bearing is less likely to lack severely behind the pitch reference compared to healthy bearings. Checking against e.g. the blade bearing on turbine DA known to be in a degraded state, these observations can't be confirmed either, as can be seen in **Figure 31**, that shows both the histogram on a linear scale to the left and on a logarithmic scale to the right.
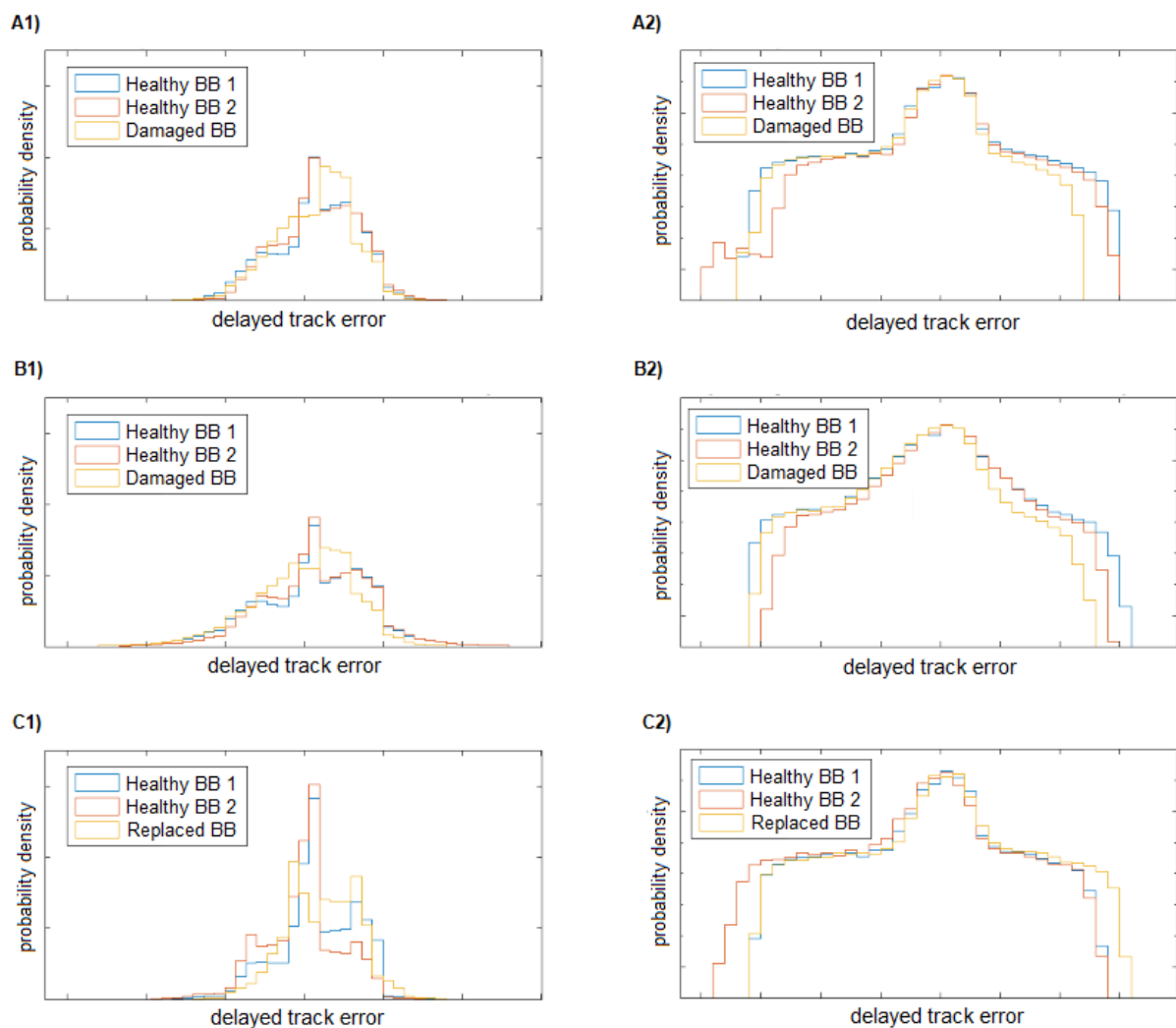
Figure 30: Histograms of delayed tracking error before and after replacement

D2.4 - Portability of failure mode
detection/prognosis orientations
CO-Confidential
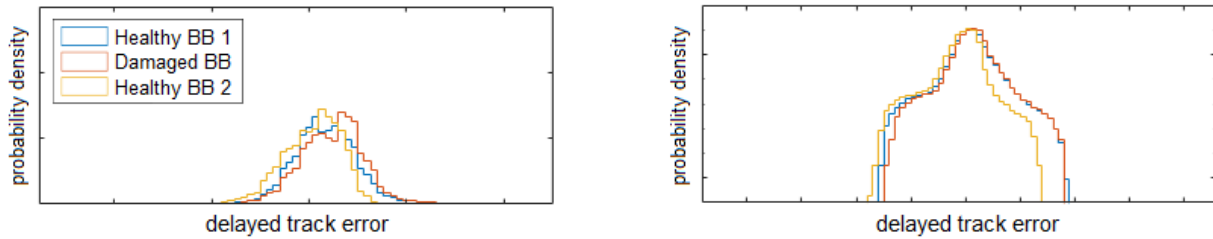
Figure 31: Histograms of delayed tracking error

Narrowing the range of operating conditions for which data is included, **Figure 32** shows an example where data for the histograms before and after the damaged blade bearing is exchanged is collected, when turbine R is operating in so strong winds, that it is actively pitch adapting to the wind. In this case we focus on the instant tracking error and from the distributions the damaged bearing does not distinguish itself in any significant way from the healthy bearings. In the figure panel A shows distributions for each blade bearing from a period before the damaged bearing was replaced and panel B shows them for a period after the replacement.
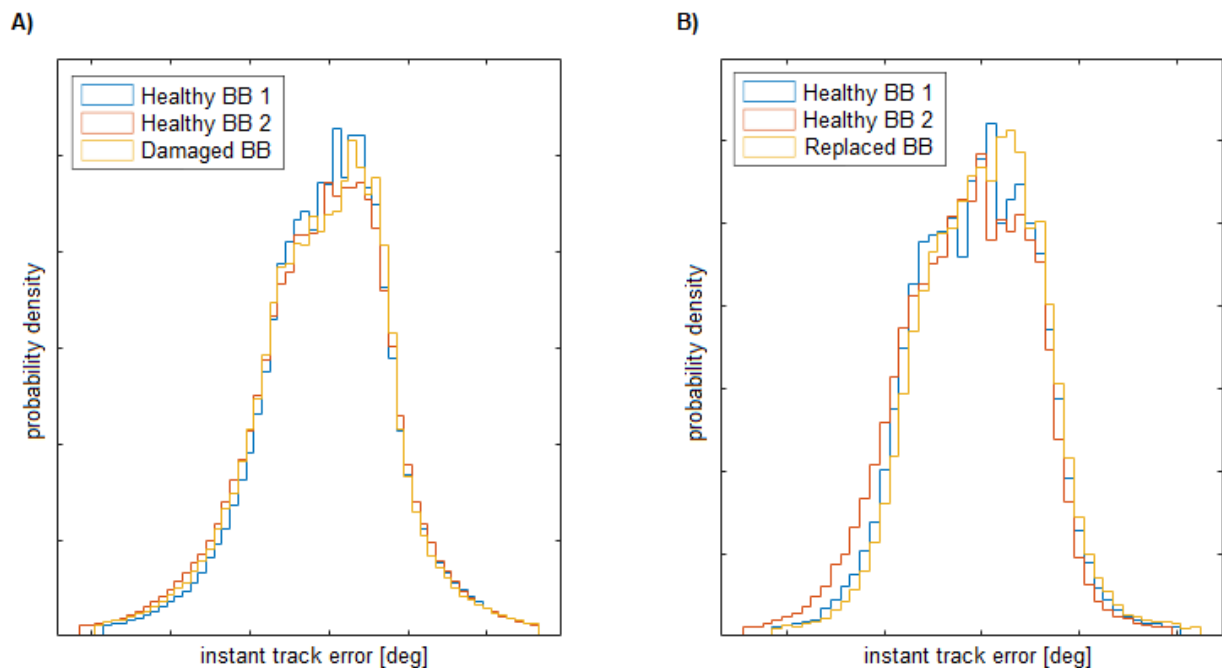
Figure 32: Histograms of instant tracking error

To facilitate an overview of how the distribution changes in time for the bearings in some of the turbines operating with a damaged bearing an in-house data browsing app have been built. This allows to accumulate the distribution over various time intervals, apply different filters and compare both the turbines known to operate with a degraded blade bearing and turbines, where there is no indication of any damages. The data browsing app comes in two modes, one displaying the time evolution of histograms in waterfall mode and the other in a heat map mode, screenshots are shown in **Figure 33** and **Figure 34**, respectively.

D2.4 - Portability of failure mode
detection/prognosis orientations
CO-Confidential
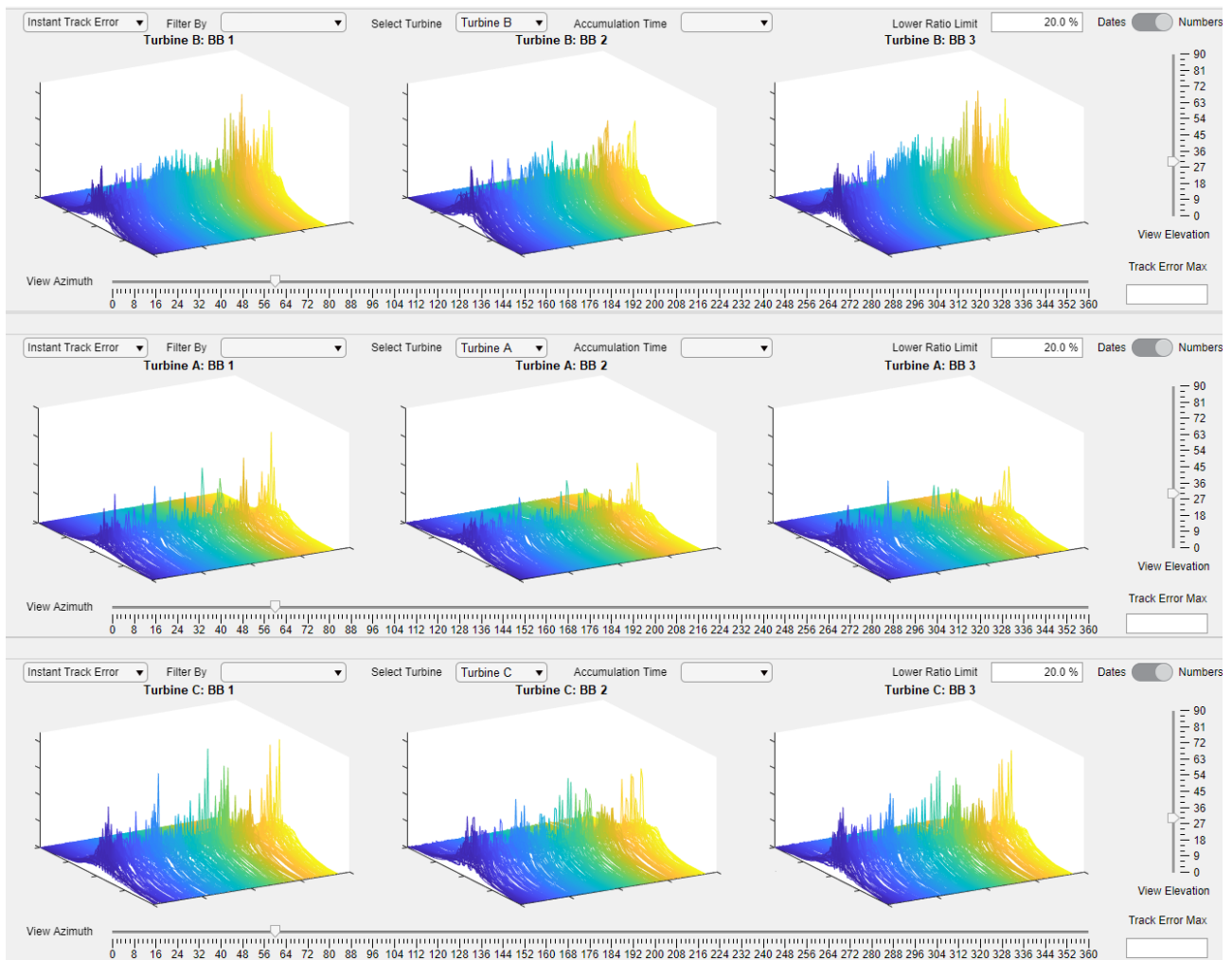
Figure 33: Screenshot from tracking error data browsing app

D2.4 - Portability of failure mode
detection/prognosis orientations
CO-Confidential
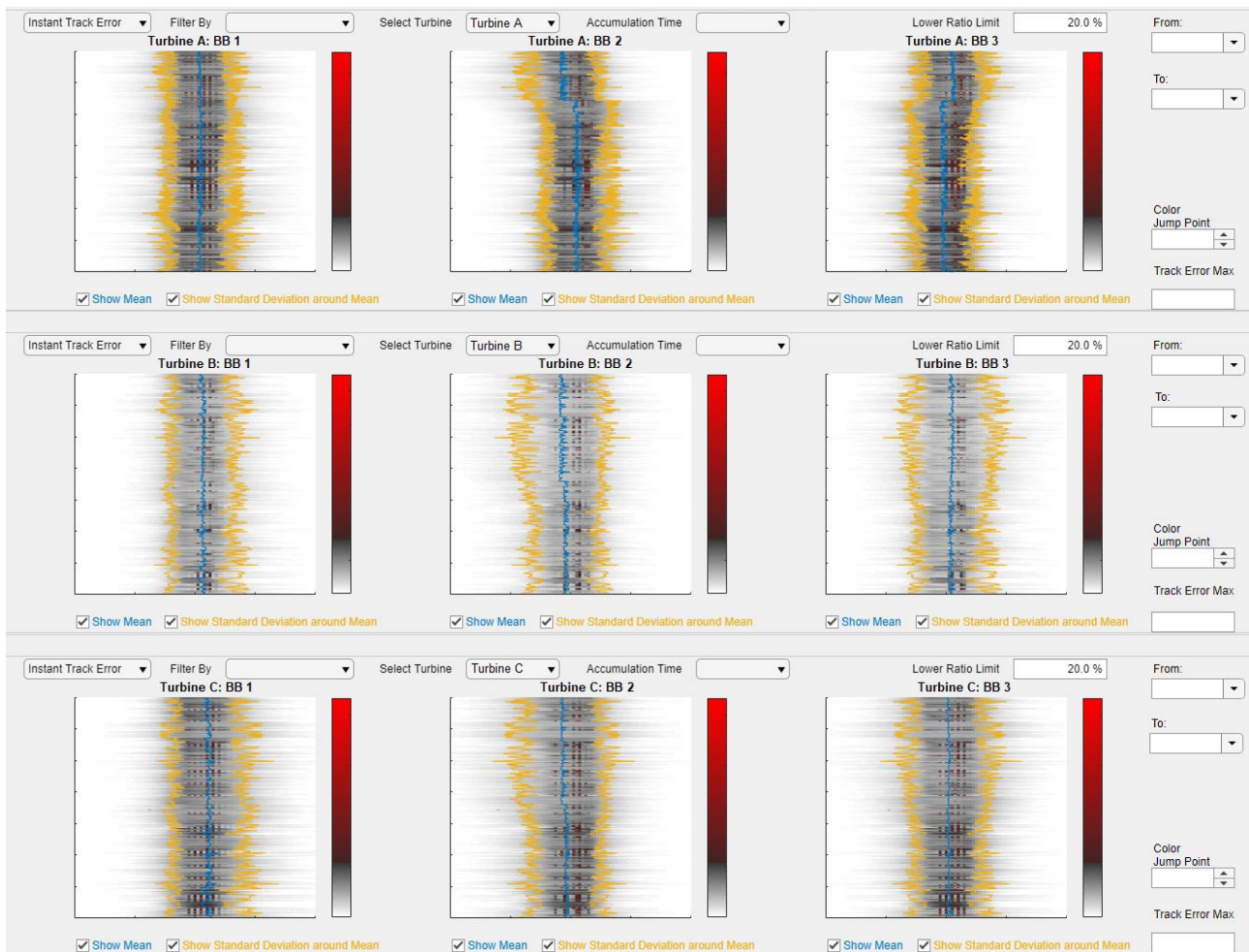
Figure 34: Screenshot from tracking error data browsing app

To move beyond the side by side comparison of the tracking error distributions for the blade bearings we move to density scatters. Here **Figure 35** displays an example of the joint distribution of the instant track error for the blade bearings for turbine DA known to operate with a damaged bearing. In three sets of panels the pairwise marginals of the joint distribution are shown. The panels on the left shows the marginals on a logarithmic scaled heatmap and the panels on the right shows them on a linear scale. As a guide for the eye, the ideal symmetry axis is plotted on top of the heat map. As an alternative to looking at the three pairwise joint distributions we can visualize the joint distribution for the tracking errors for all 3 blades by projecting it onto the 1,1,1-plane (that is the plane in 3D perpendicular to the ideal symmetry axis). This is done in **Figure 36**, still using the data from turbine DA, where the projection of the 3D tracking error axes for each of the blade bearings are also drawn on top of the heatmap as guides to the eye. For **Figure 36** the panel to the left is again a logarithmic scaled heatmap and on the panel to the right the projection is shown on a linear scaled heatmap.

As was the case when just looking at different time instances of the histograms, as exemplified with **Figure 30** and **Figure 31**, it is possible to hypothesise various features that would distinguish the bearing that is degrading in **Figure 35** and **Figure 36**, but comparing with the turbine R or DB or turbines operating with only healthy blade bearings, these hypothesis will not be confirmed. Here the limited number of cases of degraded blade bearings greatly influences the ability to reach general conclusion.

D2.4 - Portability of failure mode
detection/prognosis orientations
CO-Confidential
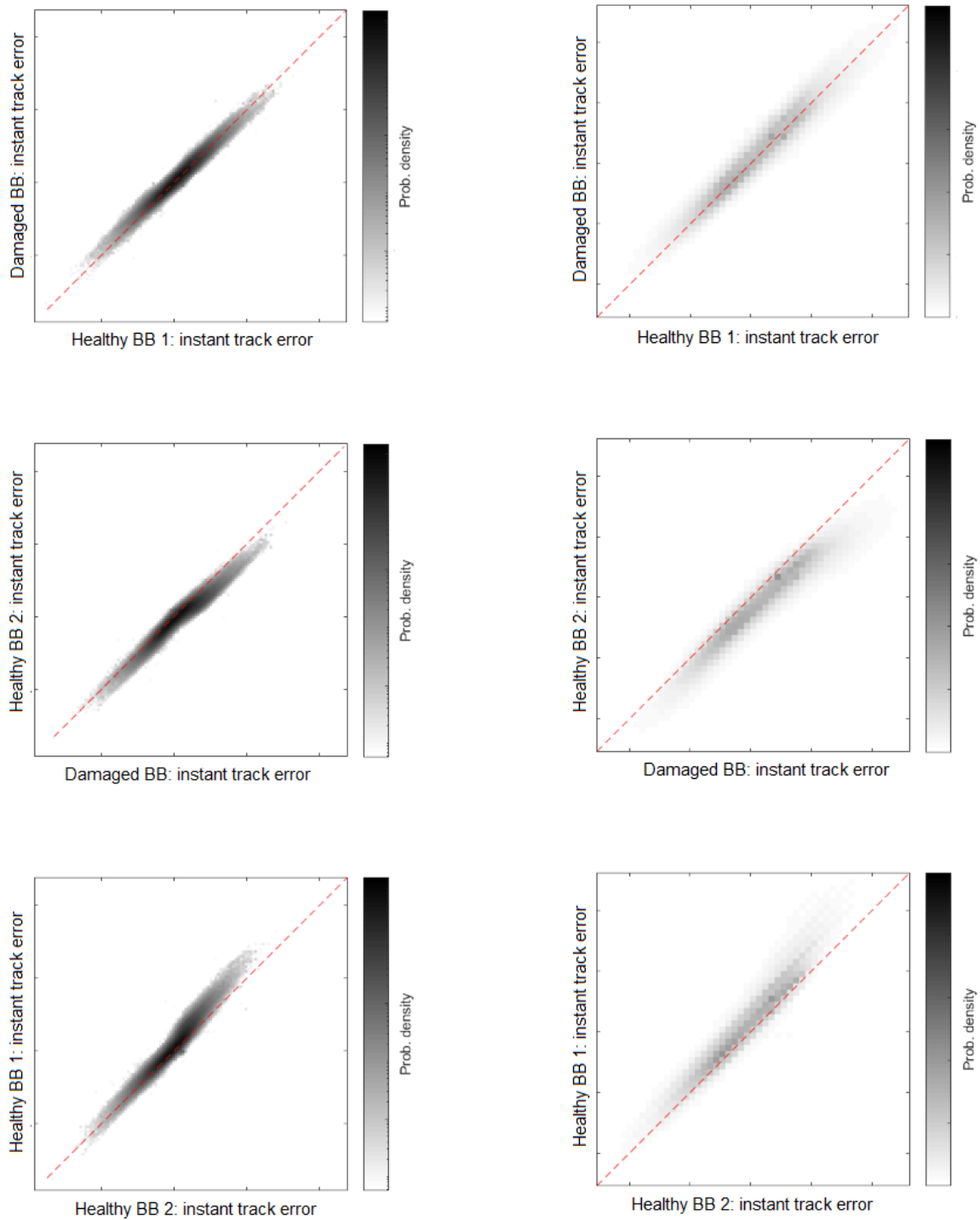
Figure 35: Pairwise marginals of the joint distribution of tracking errors

D2.4 - Portability of failure mode
detection/prognosis orientations
CO-Confidential
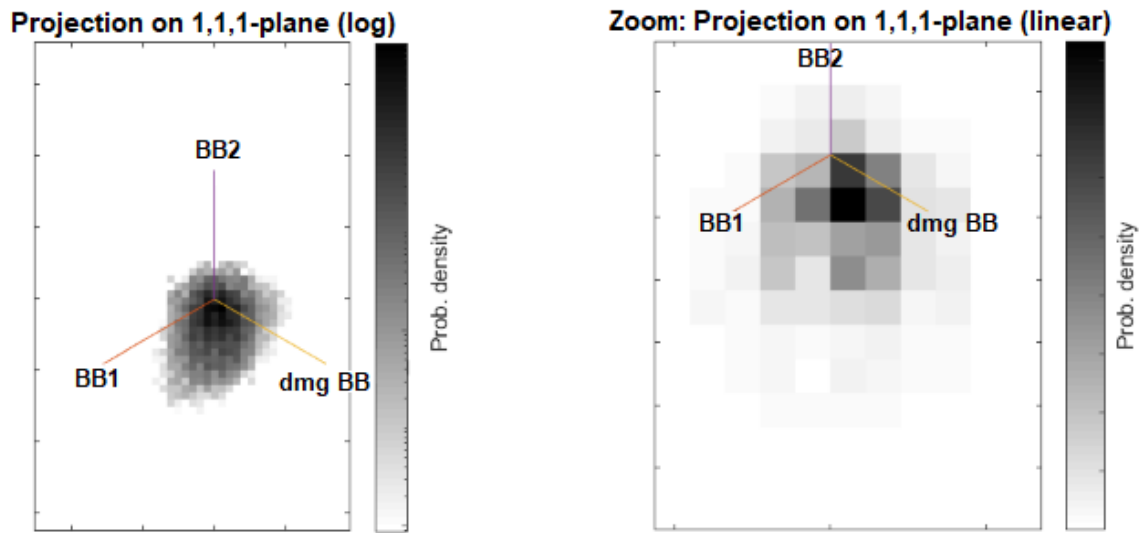
Figure 36: Joint distribution of instant tracking errors projected on the 1,1,1-plane

3.2.9. Pitch tracking delay distribution monitoring

3.2.9.1. Description

As described in the previous section, the focus in the pitch tracking delay distribution monitoring approach will be to estimate the time delay from a pitch reference is set before the position is obtained. This is done under the assumption that as a blade bearing is damaged and degrades, debris will increase the friction in the blade bearing and lead to a damaged blade bearing lagging behind compared to a healthy blade bearing. The distribution of these delays is compared for blade bearings that are known to be damaged or healthy. These delays will be denoted tracking delays.

Beside depending on the state of the pitch system including here the state of the blade bearing and the amount of friction a given damage cause, then the delay from a reference is set before the pitch position reach this value also simply depends on how far the current reference is from the current position and accordingly how fast the reference is changed.

3.2.9.2. Inputs

Pitch position, pitch reference and various signals that indicate the operation mode of the turbine together with environmental signals such as wind speeds.

3.2.9.3. Calculations

In order to estimate the tracking delay a time window of the pitch position trace and the pitch reference trace is needed. The time window of the reference is then temporally displaced until the overlap of the

D2.4 - Portability of failure mode
detection/prognosis orientations
CO-Confidential

two traces are minimal, this is then considered the delay for the last instant in the time window of the position trace. **Figure 37** depicts the principle. The left panel show a small window of the pitch position trace (in black) together with several pitch reference traces delayed by different amounts (coloured). The right plot shows the discrepancy between the position and the delayed reference calculated by a cost function. The minimum is marked by a red circle.
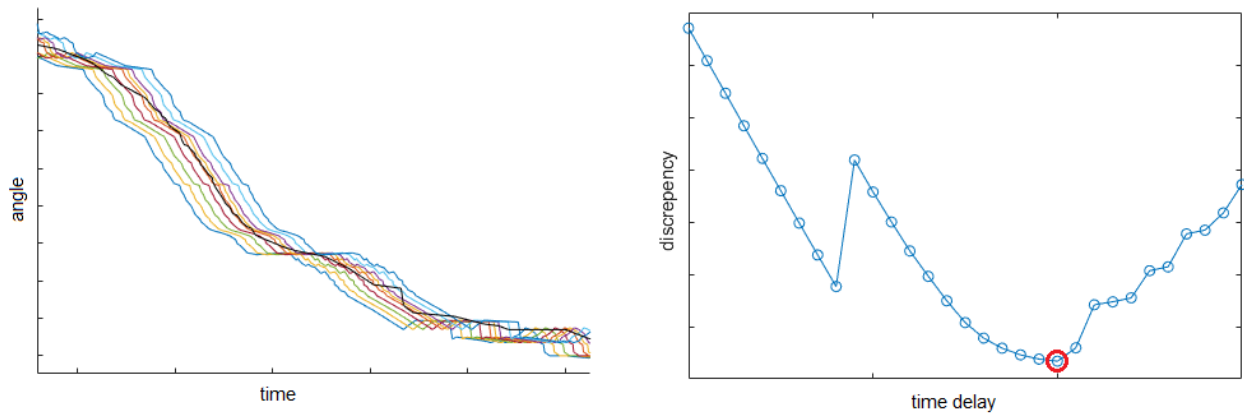
Figure 37: Principle of the tracking delay estimation technique

The tracking delays have been estimated for turbine R and DA and several turbines with healthy blade bearings. In **Figure 38** the histograms of tracking delay constructed for a period of operation before replacement (the panels A) and for a period of operation after replacement (panels B) for turbine R is shown as an example. The subfigures 1 shows the histograms on linear scale and the subfigures 2 show them on a logarithmic scale. Like the situation when analysing the tracking errors in the previous section, different hypotheses can be formed when looking at the single distributions in **Figure 38**, but when checked against the tracking delay distributions for the other turbines, it have not been possible to confirm any.

D2.4 - Portability of failure mode
detection/prognosis orientations
CO-Confidential

A1)

A2)

B1)

B2)
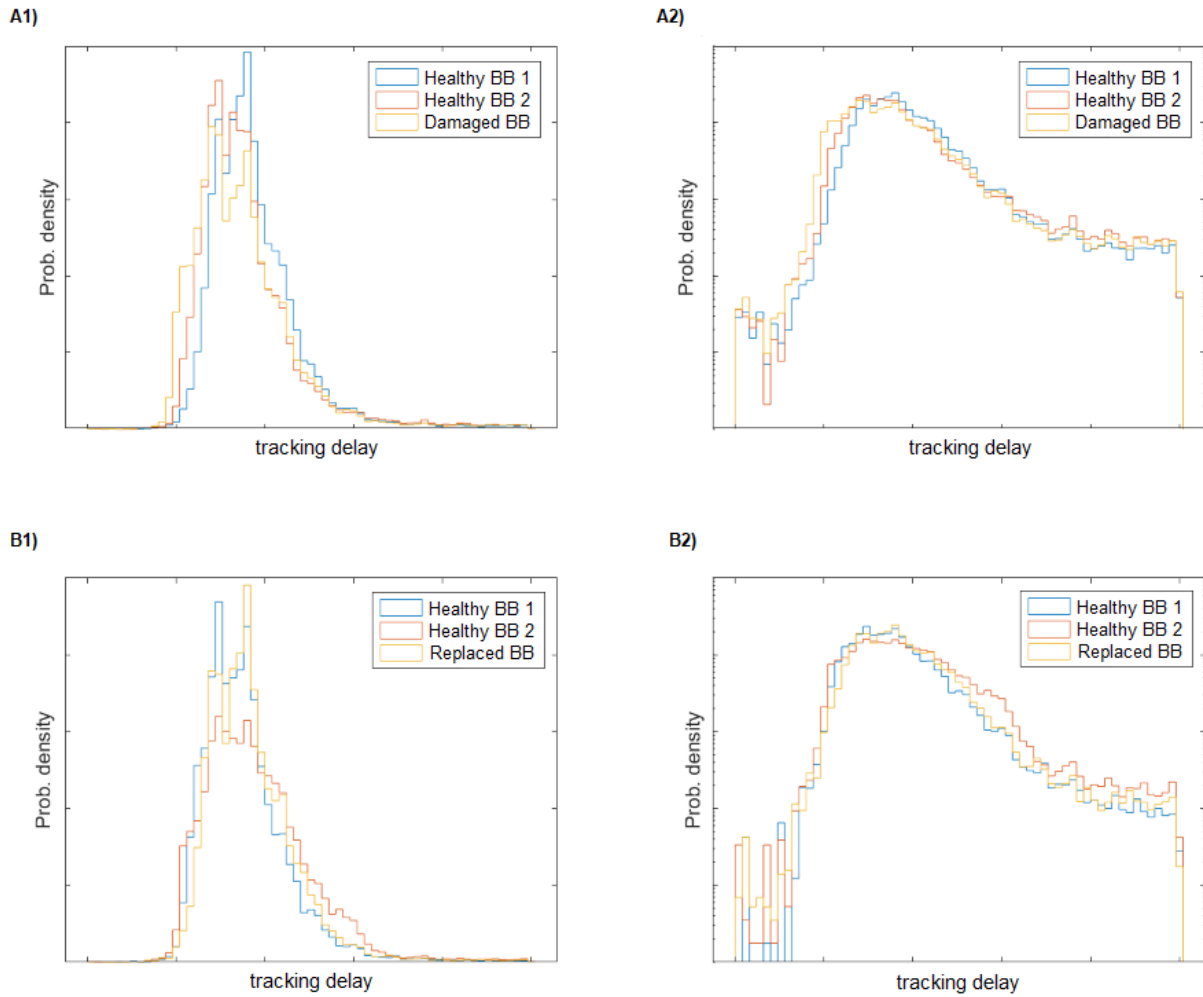
Figure 38: Histograms of tracking delays

Like for the tracking error analysis in the previous section, it is also possible to study the joint distribution of tracking delays for all three blades of a turbine instead of the single blade distributions. In **Figure 39** the pairwise marginals of the joint histogram constructed from the same data as in **Figure 38** are shown. The marginals are depicted in subfigure A, B and C represent the joint histogram before turbine R had the damaged bearing replaced and D, E and F depict the marginal from after replacement. The heatmaps are all on a linear scale.

D2.4 - Portability of failure mode
detection/prognosis orientations
CO-Confidential
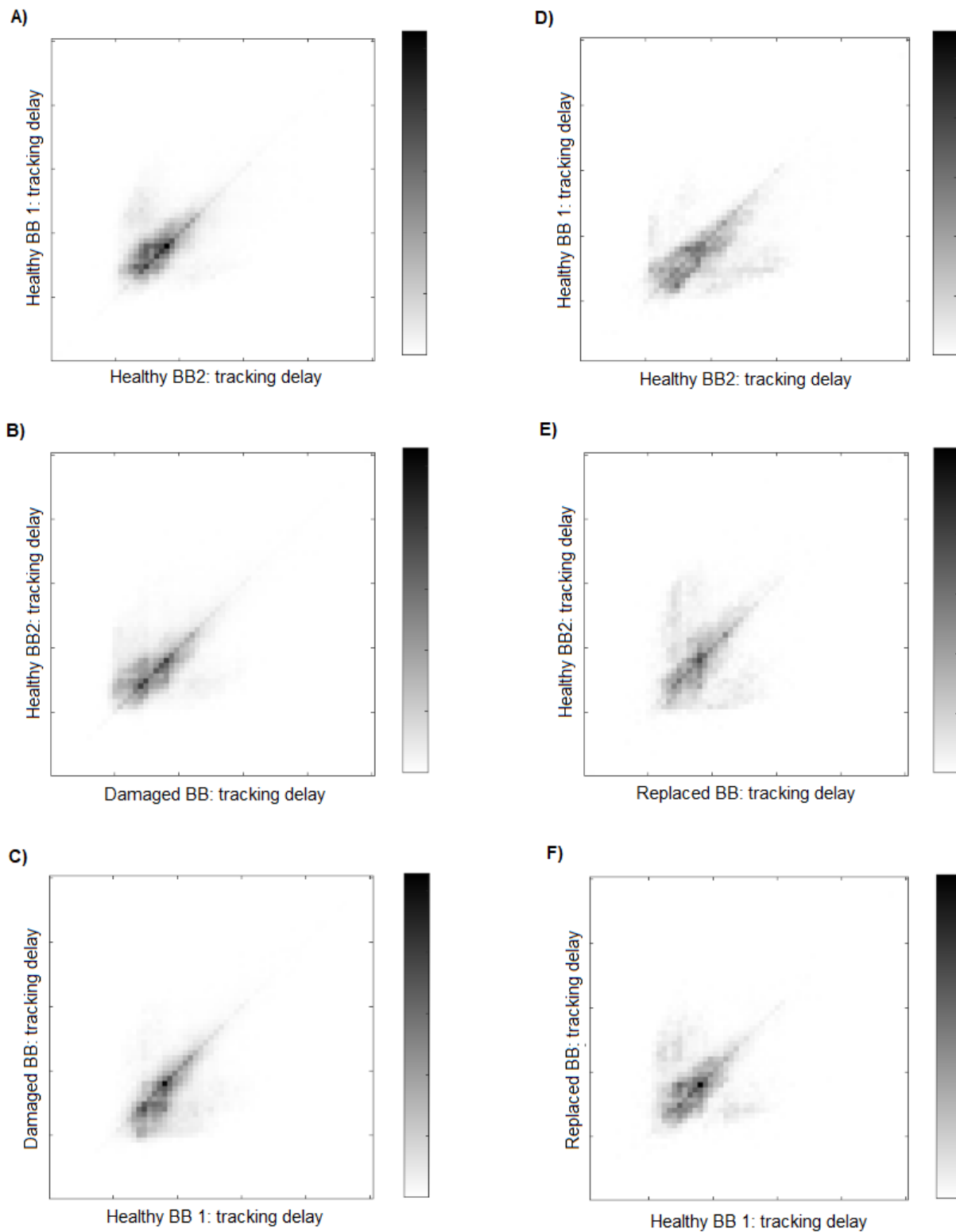
Figure 39: Joint distribution of tracking delays

3.2.10. Monitoring of hydraulic work vs pitch movement

3.2.10.1. Description

The blades are pitched by a hydraulic actuator using pressure provided through accumulators. The pressure in the accumulators are maintained by a pump, that ensures the pressure is adequate for the turbine operation. A valve controls the pressures in each chamber of the actuator, thus causing the piston to move as desired, depending on the difference between the pitch position and reference. Thus, when the pitch position needs to reach a specific pitch reference some amount of hydraulic work is performed and this is controlled by the valve, how open it is and for how long time. The idea behind this method of monitoring how much hydraulic work is done to pitch a blade is, as in previous methods the assumption, that as a blade bearing degrades an additional frictional load must be overcome in order to move the blade bearing. The hydraulic pitch system might be able compensate this extra load by providing an additional amount of work. This can explain why at first the pitch position of a damaged blade bearing cannot be seen to lag further behind the reference compared to the pitch position of a healthy blade bearing, as have been studied in the two previous sections. At later stages it might not be possible for the hydraulic system to compensate the additional load and then the pitch position will start to lag further behind the reference. Thus, this method aims to estimate the hydraulic work need to pitch a blade and then compare how this work differ under different circumstances. The hydraulic work is the product of the pressure in the chambers of the actuator and the movement of the piston, but the pressure in the actuator is not monitored. Instead, as a proxy for the pressure in the actuator, the focus here is on the accumulator pressure and the relative opening of the valve. So, this method assumes that a potential need for excess work to overcome extra friction from debris would be possible to see in changes of the statistical behaviour in the relative opening of the valve, the accumulator pressure and the piston position. In the calculation section below two approaches aiming to use proxies for the hydraulic work are presented.

As for the other approaches the ever-present challenge is that the work needed to pitch the blade is influence not only by how degraded the bearing is, but anything that changes the friction in the blade bearing, e.g. the dynamic loading that the bearing experience.

3.2.10.2. Inputs

Piston position, piston reference, relative opening of the valve, accumulator pressure,

3.2.10.3. Calculations

In order to check if the hydraulic work needed to overcome any additional friction, that might arise from the degradation of a blade bearing, requires the valve to open up more to accommodate any given tracking error, the relation between the tracking error and the valve opening is studied. For the case of turbine DB, which is operating with a degraded blade bearing, the density scatters between the instant tracking error and the valve opening are displayed in **Figure 40** for all three blades. The idea here is that

D2.4 - Portability of failure mode
detection/prognosis orientations
CO-Confidential

the relation for the degraded bearing would change substantially compared to the healthy bearings and cannot be confirmed with the data available.
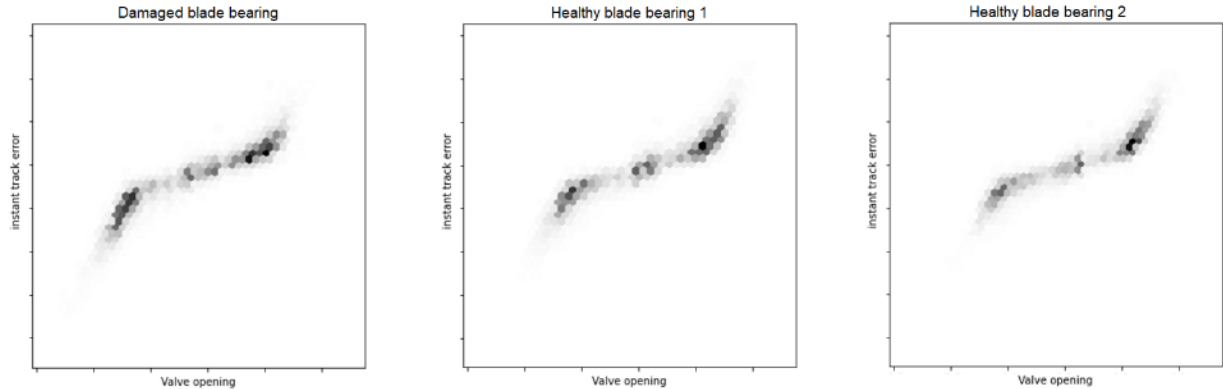
Figure 40: Relation between the instant tracking error and valve opening

Figure 41 displays an example of another approach, where just the valve openings are compared. Here two marginals of the joint distribution of the valve opening scaled by a power of the pressure for each of the pitch systems in a turbine is displayed. Since at every instant accumulator pressure and valve opening should be similar across the pitch systems in a turbine, we expect a symmetry among the pitch systems and a degraded blade bearing could potentially disturb this symmetry. This is the case in the figure, where the data from turbine DB is reused, but if this is indeed a general trend can yet not be determined for lack of cases with enough data.
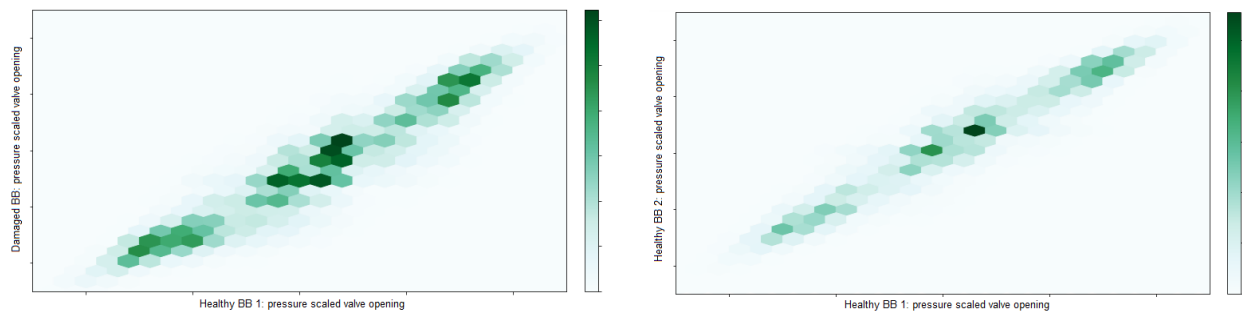
Figure 41: Joint distribution of valve opening

3.3. Electrical Drive

3.3.1. Introduction to Converter work

As part of the WP2, the aim of this portability subtask is to bring condition monitoring techniques for the failure mode "blow up of inverter modules of converters" (see section 3.3.3).

These condition monitoring techniques will have to be able to detect failures showing degradation before failure for an enough reaction time. This statement of the work is needed, due to the nature of the failure when it is ported into direct drive systems.

D2.4 - Portability of failure mode
detection/prognosis orientations
CO-Confidential

To reach this objective, the following three tasks have been identified:
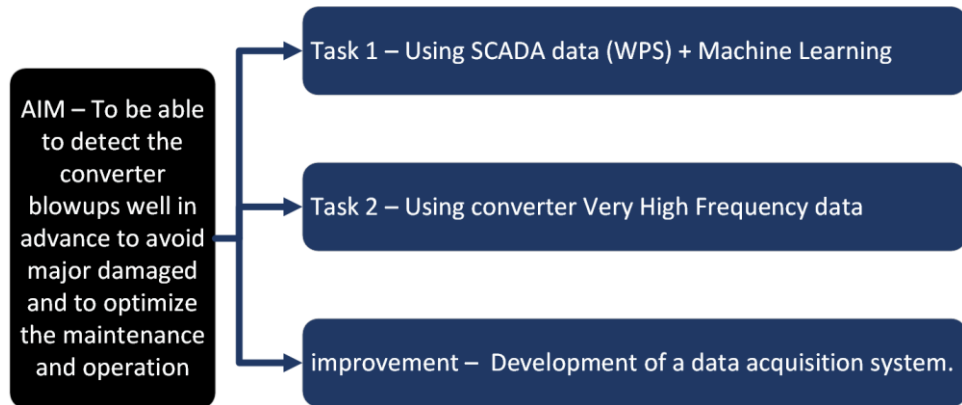
Figure 42. Aim and tasks
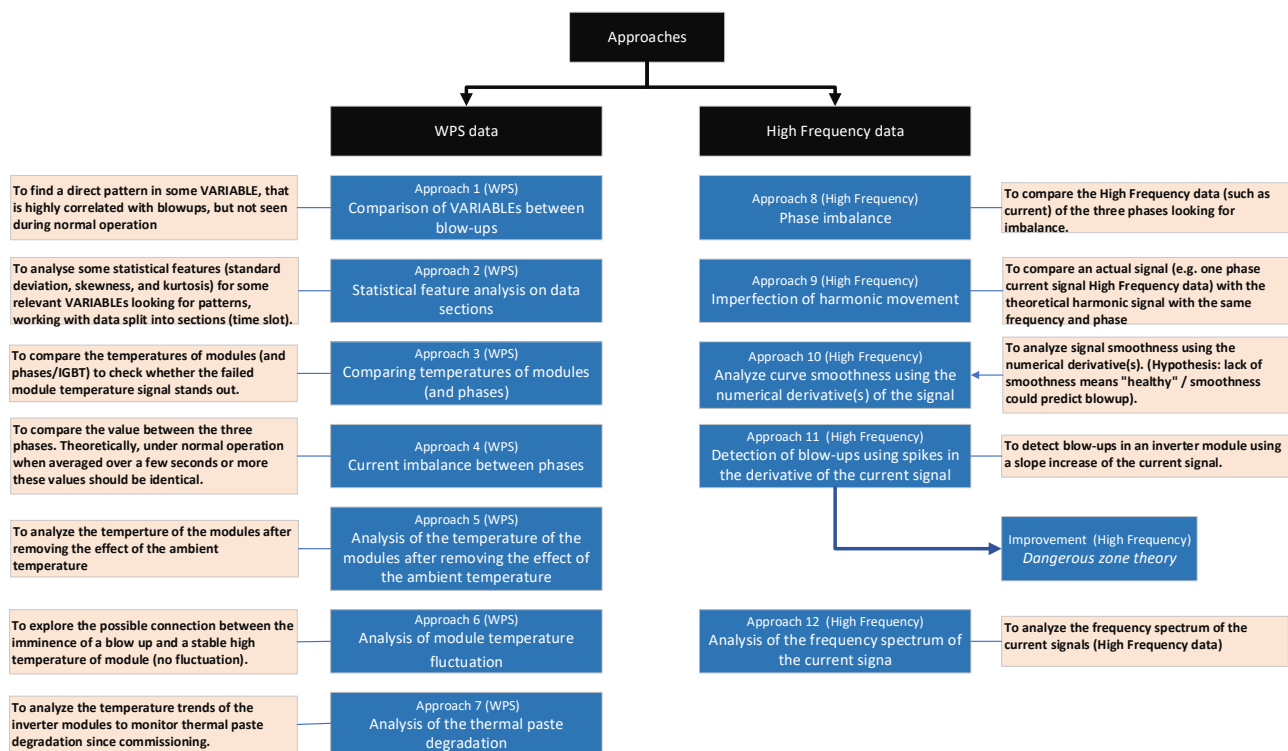
"EDT-converter ROMEO-approaches-report R1"

Blow-ups are a widespread problem. The data that this project has been concerned with have only been extracted from turbines with the SICS controllers – that being almost the entire fleet of DD turbines. It is not unlikely though that a potential failure detection algorithm designed for the SICS controller-based data, will also be compatible with data from the geared turbine fleet.

The algorithm will likely require data acquisition changes in the turbine controller system, which has been defined and assigned, but is currently awaiting execution. See Section 5.3.

3.3.2. System Description Common for Converter

3.3.2.1. Summary of the system

The converter system of a wind turbine, more specifically the *frequency* converter, is the key ingredient to connect the turbine generator to the electrical grid. The rotor of a wind turbine spins at variable frequency, depending on the wind speed, but the electrical grid has a fixed frequency of 50 or 60 Hz (depending on where in the world the turbine is located). Originally, the rotor of the turbine was connected directly to the grid, meaning that power production was only possible within very specific wind conditions. To allow for utilization of all wind conditions, the frequency converter was introduced. The frequency converter has the following purposes:

- Regulation of power from the variable speed generator to the grid
- Smoothing of power flow caused by wind speed fluctuations, and generator torque ripple
- Damping of mechanical resonances in the drive train and tower
- Regulation of the local grid voltage
- Support of local grid voltage during grid fault conditions

The frequency converter converts the variable frequency of the AC generator signal to a DC signal. Then it takes that DC signal and converts it back to an AC signal with the fixed grid frequency.

Because the converter/inverter is rated for a significantly lower power than the rated power output of most turbines, multiple *inverter modules* (IM) are installed in parallel. Small fluctuations between the signals of the inverters are "evened out" by the balancing reactors. The full overview is shown in Figure 43.

D2.4 - Portability of failure mode
detection/prognosis orientations
CO-Confidential
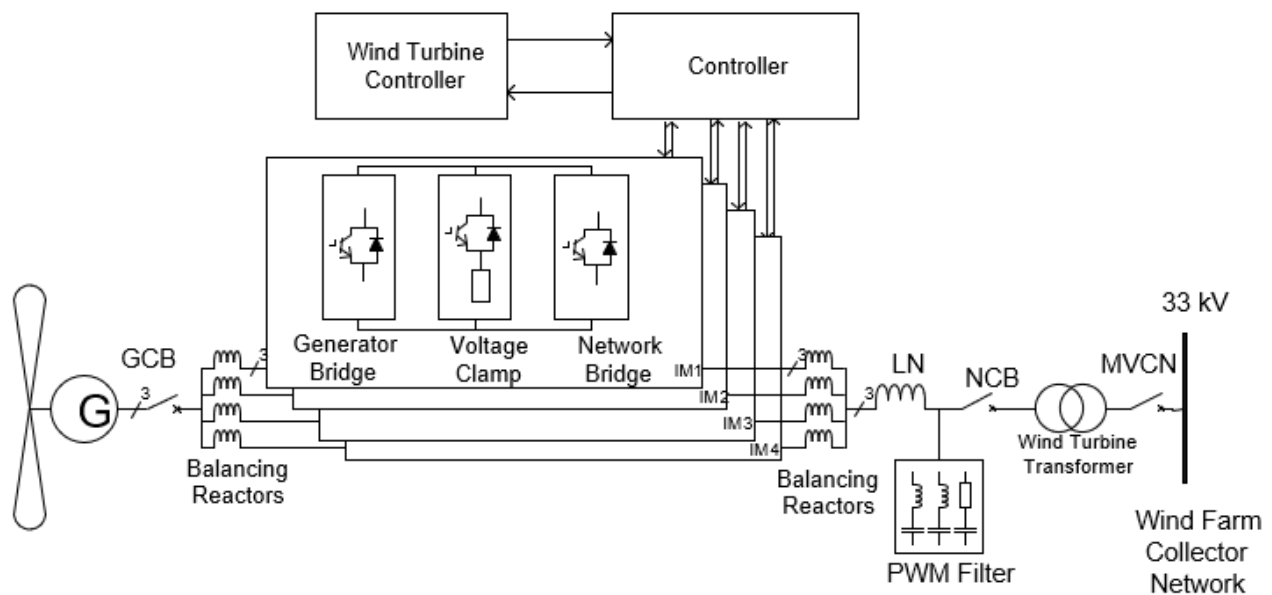
Figure 43. Full overview of converter system

Figure 44. Converter

The regulation of the power signal is done using what is known as *Pulse Width Modulation* (PWM), in which transistors turn on and off very rapidly, in order to modulate the conductance of current through the system. A transistor is represented as the Generator- and Network Bridge symbols in Figure 43, each side of the converter has three phases, each of which is modulated by two such transistors (upper and lower). Each of these pairs are what's known as the *Insulated Gate Bridge Transistor* (IGBT), and this is the component in question, when dealing with blow-ups.

D2.4 - Portability of failure mode
detection/prognosis orientations
CO-Confidential

3.3.2.2. Instrumentation

Since the project is requiring any given solutions for predictive maintenance of the converter to not require new hardware installations, all the hardware that is required to potentially detect the failure, must be available in the current monitoring design. Software changes are allowed.

The details regarding the data sources that have been handled throughout portability are reviewed in [D2.3]. The instrumentation installed in the electrical drive train are shown in Figure 4 and Figure 5 below.
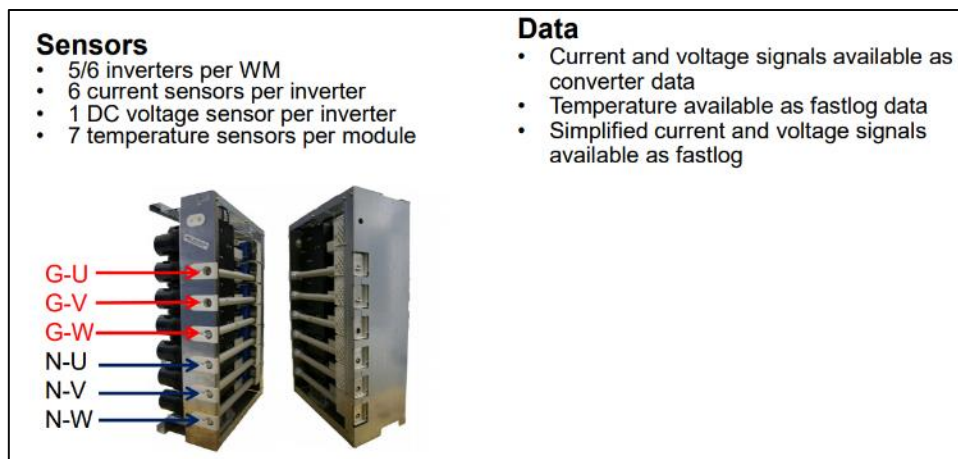
Figure 45. Sensors placed on the inverters
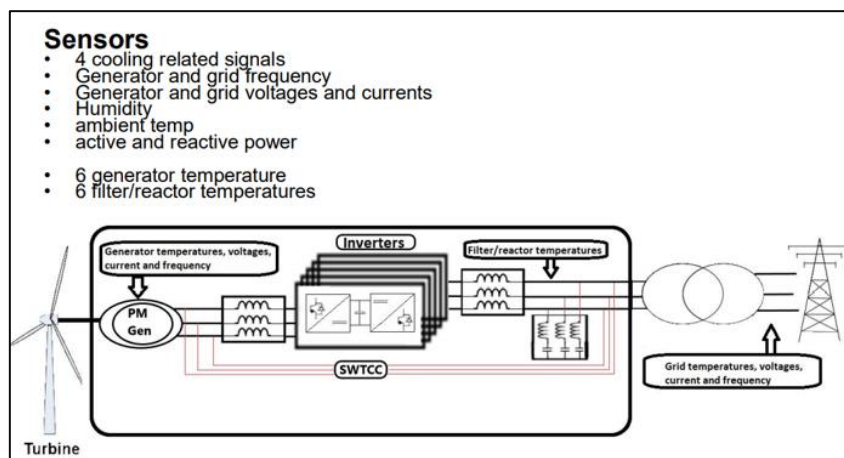
Figure 46. Surrounding sensors

3.3.3. Failure Description Common for Converter

The failure itself happens in only one of the IGBTs/phases of a specific converter module, but it causes a total failure of all three phases of the module, sometimes even affecting neighbouring modules as well, and the result is an emergency shutdown of the turbine. Only a complete exchange of the converter module in question will allow the turbine to restart, and as the failure is not always obvious, the failure

D2.4 - Portability of failure mode
detection/prognosis orientations
CO-Confidential

will sometimes require two turbine visits – one for inspection, and another for the exchange. This is obviously a costly affair, and a successful blow-up detection model will therefore significantly improve our predictive maintenance capabilities on the electrical drive train.

Illustrations of the failure are shown below.

Figure 47. Pictures of converter system after blow-up

3.3.4. Post-mortem detection using the Smoke alarm

Detecting a blow-up using offline data is relatively easy, and reasonably accurate. The detection is done using the alarm log and Snapshot data from the SCADA system. Generally, there are three simple criteria we're searching for:
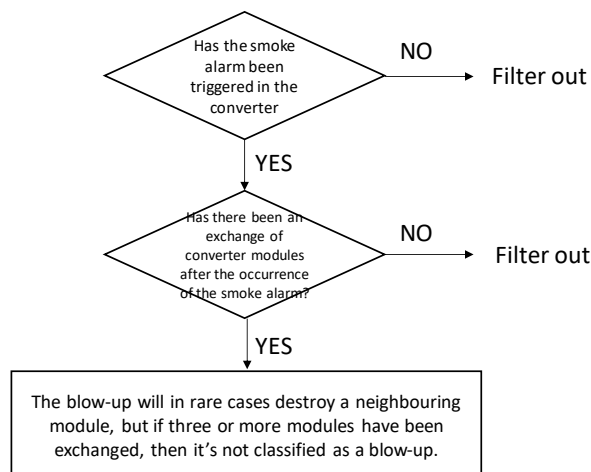
Figure 48. Process of retro-analysing data after failure.

1.   Has the smoke alarm been triggered in the converter?
The timestamp of this alarm will almost always represent the time of failure
2.   Has there been an exchange of converter modules after the occurrence of the smoke alarm?

D2.4 - Portability of failure mode
detection/prognosis orientations
CO-Confidential

3.   The blow-up will in rare cases destroy a neighbouring module, but if three or more modules have been exchanged, then it's not classified as a blow-up.

This discovery has been used in order to provide info to the rest of the failure detection methods.

3.3.5. Short circuit / current increase (WPS data)

The second way to identify a blow-up is using SCADA data. The blow-up is essentially a short-circuit of the wiring inside the converter, which causes the current flow to drastically increase. This will obviously be reflected in the measurements, and the VARIABLE "AmpPhX" (X being either phase R, S or T) will clearly show this, as illustrated below.
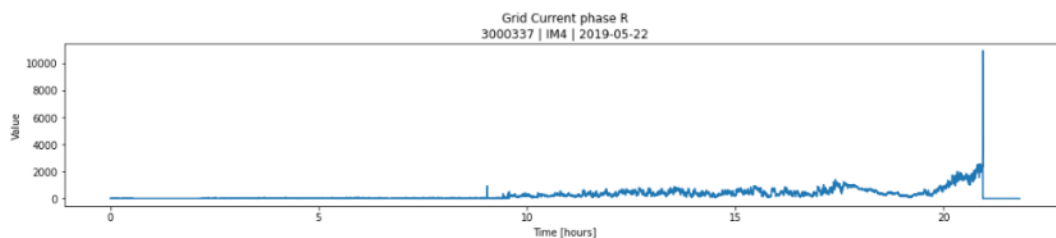
Figure 49 – Short circuit → current increase

The occurrence of a blow-up is probably not the only explanation for this behaviour. Again, the Offline data approach is not perfect, and many of the blow-up identifications done through Offline data do not correspond to an actual blow-up, so it would therefore be sensible to use the SCADA data approach in combination with the Offline approach, to increase the likelihood of correctly identifying a blow-up that has already happened, if that's the goal.

3.3.6. Portability legacy of previous approaches for converter semiconductor failures

TBD SGRE

3.3.7. High Frequency data file generation

The last way to detect the occurrence of a blow-up with reasonable accuracy – with almost perfect accuracy, as the matter of fact, considering the current setup – is via the converter (or High Frequency) data.
The reason this is almost perfect is because a datafile is only created in case something happens in the converter, so unless the datafile is corrupted somehow, a blow-up is clearly indicated in the High Frequency file. The below figure shows the appearance of all three phases of the current signal, in a blow-up file compared with normal operation. In the fault file we can see that phase T rises rapidly before saturating moments later. At the same time, we see phase R and S dropping to zero almost instantaneously.
The problem with this method is that the generation of a High Frequency file is not really monitored and accessing and reviewing the file is currently a complicated manual process.

D2.4 - Portability of failure mode
detection/prognosis orientations
CO-Confidential

Hence, identifying a blow-up is probably best done with SCADA data, but as we will see in later sections, the most promising detection algorithms have been developed using the High Frequency data.
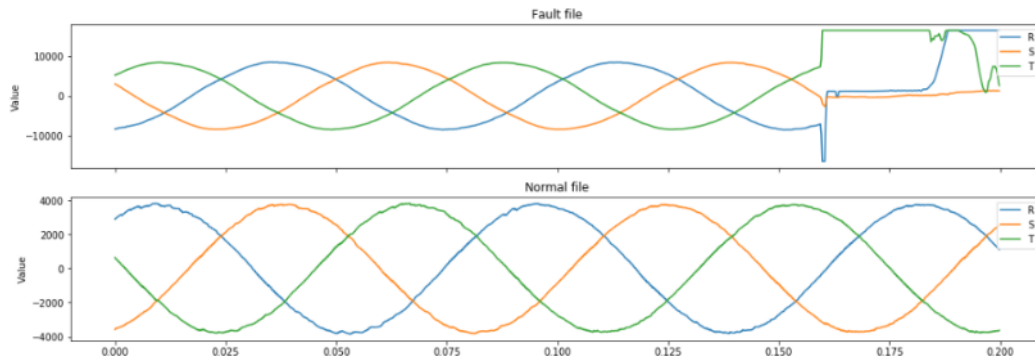
Figure 50 – Blow up in High Frequency data

3.3.8. Converter failure detection with comparison between variables

3.3.8.1. Aim

The aim of this approach is to find a direct pattern in some VARIABLE, that is highly correlated with blow-ups, but not seen during normal operation. This algorithm works with data from converter in which any blow up has happened and visualizes the trend of relevant VARIABLEs in the immediate minutes/hours/days before the failure.

Spotting anomalies in one specific example of a failure is difficult, as "outliers" in the data can have many explanations, so to overcome this problem, multiple failure examples from different turbines have been compared in the short term and long term respectively. Here, "short term" is taken as the data from the day of the failure, i.e. from midnight to the time of failure, and "long term" is a variable time frame, which in the following results have been chosen as 10 days.

3.3.8.2. Inputs / Outputs

Inputs	Outputs
Variable – The VARIABLE of which the trend will be analysed tCr – "Critical time" (i.e. the recorded time of failure) nFiles - Number of files to consider, with each file representing 24 hours of data (for long term comparisons)	The arrays required to plot the data: value array time array failure timestamp

D2.4 - Portability of failure mode
detection/prognosis orientations
CO-Confidential

3.3.8.3. Results / Conclusions

For the purpose of exemplification, the VARIABLE called "AmpPhR", which measures the grid current in phase R of the three-phase converter system, is shown on the following figure, with 10 days considered.
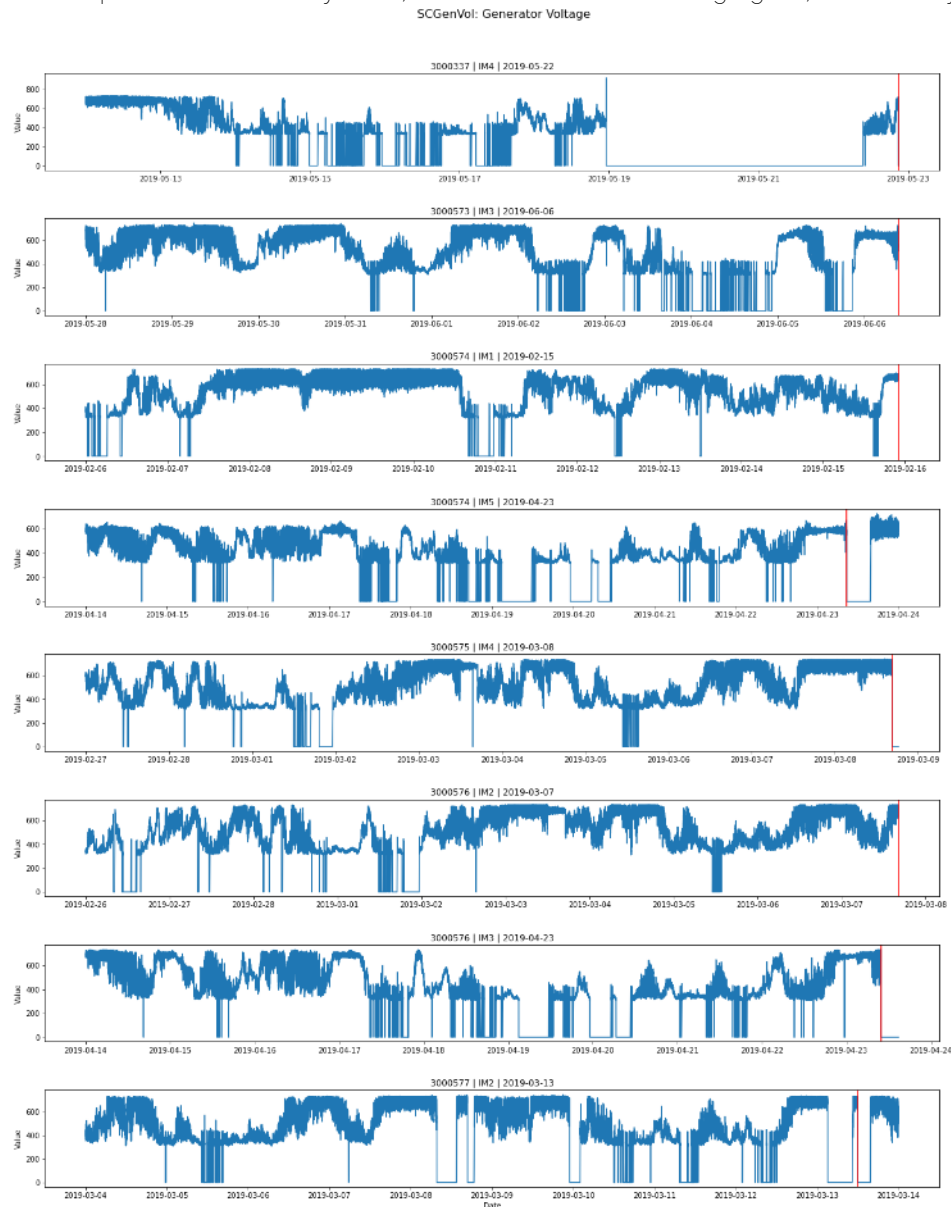
Figure 51 – Example of approach 1 "Comparison of VARIABLEs between blow-ups"

3.3.9. Converter failure detection with feature analysis in data sections

3.3.9.1. Aim

This approach analyses some statistical features (standard deviation, skewness, and kurtosis) for some relevant VARIABLEs looking for patterns. To do it along all the record time is computationally heavy, so the data have been split into section of a certain time slot.

D2.4 - Portability of failure mode
detection/prognosis orientations
CO-Confidential

3.3.9.2. Inputs / Outputs

Inputs	Outputs
Variable – The VARIABLE of which the trend will be analysed tCr – "Critical time" (i.e. the recorded time of failure) IntervalSize – Time length, in hours, of the intervals to calculate features (data sections)	The arrays required to plot the data: value array time array failure timestamp
Feature calculation (to be chosen): Standard deviation Skewness Kurtosis	Comment: the resolutions of these plots are smaller than the ones for the approach 1 due to the division into sections

3.3.9.3. Results / Conclusions

The advancement of the standard deviation leading up to the blow-up in the grid current of phase T, with interval length of 1 hour, is used as an example of the results (as with approach 1, the results here consider 10 days of data):

D2.4 - Portability of failure mode
detection/prognosis orientations
CO-Confidential

Figure 52. Example for approach 2 "Feature analysis in data sections"

At first glance, an increasing trend can be seen in the first plot (3000337), just before the blow-up happens. Looking at the other plots though, this increase is not consistent, and thus not likely to be correlated with the occurrence of a blow-up.

The extent of this analysis quickly becomes very large when considering many VARIABLEs, different lengths of each section, and different features to analyse. For this reason, there may well exist a combination of those three statistical features that can give more information.

D2.4 - Portability of failure mode
detection/prognosis orientations
CO-Confidential

3.3.10. Converter failure detection comparing temperatures/phases between converter modules

3.3.10.1. Aim

The aim of this approach is to compare the temperatures of modules (and phases/IGBT) to check whether the failed module temperature signal stands out.

Relevant VARIABLEs:

IMX Gen IGBTY temp	SCIIBTmX.GenTempY
IMX Net IGBTY temp	SCIIBTmX.NetTempY
IMX Voltage Clamp IGBT temp	SCIIBTm1.VolClTmp
X= module number (1 – 5) Y= phase/IGBT number (1 – 3) So, there are 15 of "SCIIBTmX.GenTempY", 15 of "SCIIBTmX.NetTempY", and 5 of "SCIIBTm1.VolClTmp"	

3.3.10.2. Inputs / Outputs

Inputs	Outputs
Variable – The VARIABLE of which the trend will be analysed. See 8.2.3.3 Algorithm. tCr – "Critical time" (i.e. the recorded time of failure) convSide – Converter side (gen/net) phase	The arrays required to plot the data: value array time array failure timestamp

3.3.10.3. Results

The following figure shows an example (in the third subplot) where a parameter stands out.
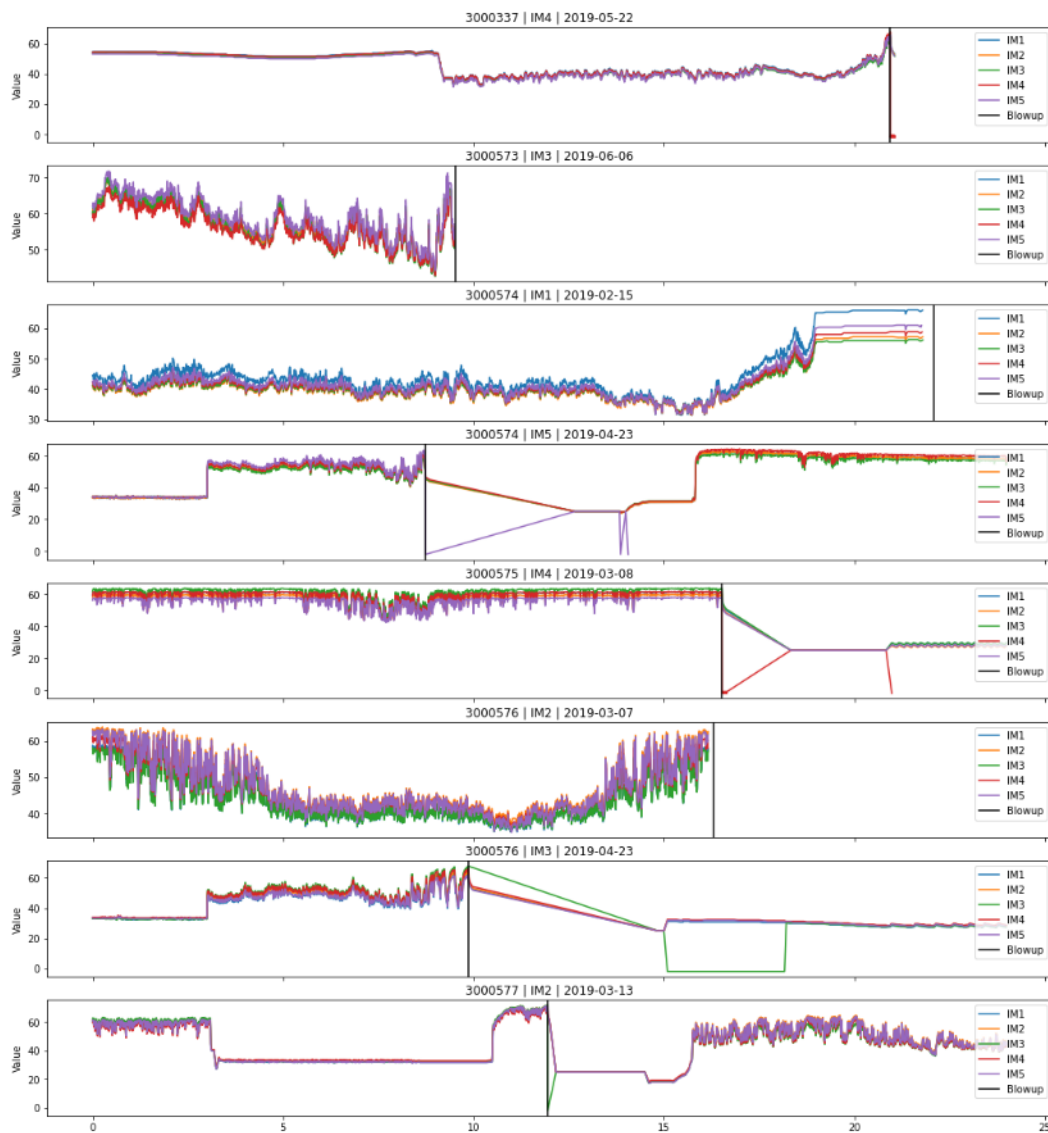
Figure 53. Example for approach 3 "Comparing the temperatures of modules (and phases)"

In the final hours before the blow-up, the five modules reach a maximum, and the IM1 module is clearly at a higher level than the others. There was a blow up in the module IM1, so this example appears to confirm this approach for detecting blow ups.

But this hypothesis has not been confirmed analysing the data of the other blow up examples. This could be just a coincidence or maybe a method that, though is able to detect blow ups, presents high number of false negatives.

3.3.11. Converter failure detection with current imbalance between phases

3.3.11.1. Aim

To compare the value between the three phases. Theoretically, under normal operation, when averaged over a few seconds or more, these values should be identical.

Note: This approach was inspired by a similar investigation by Module 03 from WP3, applied on converters in AD5 turbines. It compares the value between the three phases. Theoretically, under normal operation, when averaged over a few seconds or more, these values should be almost identical. Apart from the time of failure, nothing stands out.

3.3.11.2. Inputs / Outputs

Inputs	Outputs
Variable – current signal of each phase (AmpPhR; AmpPhS; AmpPhT) tCr – "Critical time" (i.e. the recorded time of failure)	The arrays required to plot the data: value array time array failure timestamp
	Plotting the absolute value of the difference between phases. 3 plots: phase R vs phase S phase S vs. phase T phase T vs phase R

3.3.11.3. Results

The following figure is an example of this approach.
The three plots below show the three combinations of current imbalance between the phases.
The plots represent ten days of data.

Comments
- The scale of the plots S-T and R-T are considerably higher than the scale of the plot S-R
- The plots S-T and R-T have an upwards moving trend in the final hours before the blow-up, that is not seen in the S-R plot.

D2.4 - Portability of failure mode
detection/prognosis orientations
CO-Confidential
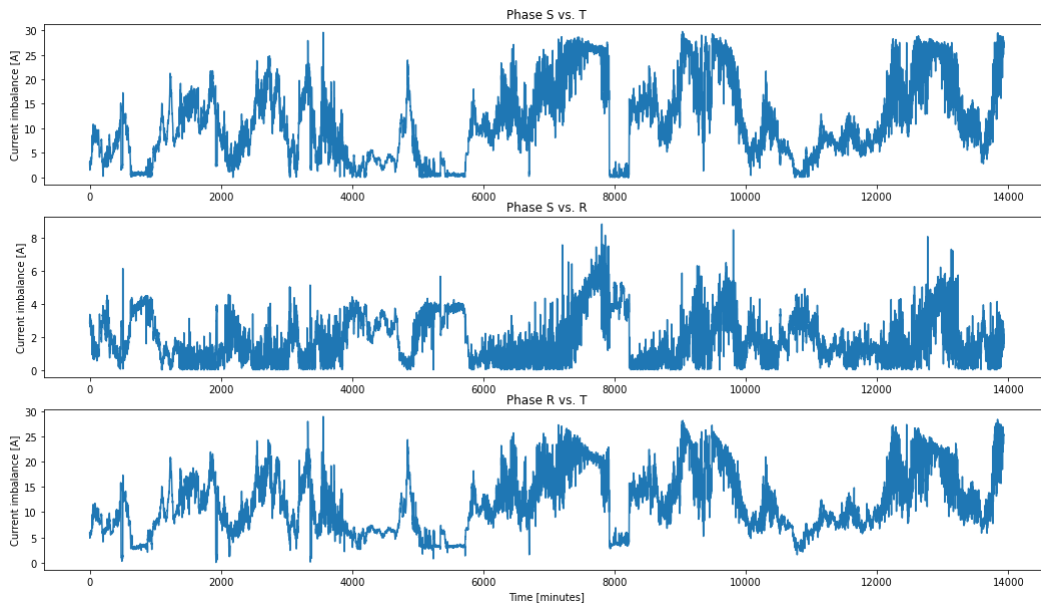
Figure 54. Example 1 for approach 4 "Current imbalance between phases"

- This result appears to show that the phase T is the one which is going to blow up, and that this approach is useful to detect it.

- This approach might not be directly usable because:

  1. In example 2, next figure, no upwards moving trend in the final hours before failure is seen. It is not possible to set which phase has blew up.
  2. On the other hand, the trend increase detected in example 1 is also seen in some healthy converters
  3. Finally, this method is not able to distinguish between different modules. So, a failure detection implies to replace the five modules.

D2.4 - Portability of failure mode
detection/prognosis orientations
CO-Confidential
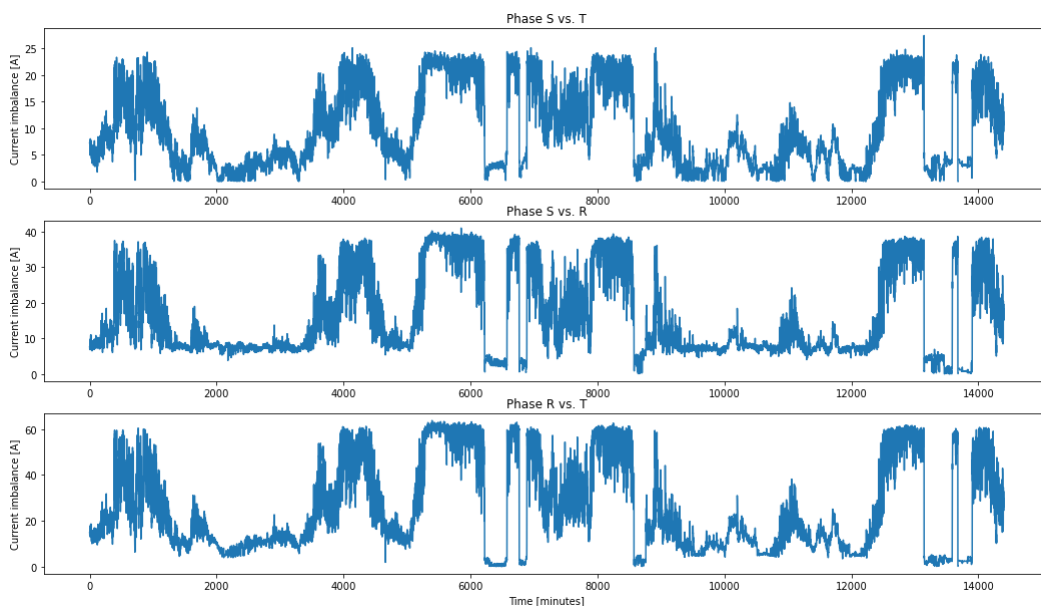
Figure 55. Example 2 for approach 4 "Current imbalance between phases"

3.3.12. Converter failure detection using analysis of the temperature of the modules after removing the effect of the ambient temperature

3.3.12.1. Aim

To analyse the temperature of the modules after removing the effect of the ambient temperature

What the algorithm does is: first, to manipulate (synchronize, truncate the longer signal) the module temperature VARIABLE and the ambient temperature VARIABLE, and subtract them. If the ambient temperature in the turbine is removed from the temperature of the inverter modules, any fluctuations happening in the temperature must be explained by something other than mere temperature fluctuations in the environment.

3.3.12.2. Inputs / Outputs

Inputs	Outputs
Variable1 – inverter module temperature (e.g. SCIIBTm1_GenTemp1) Variable 2 – ambient temperature tCr – "Critical time" (i.e. the recorded time of failure)	The arrays required to plot the data: value array time array failure timestamp

3.3.12.3. Results

As an example, the plot below shows the converter module temperature data in the top plot, and the bottom plot shows that same Variable, only with the ambient temperature in the nacelle subtracted from it. It's clear that removing the effects of the ambient temperature reveals no hidden information, and this has been the conclusion in all the considered analyses in this approach.
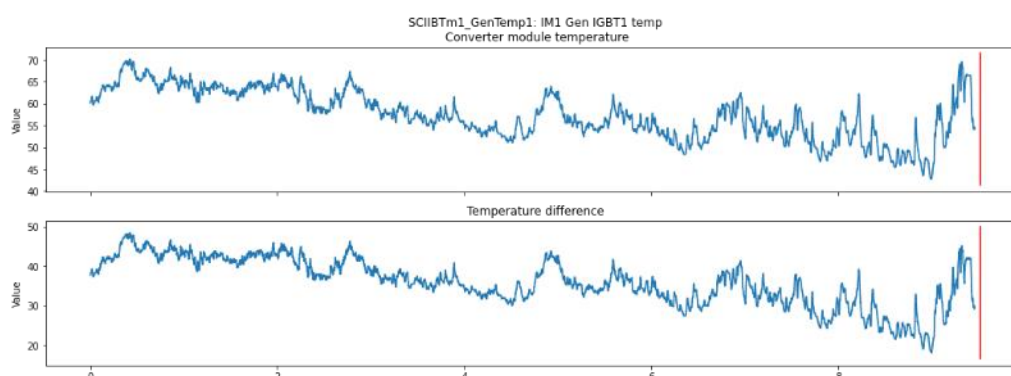
Figure 56. Example for approach 5 "Analysis of the temperature of the modules after removing the effect of the ambient temperature"

D2.4 - Portability of failure mode
detection/prognosis orientations
CO-Confidential

3.3.13. Converter failure detection with fluctuation analysis

3.3.13.1. Aim

The analysis of the first Medium-High Frequency files from failure examples appeared to show that the inverter module temperature stabilizes considerably in the hours leading up to the failure, as opposed to during the days prior, when they had considerably higher fluctuation.

The aim of this approach is to explore the possible connection between the imminence of a blow up and a stable high temperature of module (no fluctuation).

3.3.13.2. Inputs / Outputs

Inputs	Outputs
Variable – inverter module temperature (e.g. SCIIBTm1_GenTemp1) thr – threshold above which the temperature is assumed "critical" if found steady for an extended period heatTimeCr – duration of time with steady temperature above a critical value	In case of detection of an imminent blow up, the algorithm will show a warning message: "Converter failure is imminent in file ___"

3.3.13.3. Results

The analysis of new high frequency data files from failure examples have given several examples against the hypothesis on which is based this approach.

The deployment of this algorithm has reached the following state of the art:
(1) improvement of the detection algorithm was stopped before it became reliable – in the most updated state, it generates a large portion of false positives
(2) pursuing a robust detection of the behaviour had decreased accuracy, since the behaviour was inconsistent with blow-ups.

The figure below (on the left) shows an example of the behaviour that led to the original idea. It shows the temperature in one of the inverter modules, compared with the active power output. In the hours before the blow-up, it can be seen a high production of the turbine, and a very steady temperature level. Note that the y-label on the Active Power plot is wrong – the scaling is in kW.

The reasoning behind the idea is shown in the figure below (on the right) this paragraph, which shows the same Variables in the same turbine, one day prior to the above plots. Here we again see high production, but with much more fluctuation in the temperature.

D2.4 - Portability of failure mode
detection/prognosis orientations
CO-Confidential
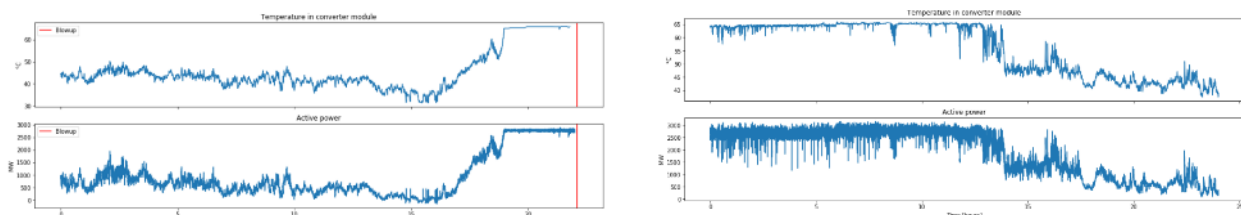
Figure 57. Example 1 for approach 6 "Analysis of module temperature fluctuation"

On the contrary, the figure below this paragraph shows one example of many, which easily disproves the hypothesis, as this shows a different converter module blow-up, which happens during a period of highly fluctuating temperature.
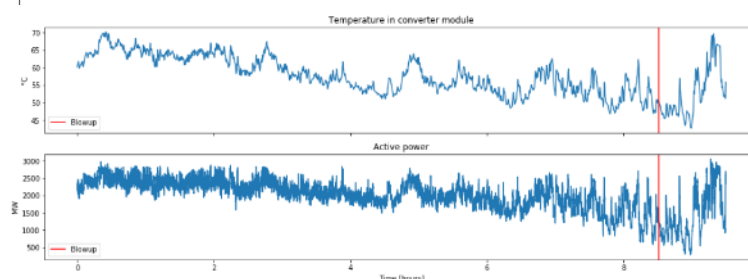
Figure 58. Example 2 for approach 6 "Analysis of module temperature fluctuation"

> Conclusion
> New examples have shown that the hypothesis on which this approach was based is not correct. The approach is discarded.

3.3.14. Converter failure detection by analysis of the thermal paste for heat conduction

3.3.14.1. Aim

To analyse the temperature trends of the inverter modules to monitor thermal paste degradation since commissioning.

In order to transmit the heat, generated by the flow of current in the converter, away from the converter modules, a so-called thermal paste is used as a bridge of thermal conductivity between the two, otherwise separate, surfaces.

Degradation in this thermal paste could made it to lose all or most of its conductivity. Which would could over time cause a short-circuit

3.3.14.2. Inputs / Outputs

Inputs	Outputs
Variable – inverter module temperature (e.g. SCIIBTm1_GenTemp1)	In case of detection of an imminent blow up, the algorithm will show a warning message: "Converter failure is imminent in file ___"

thr – threshold above which the temperature is assumed "critical" if found steady for an extended period heatTimeCr – duration of time with steady temperature above a critical value	

3.3.14.3. Results

This breakdown can take many months, often years, to develop, so to investigate the detection capabilities of the problem, it is necessary to analyse temperature data from the converter modules on a much longer term than done so far. It would be necessary to identify a recent turbine blow-up, extract the relevant data parameters, and track them all the way back to the initial commission of that turbine. Then, the trend could be carefully analysed looking for a gradual breakdown of the thermal paste represented as a gradual increase in the temperature level of the converter module.

3.3.15. Converter failure detection. Current imbalance between phases

3.3.15.1. Aim

To compare the current (Very High Frequency data) of the three phases.

This approach has been also studied using Medium-High Frequency data (approach 4) but the Very High Frequency data have a higher resolution (5kHz instead of 20Hz).

3.3.15.2. Inputs / Outputs

Inputs	Outputs
faultPath - Directory of files with failure data to consider in the analysis normalPath - Directory of files with normal operation data to consider in the analysis Very High Frequency data – current signal of each phase	faulVariableff / normalDiff - a measure of how different the signals of the three phases in the input data file are.
	When looping over multiple files, and when comparing failure data to normal operation, the outputs are two arrays, in which the individual elements are the difference measure of each data file that is analysed.

D2.4 - Portability of failure mode
detection/prognosis orientations
CO-Confidential
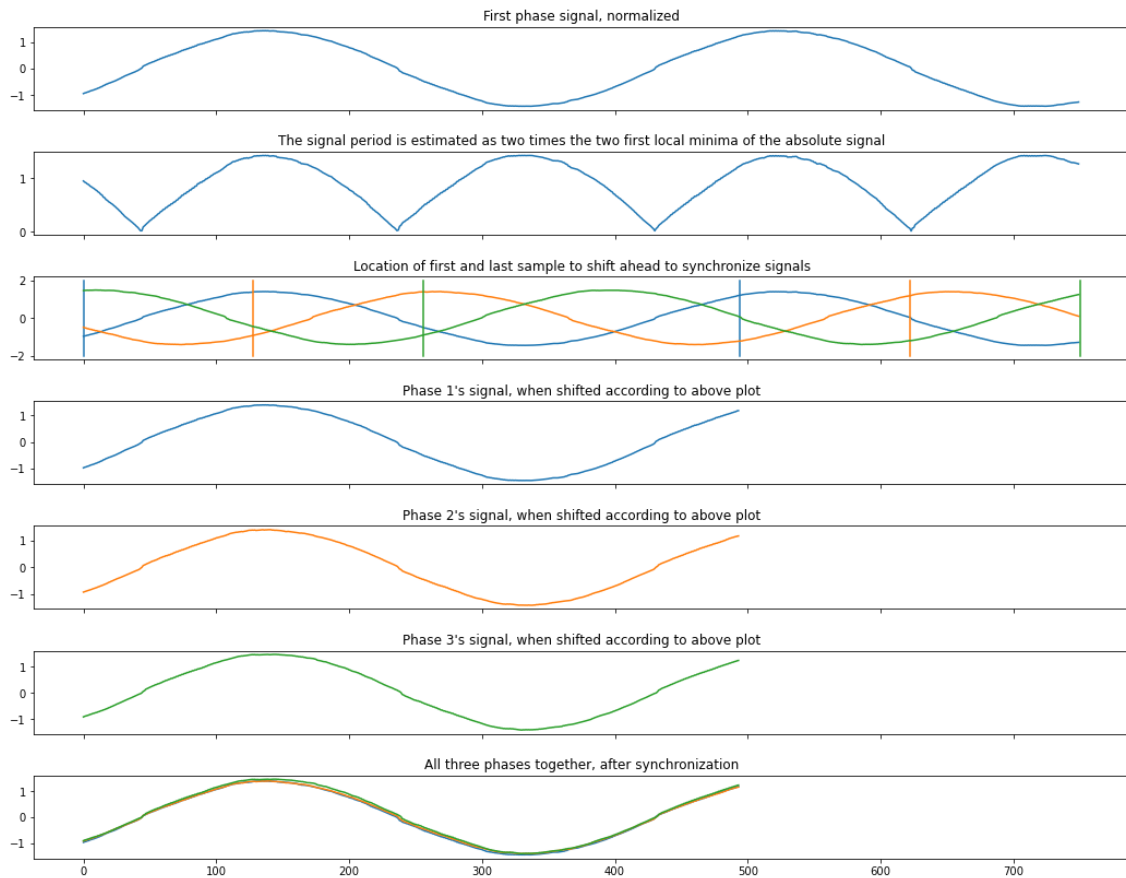
Figure 59. Algorithm for the approach 8 (Very High Frequency data) "Current imbalance between phases"

3.3.15.3. Results

The following figure shows this algorithm, when applied to 38 data files, compared with 38 randomly triggered data files from around the fleet, during normal operation.
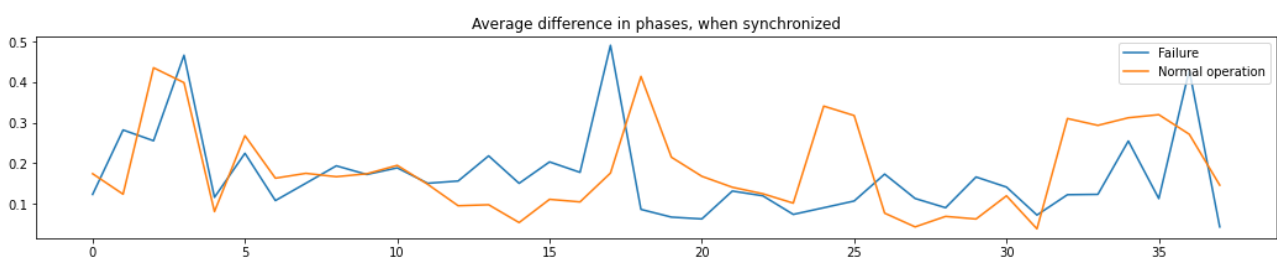
Figure 60. Example of the approach 8 (Very High Frequency data) "Current imbalance between phases"

It is difficult to say which of the lines are the result of failure data.

3.3.16. Converter failure detection approach (Very High Frequency) - Imperfection of current signal

3.3.16.1. Aim

D2.4 - Portability of failure mode
detection/prognosis orientations
CO-Confidential

To compare an actual signal (e.g. one phase current signal Very High Frequency data) with the theoretical harmonic signal with the same frequency and phase. The "error" of the physical signal is computed as the mean squared error.

3.3.16.2. Inputs / Outputs

| Inputs	Outputs
faultPath - Directory of files with failure data to consider in the analysis normalPath - Directory of files with normal operation data to consider in the analysis Very High Frequency data – current signal	faultError / normalError - the mean squared error between the theoretical sine wave and the actual current signal
	When looping over multiple files, and when comparing failure data to normal operation, the outputs are two arrays, in which the individual elements are the difference measure of each data file that is analysed.
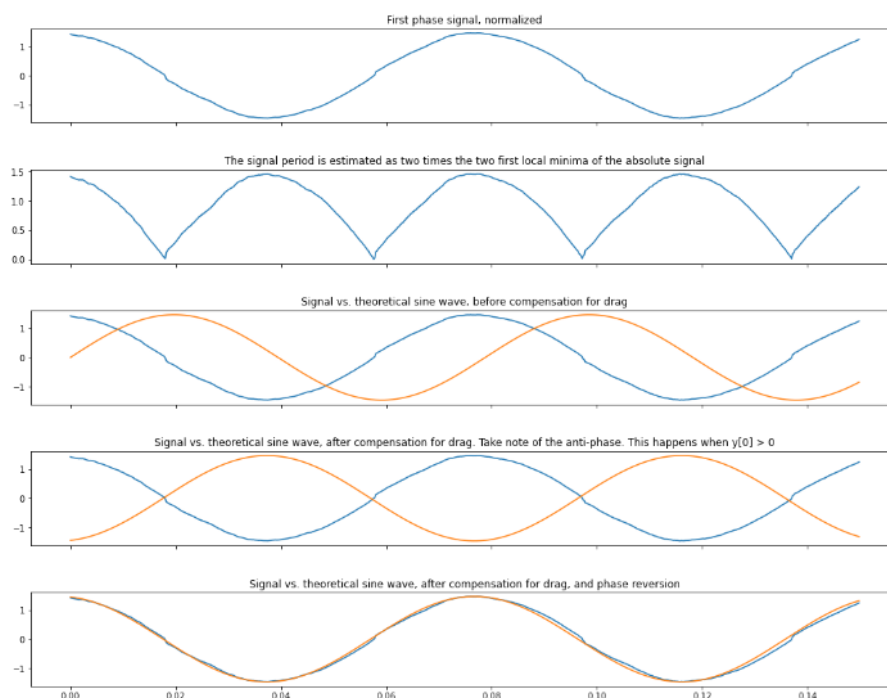
Figure 61. Algorithm for the approach 9 (Very High Frequency data) "Imperfection of current signal"

3.3.16.3. Results

The following figure compares historical data files (with blow up) with randomly triggered normal operation data.

D2.4 - Portability of failure mode
detection/prognosis orientations
CO-Confidential

As can be seen, the two plot lines have a very similar scaling.

There are two failure files where the error is considerably higher than normal operation, but 2 out of 38 files are not nearly enough for a robust detection algorithm.
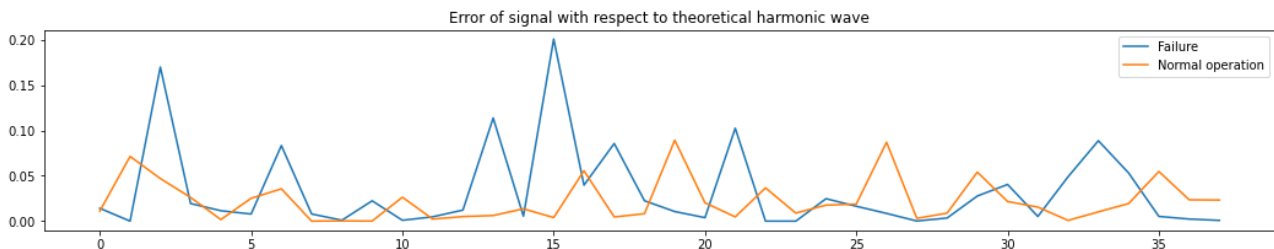
Figure 62. Example of the approach 9 (Very High Frequency data) "Imperfection of current signal"

3.3.17. Converter failure detection (Very High Frequency) - Analyse current signal smoothness

3.3.17.1. Aim

Analysing very High Frequency data extracted it was seen that the current signals from normal operation were not smooth. This "noise" was rarely seen in failures, where the signal always seemed very smooth (prior to the blow-up).

The aim of this approach is to identify this behaviour, by means of the analysis of the current signal smoothness using the first (and the second) numerical derivative of the signal.

3.3.17.2. Inputs / Outputs

Inputs	Outputs
path – directory to extract the files (selecting a file at random in the desired directory and applying the algorithm on it."	

Overview

Evaluating the smoothness of a signal is most easily done graphically, but since that's not suitable for a detection algorithm, the smoothness has been quantified somehow.

The initial idea was to extract a measure from the first or second derivative of the source signal. One way to do this is to extract the crest factor of the first derivative. The crest factor, found as $c = \frac{\max(|y|)}{RMS(y)}$, is a measure of how sinusoidal a given signal is – the theoretical crest factor being $\sqrt{2}$.

A smooth signal will thus have a relatively accurate crest factor, and a noisy signal will not. Detection could then be based on some threshold of deviation from $\sqrt{2}$.

3.3.17.3. Results

D2.4 - Portability of failure mode
detection/prognosis orientations
CO-Confidential

Collecting more data from normal operation is was seen that such data would usually have the same smoothness to it as failure data.

This hypothesis has been rejected.

3.3.18. Converter failure detection (Very High Frequency) – Detection of blow-ups using spikes in the derivative of the current signal

3.3.18.1. Aim

To detect blow-ups in an inverter module using a slope increase of the current signal.

Upon inspection of the blow-up signals, it was discovered that many of them had a sudden change of slope when the signal was close to zero, and this behaviour was almost never seen under normal operation.

Example: In the following figure, on the left, current signal (three phases) for failure signal (up) and for normal signal (down). On the right, the comparison between the first derivatives of the current signal of phase R (failure (up) and normal (down)).

Figure 63. Example 1 of the approach 11 (Very High Frequency data) "Detect blow-ups using spikes in the derivative of the current signal"

When digging a little deeper, comparing all modules in a failure example, a pattern was noticed:
- if there is a slope change around zero current in the signals, the module which blows up will always show a slope increase (leading to outward facing spikes, away from zero),
- whereas the other modules will show a slope decrease (leading to inward facing spikes, towards zero).

Note that the slope increase of the failure module will often be seen in the modules near the failure module as well.

The following figure shows an example of the module comparison. In this example, module 2 was the module that failed, thus correctly showing the slope increase, but module 1 and 3 show an increase as well, and only module 4 and 5 show the decrease which causes spikes toward zero in the derivative.
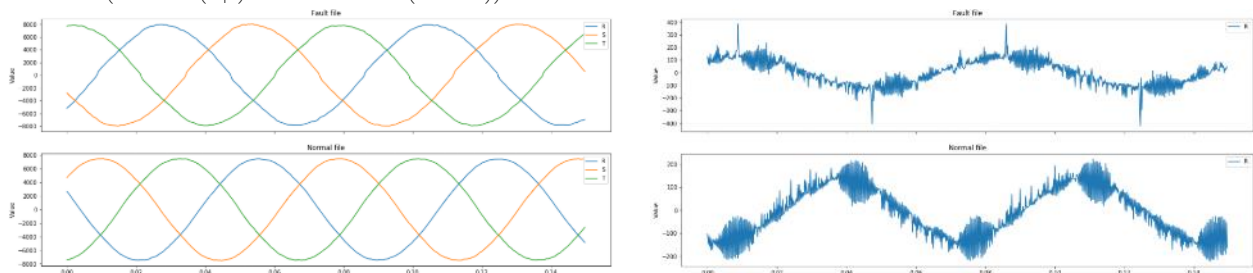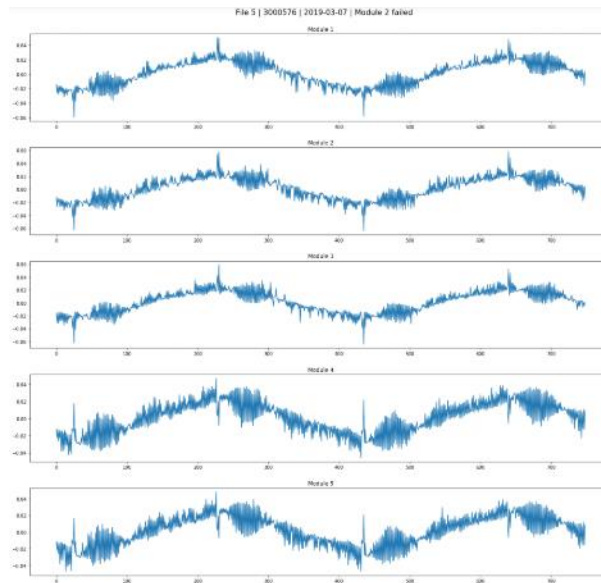
Figure 64. Example 2 of the approach 11 (Very High Frequency data) "Detect blow-ups using spikes in the derivative of the current signal"

3.3.18.2. Inputs / Outputs

Inputs	Outputs
Path – directory from which data are uploaded Phase – phase to analyse (0: phase R; 1: phase S; 2: phase T) intSize – size of the interval around 0 current, used to identify the presence of a slope change. slopeIncThr – threshold for detecting a slope increase slopeDecThr - threshold for detecting a slope decrease	False/ True – a future failure is detected

3.3.18.3. Results

- Note that A_{gen}, V_{gen} and P_{gen} (and the wind speed) are directly available as the VARIABLEs *SCGenCur, SCGenVol, SCGenPow* and *AcWindSp*, but they are not all available in scientific data, so the analysis is only possible using Medium-High Frequency data.

- Once the parameters have been extracted, they can be plotted together with the theoretical plot in the chart shown in the previous figure.

- The following figure shows the plot of the data from one Medium-High frequency files of a blow up[2]:

---

[2] Comparing the green plot of the theoretical power factor with the scatter plot of the real-world data suggests that the indirect power factor extraction is correct.

D2.4 - Portability of failure mode
detection/prognosis orientations
CO-Confidential
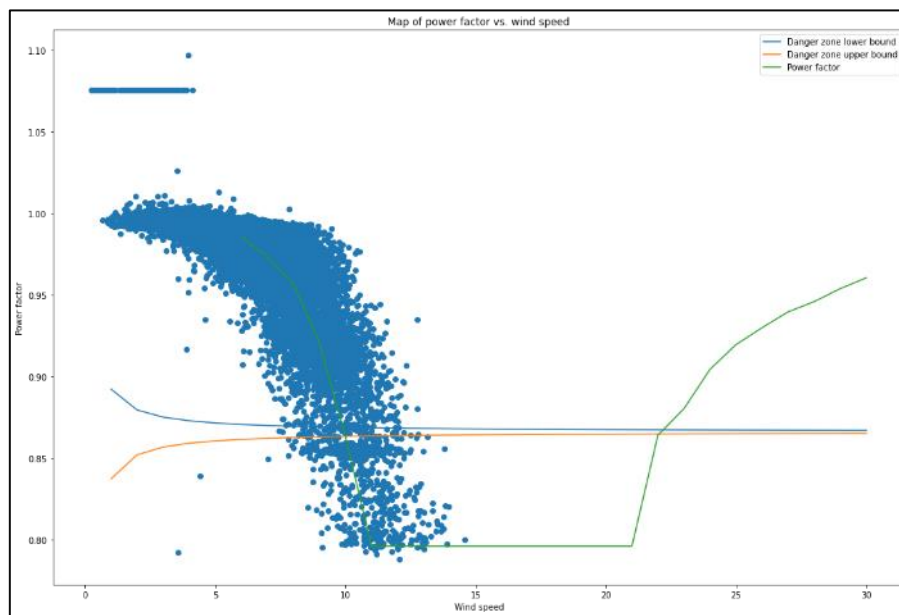
Figure 65. Example of blow up and Danger Zone

This is as far as this investigation has come, a further analysis requires a third dimension in the above graph representing the variable density of the data points.

The Danger Zone is an electrical equivalent of a Keep Out Zone for Converters.

3.3.19. Converter failure detection (Very High Frequency) - Analyse the frequency spectrum of the current signals

3.3.19.1. Aim

To analyse the frequency spectrum of the current signals.

The signal might not be perfect, and a Fast Fourier Transform may help in order to detect an abnormality.

3.3.19.2. Inputs / Outputs

Inputs	Outputs
path− =faultPath normalPath	Plots: Time domain: time signal Frequency domain: Fast Fourier Transform (FFT)

3.3.19.3. Results
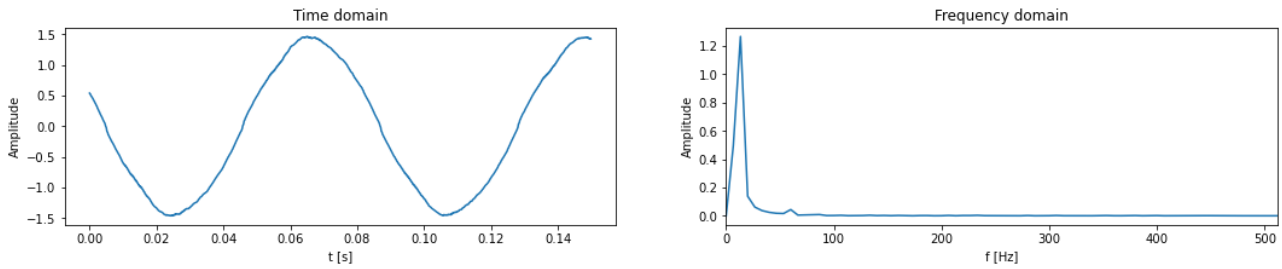
Figure 66. Example of the approach 12 "Analyse the frequency spectrum of the current signals"

3.3.20. Converter DC bus capacitor degradation

3.3.20.1. System description for DC bus capacitor of converters

Converters systems of wind turbines, whatever their configurations/topology, make use of capacitors on the DC bus, which can be of different technologies: Aluminum Electrolytic Capacitors (Al-Caps), Metallized Polypropylene Film Capacitors (MPPF-Caps) and high capacitance Multi-Layer Ceramic Capacitors (MLC-Caps). They are subject to significant failures and are so one of the systems considered within ROMEO for the diagnosis for new wind turbine generators.

The capacitor allows to balance the instantaneous power difference between the input source and output load, and to minimize the voltage variation in the DC bus within the converter. The approach carried out for the development of the diagnosis algorithm makes use of:

- Analysis and theoretical modelling of an electrical circuit, with the determination of an equivalent electrical circuit of the DC bus.
- Development, implementation and tests based on EDF R&D small scale test bench adapted within the framework of the ROMEO project. A description of the test bench is available in [D2.1]. It represents in reduced scale and electromechanical conversion system used in offshore wind application and is installed in EDF Lab Paris-Saclay facility. A detailed description of one AC/DC/AC converter of the test bench will be given in Figure 69.

The measurements considered to address this failure mode are the DC bus voltage and AC grid voltage. These measurements are available on EDF test bench and are natively measured by the wind turbine for its operation. No additional sensor is therefore needed, though sampling frequency must be high enough to enable a description of the charging and discharging phases. The diagnostic evaluation can be done:

- either with a diagnosis system integrated within the condition monitoring system
- either with an additional remote system used in each wind turbine
- or with an online calculation process, which requires to have remote information with enough sampling frequency. In this case, an event detection is recommended to restrict the amount of data transmitted

3.3.20.2. Failure description of DC bus capacitor

The converter failures caused by capacitor faults account for 30% of total converter failures [DCBUS_1]. Three types of capacitors are generally available for dc-link applications, which are the Aluminum Electrolytic Capacitors (Al-Caps), Metallized Polypropylene Film Capacitors (MPPF-Caps) and high capacitance Multi-Layer Ceramic Capacitors (MLC-Caps). The dc-link design requires the matching of available capacitor characteristics and parameters to the specific application needs under various

D2.4 - Portability of failure mode
detection/prognosis orientations
CO-Confidential

environmental, electrical, and mechanical stresses. These three types of capacitors therefore exhibit specific advantages and shortcomings. On Figure 67, comparison between their performances from different aspects in a qualitative way has been performed [DCBUS_2]. It is noticeable that Al-Caps could achieve the highest energy density and lowest cost per Joule, however, with relatively low ripple current ratings, and wear out issue due to evaporation of electrolyte. MLC-Caps have smaller size, wider frequency range, and higher operating temperatures, however, they suffer from higher cost and mechanical sensitivity. On the other hand, MPPF-Caps, besides offer some advantages such the high reliability, wider frequency, the only noticeable drawbacks are the low energy density and the low withstand to temperature.
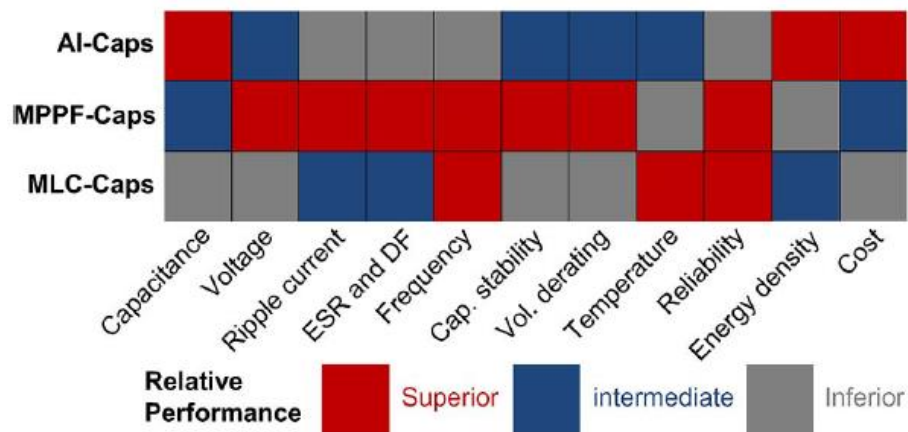

Figure 67 - Performance comparisons of the three main types of capacitors for dc-link applications [DCBUS_2]

The major failure mechanisms have been discussed in [DCBUS_3], with a focus on Al-Caps in [DCBUS_4], [DCBUS_5] for MPPF-Caps and [DCBUS_6] for MLC-Caps. Based on these prior-art research results, Table 8 gives a summary of the failure modes, failure mechanisms and corresponding critical stressors of the three types of capacitors.

The faults of DC Link capacitors are mainly caused by the design defect, material wear, operational temperature, voltage, current, moisture and mechanical stress, which can be divided into two major categories: intrinsic and extrinsic factors. These failures can also be classified as catastrophic failures and wear-out failures.

Generally, Al-Caps and MPPF-Caps suffer from open-circuit fault while the MLC-Caps is prone to short-circuit failure. Self-healing dielectric breakdown is the major cause of failures in Al-Caps and MPPF-Caps while Dielectric breakdown is prone to be the root cause of MLC-Caps failure. Meanwhile, the long-time operation in the degradation state will cause wear-out failure of DC-Link capacitors. The critical stressors as shown on Figure 67 are the ambient temperature (Ta), the voltage of the capacitor (Vc) and the capacitor ripple current (ic), humidity, vibration. The capacitor voltage and the ambient temperature being common to the 3 types of capacitors, their analysis for the detection of fault is therefore a reliable approach considering portability.

D2.4 - Portability of failure mode
detection/prognosis orientations
CO-Confidential

	Al-Caps	MPPF-Caps	MLCC-Caps
Dominant failure modes	wear out		
	open circuit	open circuit	short circuit
Dominant failure mechanisms	electrolyte vaporization; electrochemical reaction	moisture corrosion; dielectric loss	insulation degradation; flex cracking
Most critical stressors	T_a, V_C, i_C	T_a, V_C, humidity	T_a, V_C, vibration
Self-healing capability	moderate	good	no

Table 8 - Comparisons of failure and self-healing capability of the three types of capacitors [DCBUS_2]

For the electrolytic capacitors, a failure mechanism is associated to the evaporation of the electrolyte which is accelerated with temperature rise during the operation (mainly due to ripple currents). This causes a decrease of capacitance (C) and an increase of the equivalent series resistance (ESR) which further increases the losses and, consequently, the temperature. The equivalent series resistance (ESR) of the capacitor represents the sum of the frequency-sensitive resistance of the oxide dielectric, the temperature-sensitive resistance of the electrolyte and the relatively constant small contributions of the foil, the tabs and the terminals [DCBUS_7].

Another parameter of interest in the diagnosis of DC bus faults is the ripple voltage caused by the ripple current which is the residual AC current through the capacitor due to incomplete suppression of the alternating waveform within the power supply. The ripple current causes power dissipation and heating affecting negatively the state of the capacitor.

3.3.20.3. Diagnosis approach based on charging and discharging phases of DC bus.

3.3.20.3.1. Aim

The goal of the diagnosis approach is to robustly and efficiently detect incipient fault related to the capacitors of the DC bus of converters. To do so, an analysis of the evolution of the charging and discharging time constants is done.

3.3.20.3.2. Inputs / Outputs

Inputs	Outputs
Path_Analysis - Directory of files to be considered in the analysis. These files containing high Frequency data (>100Hz) – converter DC & AC voltages signal	Estimated charging and discharging time constants for each file analysed Classification of the state of the equipment by comparison of estimates with initial references
Initial reference value for the time constants.	When looping over multiple files, the output is a two-dimension array with estimates, errors and phase number used for classification.

D2.4 - Portability of failure mode
detection/prognosis orientations
CO-Confidential

3.3.20.3.3. Results

The algorithm has been developed, implemented and tested making use of EDF R&D small scale electrical bench test, which enables to simulate the electrical behaviour for evolving values of the capacitors. Figure 68 presents a photo of EDF Electrical test bench.
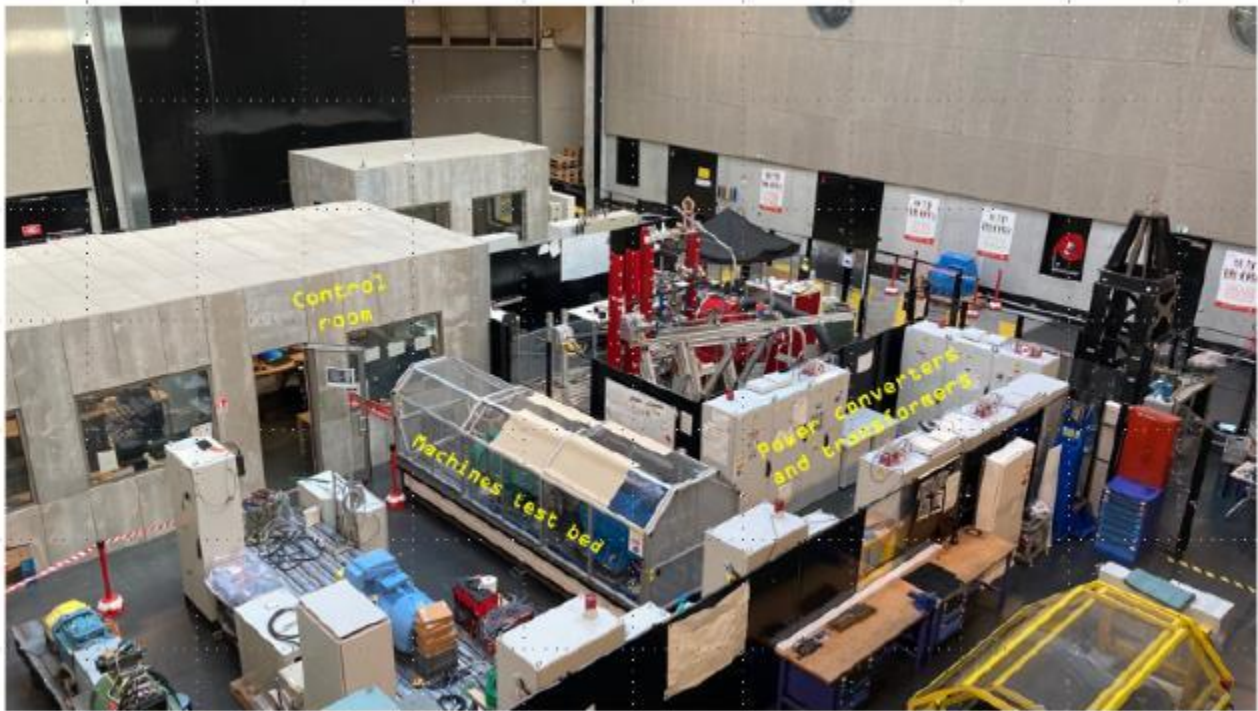

Figure 68 – 55kW EDF R&D small scale test bench implementation

The diagram of Figure 69 details the different elements of the converter system that has been used on the test bench.
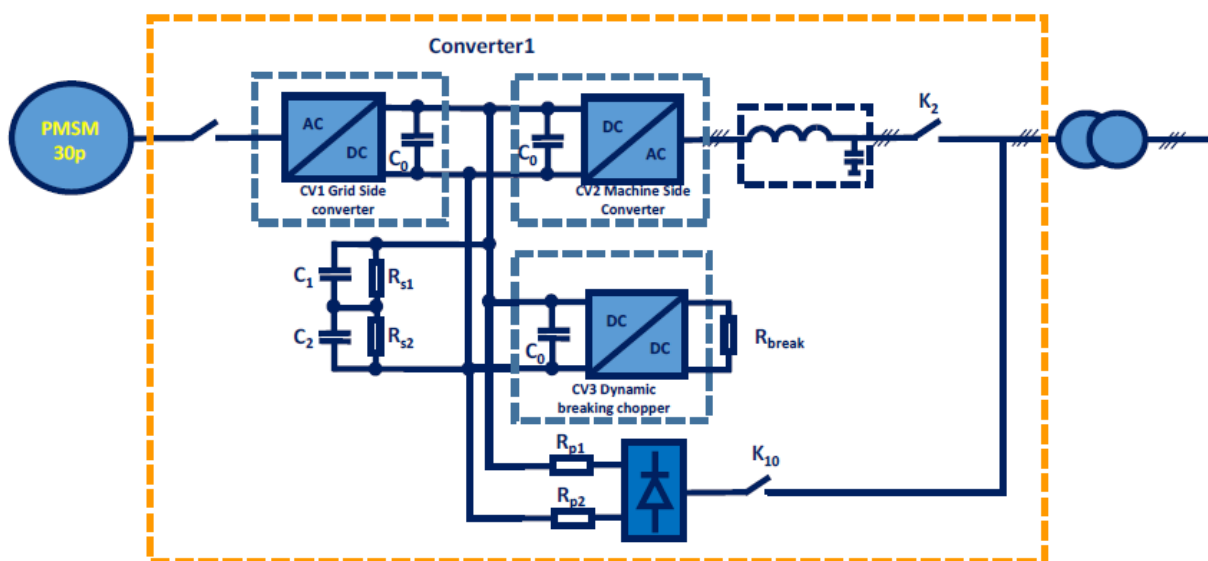

Figure 69 - AC/DC/AC Converter 1 detailed description

There are three AC/DC 3-phase IGBT power modules used for the power converter as shown on Figure 69. One of them is reconfigured to run in DC/DC for dynamic resistor breaking when the grid is off and DC bus overvoltage protection. Each AC/DC power module (CV1 used on the machine side, CV2 used on the grid side, CV3 – used for the breaking chopper) is equipped with integrated DC link (C_0) capacitors. The pre-charging circuit of DC link is done using a 3-phase diode bridge rectifier connected to the AC input and power resistors (R_{p1} and R_{p2}) on the DC side. The pre-charge contactor K10 is switched off when the DC bus reach 550V followed-up by a switch-on of K2 the line contactor. Four values are used for the additional capacitors C1 and C2 to test the system behaviour under various DC link capacitance global values. R_{s1}, R_{s2} resistors, are used to balance the voltage across the additional capacitors C_1 respectively C_2. The corresponding cases are referred in the sequel as "Configuration 1 BUS DC 1", "Configuration 1 BUS DC 2", "Configuration 1 BUS DC 3" and "Configuration 1 BUS DC 4". These cases have been tested for 15 operating points covering the operating active power range.

Figure 70 presents the control module, power module and power interface cubicles.

Figure 70 - AC/DC/AC Converter – a) control cubicle b) power modules and power interfaces cubicles

As illustration, focusing on the DC bus voltage, Figure 71 presents evolution during charging and discharging for the four configurations at maximum power.
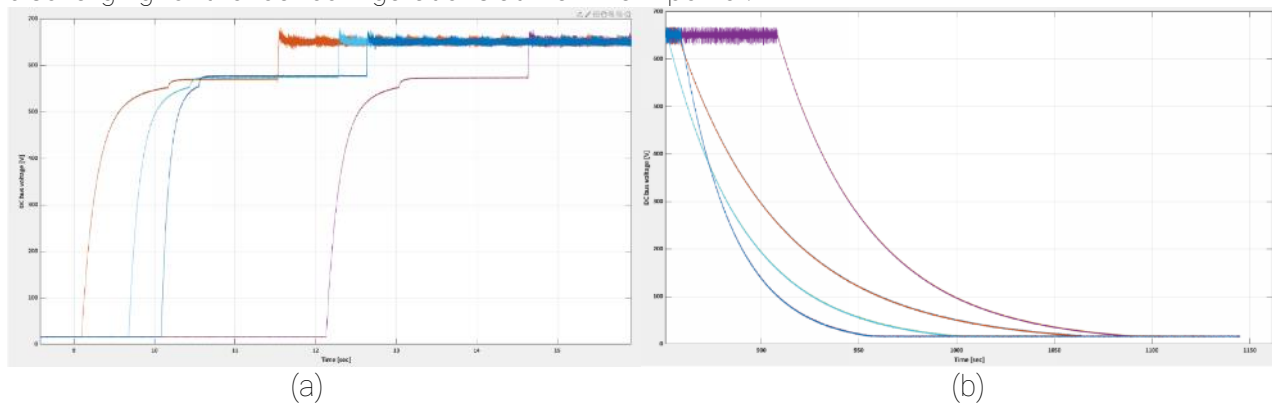

(a)   (b)

Figure 71 – sample of charging (a) and discharging (b) of the DC bus voltage at maximum power

D2.4 - Portability of failure mode
detection/prognosis orientations
CO-Confidential

The results of the diagnosis are consistent with the expected outputs, without any false positive, nor false negative:

- BUS DC 1: the 15 cases lead to Phase "0" – Normal operation
- BUS DC 2: the 15 cases lead to Phase "1" – Warning, degradation suspected
- BUS DC 3: the 15 cases lead to Phase "2" – Alert, unfitted for operation
- BUS DC 4: the 15 cases lead to Phase "2" – Alert, unfitted for operation

It is however to be noted that the degradation of the capacitor has been simulated by a variation of the capacitor value on the DC bus. Despite being a reasonable approach, considering various capacitor technologies, it is not fully representative, for instance of the expected effects of the degradation on the resistance and the temperature. The diagnosis algorithm developed will benefit from further tests and evaluations with:

- Additional small-scale test bench datasets for various normal and abnormal operations.
- Full scale operating wind turbines data.

3.3.20.3.4. Improvements and portability

- Besides traditionnal approach for fault diagnosis based on the ESR, ripples current, ripples voltage or capacitor value decrease, there is a need in setting up real-time capacitor degradation models that take into account the operating conditions (ambient temperature, voltage, ripple current, humidity, frequency, time, etc.) for more accurate stress analysis. Investigations into the interaction effect among various stressors on the lifetime of capacitors can also to be conducted.

- Hybrid models, which combine the physics-of-failure and data-driven models can also be noted. Also, regression-based degradation modeling could be a promising approach even if these models require large sample sets to increase their predictive accuracy.

- Complementary investigations might be carried out regarding the definition of the classification method and thresholds to define the different phases associated to the evolution of the failure mechanism. It could be for instance performed taking into account the specific DC bus design criteria, and from on field return of experience.

- No hardware change is identified as mandatory for improvement of the detection as, with the diagnosis method developped, the input data are available from the wind turbine controler. It however assumes that:
- o Either the diagnosis algorithm can be integrated within the wind turbine controler.
- o Either an on-event transmission of data is set in place between the wind turbine controler and a remote processing unit.

D2.4 - Portability of failure mode
detection/prognosis orientations
CO-Confidential

4. Conclusions

Similarly to D2.1, the technologies that have been subject to portability development have been summarized.

Table 9. Summary of the advances in the State-of-the-Art

Technology	Subtask	Failure Modes Covered	Advances in the State-of-the-Art
Drive train - CMSSTD	Task 2.3	Gearbox failures (all) Main bearing failures (all)	Deployment in a test bench involving a new offshore prototype. Industrialized configuration in assembly level detail.
Drive train - Imbalance	Task 2.3	Rotor & Drive train failures	Successfully deployed through models with different rotor sizes, tower and offshore foundation configurations. Inputs for the ported configuration, tested and crosschecked with experts.
Drive train – Damage Classification	Task 2.3	Main Bearing failures (all)	Successfully deployed through models with different rotor sizes. Industrialized configuration. Considerations about the usage of displacement sensor algorithm developed in D2.1 Inputs for the ported configuration, tested and crosschecked with experts.
Blade bearing CMS and diverse detection techniques	Task 2.4	Raceway/Ball fatigue Raceway/Ball wear out	Adaption of a wide spectrum of techniques to the offshore fleet. Focused methods have been studied in better detail. Diverse techniques provide also valuable approaches in order to understand better the failure behaviour.
Electrical drive train detection techniques	Task 2.5	Converter DC capacitor Converter semiconductor failure detection	Building of a test bench replicating an offshore wind turbine for the most complicated tests. Adaption of a wide spectrum of techniques to the offshore fleet.

5. References

[D2.1]   K. Krügel, P. Bousseau, C. Rodenas, *et al.*, Failure mode diagnosis/prognosis orientations. 2019. ROMEO.

[D2.2]   K. Krügel, D. Andreasen, I. Reinares, *et al.*, Preliminary failure datasets (Blade Bearing / Drive Train)

[D2.3]   P. Bousseau, A. Olsen, C. Rodenas, *et al.*, Preliminary failure datasets (Electrical Drive Train)

[DCBUS_1] Brunson C, Empringham L, De Lillo L, Wheeler P, Clare J. Open-circuit fault detection and diagnosis in matrix converters. IEEE Trans Power Electron 2015;30(5):2840–7.

[DCBUS_2]   Wang H, Blaabjerg F. Reliability of capacitors for dc-link applications in power electronic converters-an overview. IEEE Trans Ind Appl 2014;50 (5):3569–78.

[DCBUS_3]   Yang Z, Chai Y, A survey of fault diagnosis for onshore grid-connected converter in wind energy conversion systems, Renewable and Sustainable Energy Reviews 66 (2016) 345–359

[DCBUS_4]   Alwitt R, Hills R. The chemistry of failure of aluminum electrolytic capacitors. IEEE Trans Parts Mater Package 1965;1(2):28–34

[DCBUS_5]   H. Li, Z. Li, F. Lin, Y. Chen, D. Liu and B. Wang, "Measurement and analysis of insulation resistance of metallized polypropylene film capacitor under high electric field," 2012 IEEE International Power Modulator and High Voltage Conference (IPMHVC), 2012, pp. 617-619

[DCBUS_6]   Liu DD, Sampson MJ. Some aspects of the failure mechanisms in batio3-based multilayer ceramic capacitors. In: Proceedings of the CARTS International, 2012. p. 49–61.

[DCBUS_7]   J. W. Kolar, T. M. Wolbank and M. Schrodl, "Analytical calculation of the RMS current stress on the DC link capacitor of voltage DC link PWM converter systems," 1999. Ninth International Conference on Electrical Machines and Drives (Conf. Publ. No. 468), 1999, pp. 81-89,